2019

Programmable Low Loss Orthogonal Frequency Coded Surface Acoustic Wave Correlator Filters

Marshall Smith
University of Central Florida

STARS Citation

Smith, Marshall, "Programmable Low Loss Orthogonal Frequency Coded Surface Acoustic Wave Correlator Filters" (2019). *Electronic Theses and Dissertations*. 6620.
https://stars.library.ucf.edu/etd/6620

PROGRAMMABLE LOW LOSS ORTHOGONAL FREQUENCY CODED SURFACE ACOUSTIC WAVE CORRELATOR FILTERS

by

MARSHALL SCOTT SMITH III
B.S.E.E. University of Central Florida, 2014
M.S.E.E. University of Central Florida, 2016

A dissertation submitted in partial fulfillment of the requirements
for the degree of Doctor of Philosophy
in the Department of Electrical and Computer Engineering
in the College of Engineering and Computer Science
at the University of Central Florida
Orlando, Florida

Fall Term
2018

Major Professor: Donald C. Malocha

ABSTRACT

Simultaneous Transmit and Receive (STAR) communication is being developed as a means of improving spectral efficiency in wireless communication systems. If the obstacle of self-interference can be sufficiently overcome, it is possible to double the spectral efficiency of an equivalent time or frequency division duplexed system. Spread spectrum techniques can reduce self-interference by using orthogonal or pseudo-orthogonal codes to encode the transmit signal and decode the receive signal.

Hardware correlator filters are developed for use with STAR radio systems using orthogonal frequency coded (OFC) surface acoustic wave (SAW) devices. OFC is a type of spread spectrum communication that can be implemented using SAW transducers to create a correlator filter, also known as a matched filter. OFC allows code division multiple access and processing gain, similar to other spread spectrum techniques, but is more well-suited to low loss inline SAW design due to the use of multiple orthogonal carriers.

The development of low loss fixed code OFC SAW correlator filters is documented, including design criteria and multiple approaches that progressively reduce insertion loss. Using the results from progressive designs and experiments, a pair of correlator filters with matched codes are presented with approximately 6 dB insertion loss at 950 MHz.

A second development focusing on OFC SAW correlator filters with programmable codes using RF switches is also described. The programmable correlators use a fixed OFC code with programmable binary phase shift keying (BPSK), and demonstrate positive results. The programmable correlators presented require less than 1 mW of DC power.

ACKNOWLEDGMENTS

First, I would like to acknowledge my advisor, Dr. Donald Malocha, for his guidance throughout my graduate career at UCF. Your wealth of knowledge and experience has been an invaluable resource, and it has been a privilege working with you. Additionally, I thank Dr. Arthur Weeks for many helpful discussions and his commitment to education. Also, I would like to thank my committee including Chair, Dr. Donald Malocha, Dr. Arthur Weeks, Dr. Samuel Richie, Dr. Kalpathy Sundaram, and Dr. Robert Youngquist for their time and support.

I thank my colleagues at the Consortium for Applied Acoustoelectric Technology (CAAT) research group at UCF. I especially want to thank Mark Gallagher, Daniel Gallagher, Trip Humphries, Jose Figueroa, Chris Carmichael, Luis Rodriguez, and Brian Fisher. Without the strong foundation built through hard work of the group members that came before me, the work presented would not have been possible.

This work would not have been possible without the DARPA SPAR program, which funded much of the work presented in this dissertation. Additionally, support from Rockwell Collins and fabrication expertise from Qorvo contributed to the achievements presented. I would also like to thank Quality Manufacturing Services for providing PCB assembly services.

Perhaps the greatest thanks I owe to my parents, Jill and Scott Smith. You encouraged me at every turn and instilled within me the drive to be better. Julie, Jonathan, and I could not have asked for better role models. To all of my family and friends, your encouragement made this undertaking more bearable. Thank you for the memories made along the way, and for keeping me sane.

TABLE OF CONTENTS

LIST OF FIGURES

LIST OF TABLES

CHAPTER 1: INTRODUCTION

The widespread use of mobile communication systems employing wireless communication links places continually increasing demands on the limited wireless spectrum. The need to support such a large body of users on a limited electromagnetic spectrum demands increased spectral efficiency in wireless communication systems. Spectral efficiency is defined simply as the number of information bits reliably communicated per second per Hz. Spectral efficiency has been improved by advances in modulation and coding but it has been suggested that these approaches have largely been exhausted. Many of today's systems employ either frequency or time division duplexing to avoid interference at the receiver due to the transmitter, which reduces the system's spectral efficiency by a factor of two due to duplexing. It is possible to eliminate the loss due to duplexing, allowing spectral efficiency to be increased by a factor of two over time or frequency duplexed systems by using simultaneous transmit and receive (STAR) operation [1].

STAR operation, also called in-band full duplex (IBFD) operation, can increase spectral efficiency, but only if self-interference can be mitigated. Isolation and both analog and digital cancellation methods can significantly reduce self-interference. Incorporating a spread spectrum hardware correlator, further isolation between the transmitter and receiver can be achieved by using mismatched codes. The spread spectrum correlator also provides complex signal processing in real time at full radio frequency (RF), and can improve immunity to both internal and external jamming signals. In addition to the spectral efficiency advantages, it has been suggested that STAR operation can provide a significant advantage in military tactical communications. A STAR system can hinder eavesdropping by simultaneously broadcasting a jamming signal while receiving messages [2]. Incorporating spread spectrum technology further enhances the security of this transmission and is a natural extension for STAR systems.

Spread spectrum communication can be implemented using correlator filters, also referred to interchangeably as matched filters in surface acoustic wave (SAW) literature [3, 4]. A full duplex STAR system uses one correlator filter to encode the transmit signal, and a second correlator to decode the received signal. To improve isolation between the transmitter and receiver, the transmit correlator and receive correlator should have codes that are orthogonal. If codes are orthogonal, the transmit signal is completely rejected and the system operates free from self-interference. Orthogonal codes are possible but require perfect synchronization, which is not feasible to maintain for many network topologies. For systems that are not synchronized, codes can only be pseudo-orthogonal, and some level of self-interference remains.

Correlator filters can be implemented using SAW devices, and these devices have been used extensively in radar and spread spectrum communication systems [3-5]. These correlator filters allow asynchronous communication, and are therefore particularly advantageous in situations where synchronization is difficult or too time consuming. The correlators in the literature often use some form of phase shift keying (PSK) to implement direct-sequence spread spectrum (DSSS) and have high loss, typically 30-50 dB [3], but as low as 14 dB have been presented [6]. More recently, orthogonal frequency coded (OFC) correlators have been demonstrated for use in ultra-wideband (UWB) communication systems with insertion loss around 20-30 dB [7]. The OFC correlators presented didn’t focus on achieving low insertion loss, and significant improvements in loss are possible. Many of the correlators presented in literature were designed for use in the intermediate frequency (IF) section of heterodyne radios and therefore loss was less of a concern.

For STAR radio applications, the correlators are used directly in the RF section to protect sensitive receiver components from strong jamming signals, and must have low insertion loss. Another concern for correlators is the ability to dynamically change the codes used, allowing increased security and selective communication within a network. Programmable correlators can be implemented using external switching elements [6, 8], integrated switching devices on silicon using a piezoelectric film [9], or using a nonlinear SAW convolvers [10].

This first chapter serves as a brief introduction to the material that will be presented and provides an overview of the organization of the content to follow. Chapter 2 focuses on providing the background theory necessary to understand the need for this work and the potential applications. An overview of simultaneous transmit and receive (STAR) radio operation and its advantages is provided, spread spectrum communication and receivers are discussed with schematic diagrams and example signals to illustrate concepts, and finally, orthogonal frequency coding (OFC) is introduced. OFC coding is described as a form of multi-carrier spread spectrum communication and the implementation of a correlator filter using a SAW device with an OFC impulse response is introduced.

Chapter 3 details the process used to design low loss OFC SAW filters with fixed codes. The chapter begins with the design goals and basic embodiment of the device, including a brief description of the substrate and electrode materials used, and a quick summary of some related work from the literature. Interdigital transducers are described and the concept of unidirectional transducers and their applications to low loss design are outlined. Experimental results for simple two transducer filters are presented demonstrating low insertion loss. Propagation effects are discussed focusing on measured results for actual devices and loss mechanisms are described, with the end result being that devices need to have short delays to minimize loss. The short delays reduce loss, but give rise to the problem of electromagnetic feedthrough. Differential SAW transducers are presented and implemented as a means to significantly reduce electromagnetic feedthrough through common mode rejection (CMR). Circling back to propagation effects, waveguides with multiple modes and diffraction issues are discussed and an empirical approach is used to optimize the device beamwidth giving lower insertion loss and reduced loss through the transducer. Finally, the experiments performed along the way are progressively combined into a final pair of low loss fixed-code OFC SAW correlator filters with matched codes. The pair of devices have insertion loss around 6 dB with ideal electrical matching. A single correlator filter was also presented as part of this work that achieved insertion loss as low as 5 dB [11], but a matched filter pair was not fabricated.

Chapter 4 describes a second significant achievement, programmable SAW correlator filters. The desire for programmable correlators has been long known [5] and a number of devices have been presented with varying levels of success. Most devices in the literature have high insertion loss and low operational frequencies. The devices presented are not optimized for low loss as in Chapter 3, but it expected that the work presented can be extended to achieve insertion loss only slightly higher than that for fixed correlators. Several embodiments for creating programmable correlators are described, and the feasibility in terms of SAW design and switch integration are discussed, with the end result being that programmable binary phase shift keying (BPSK) is the simplest and most feasible to implement. SAW correlators with fixed OFC code and programmable BPSK code are designed, and a printed circuit board (PCB) is used to integrate the SAW device with switches, collectively creating a programmable SAW correlator filter. Results are presented demonstrating small code sets, and the results compared with a fixed-code correlator of similar design.

The final chapter ties together what was achieved, and why it is important to the advancement of spectrally efficient wireless communication systems. The overall results are summarized, and potential avenues for performance improvements along with some difficulties and limitations are described.

CHAPTER 2: BACKGROUND THEORY

Many communication systems contain a transmitter and a receiver in order to support bidirectional communication. The power of the signal generated by the transmitter is typically several orders of magnitude greater than the signal the receiver is trying to detect. When the transmitter and receiver are on at the same time, some of the transmit signal arrives at the receiver due to finite isolation. This is referred to as self-interference, which is sometimes abbreviated SI. The problem of self-interference is illustrated below in Figure 2.1 for both separate and shared antenna systems. Self-interference can often be treated as a jamming or noise type of signal, effectively increasing the noise level of the receiver and degrading the signal to noise ratio (SNR). In this dissertation the noise referred to in SNR will also include all additive interferences, sometimes referred to as signal to interference plus noise ratio (SINR).

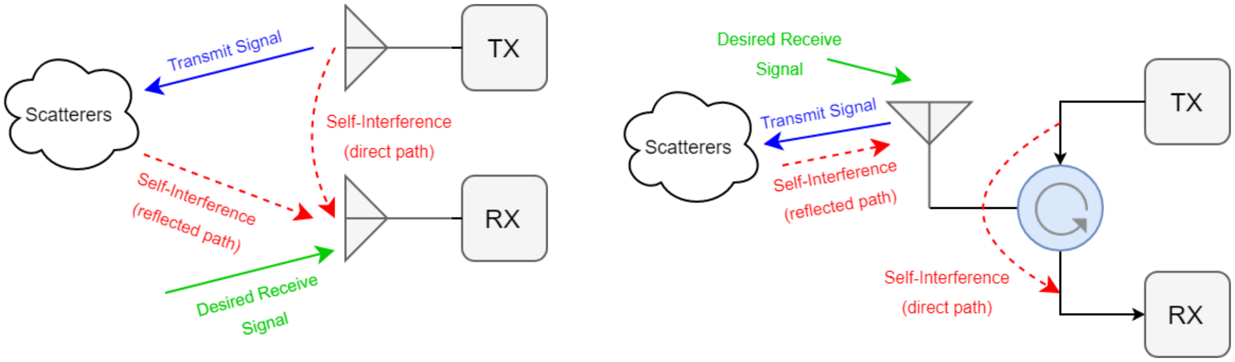

Figure 2.1: Illustration of the self-interference signals (direct and reflected paths) in contention with the desired signal for separate antenna (left) and shared antenna systems using a circulator (right).

Interference at the receiver, due to the transmitter, is a well-known problem and a number of solutions have been devised and implemented. One option is to eliminate the problem by turning off the transmitter while receiving, this is referred to as time-division duplexing (TDD). In a point-to-point duplex communication system, two systems can communicate with one another in both directions – both systems can transmit and receive. In a half-duplex system only one system can transmit at a time while the other receives, a common example of this is walkie-talkies. On the other hand, full-duplex systems allow both systems to transmit and receive at the same time. A common example of this is a telephone call, where it is possible for both parties to talk at the same time. TDD doesn't allow full-duplex operation, however, by switching between transmitting and receiving quickly the communication system can emulate full duplex operation at half speed. Another option is to have the transmitter and receiver operate over different frequency bands and filter the undesired transmission signal from the received signal, this is referred to as frequency-division duplexing (FDD). FDD allows full-duplex operation but at the cost of using doubling the bandwidth over a signal transmitting and receiving on the same frequency band. A third option is to increase isolation between the transmitter and receiver enough that they can simultaneously operate over the same frequency band without substantially degrading the SNR. This is referred to as simultaneous transmit and receive (STAR), or in-band full-duplex (IBFD) operation to distinguish itself from FDD full-duplex operation.

In this chapter the principles of STAR operation are discussed. STAR operation is compared with TDD and FDD operation and a quick overview of spread spectrum communication is given with applications to STAR operation. Orthogonal frequency coding (OFC), a type of spread spectrum communication which can be implemented in hardware using surface acoustic wave (SAW) filters, is described and brief overview of SAW devices presented.

2.1 Simultaneous Transmit and Receive (STAR) Operation

STAR operation as a concept has been known and in limited use since at least the 1940s in continuous wave (CW) radar systems. CW radars operate in contrast to pulsed radar systems, which turn the transmitter off while listening for target echoes – effectively TDD operation. CW radars continue to be used but are typically limited to short range targets due to the issues associated with self-interference. Other than the limited market of CW radars and repeaters, STAR operation has not seen widespread commercial use [1].

Most modern communication systems employ TDD or FDD in order to achieve bi-directional communication by trading spectral efficiency for self-interference reduction. STAR does not compromise spectral efficiency and can achieve up to double the spectral efficiency of the same system using TDD or FDD if self-interference can be mitigated. Spectral efficiency can be measured by the number of information bits reliably communicated per second per Hz. Self-interference presents a serious problem in STAR operation and has been the primary limiting factor preventing widespread use. Significant interest in STAR operation has surfaced recently driven by the belief that traditional methods for increasing spectral efficiency are becoming exhausted leading engineers to try other approaches. Additionally, the trend toward smaller cells for cellular and other wireless communication networks reduces self-interference due to lower transmission power and makes the problem much more manageable [1]. In addition to the commercial benefits of STAR, the ability to transmit and receive simultaneously has applications in the field of secure transmissions and communication disruption. STAR operation can enable a system to receive while simultaneously jamming the same frequency band, a form of physical layer security [2].

In STAR operation, self-interference cancellation is of prime importance. Without sufficient self-interference cancellation STAR operation cannot compete with TDD or FDD spectral efficiency, however, with good cancellation it is possible to increase spectral efficiency by up to a factor of two over TDD and FDD [1]. In order to achieve an SNR equal to that of a TDD or FDD system, the self-interference must be reduced to below the noise floor of the system. For a system operating at room temperature with a 50 MHz bandwidth and 4 dB Noise Figure (NF), the noise floor is approximately -93dBm. For a transmission power of 30dBm, the total isolation between the transmitter and receiver must be greater than 123dB. A similar example for femto-cell cellular systems is provided in [1].

In principle, self-interference cancellation is a simple problem that can be solved by subtracting a scaled transmit signal from the received signal, however, practical issues and the degree of suppression required make the task much more difficult. A number of cancellation methods exist which have been detailed in the literature [2, 12] and will be summarized here. Cancellation methods can be partitioned into three different categories – propagation-domain, analog-circuit-domain, and digital-domain.

Propagation-domain cancellation is mostly applicable to systems using separate antennas for the transmitter and receiver. In systems using a shared antenna for the transmitter and receiver the propagation-domain cancellation is typically accomplished by a circulator. In systems using separate antennas, antenna placement, polarization, directivity, beamforming, shielding, and absorptive material can be used to isolate the transmit and receive antennas. Propagation-domain cancellation consists mostly of passive techniques, but active beamforming based on channel information can also be used to cope with multipath and external reflections. Typically, systems using separate transmit and receive antennas can achieve much higher suppression than systems using shared antennas.

Analog-circuit-domain cancellation is applicable to virtually all systems and is accomplished by subtracting a modified version of the transmit signal from the receive signal. Analog-circuit-domain cancellation can occur anywhere on the receive chain before the analog-to-digital converter (ADC). Analog-circuit-domain cancellation may be passive or active and may be static or dynamically controlled based on channel information.

Digital-domain cancellation is applicable to virtually all systems and is the most versatile of the three methods. Digital-domain cancellation is performed in software and is thus easily adaptable and allows complex signal processing to be performed which makes it most well equipped to handle dynamic channel effects. Digital-domain cancellation can be seen as the last line of defense and occurs after the ADC, which constitutes its primary shortcoming. An ADC has a finite dynamic range, the ratio between the largest and smallest values that can be digitized. If the difference between the self-interference signal at the ADC and the receiver noise floor is greater than the dynamic range of the ADC, then even with perfect cancellation the signal will still suffer from errors due to quantization noise. Additionally, some headroom to avoid clipping and some space between the quantization floor and the noise floor should also be allowed when designing the system leaving the effective dynamic range of the ADC several dB below the actual dynamic range. Digital-domain cancellation can be expected to suppress self-interference no more than the value of the ADC's effective dynamic range [1].

In addition to the limitations of cancellation methods described above are the practical limitations of implementation including oscillator phase noise, nonlinearities, I-Q mismatch (for direct conversion receivers), channel estimation error, and fabrication tolerances. In many cases it is impossible to cancel self-interference to below the noise floor using a single cancellation method and multiple methods must be combined. A diagram showing the discussed cancellation methods is shown in Figure 2.2.

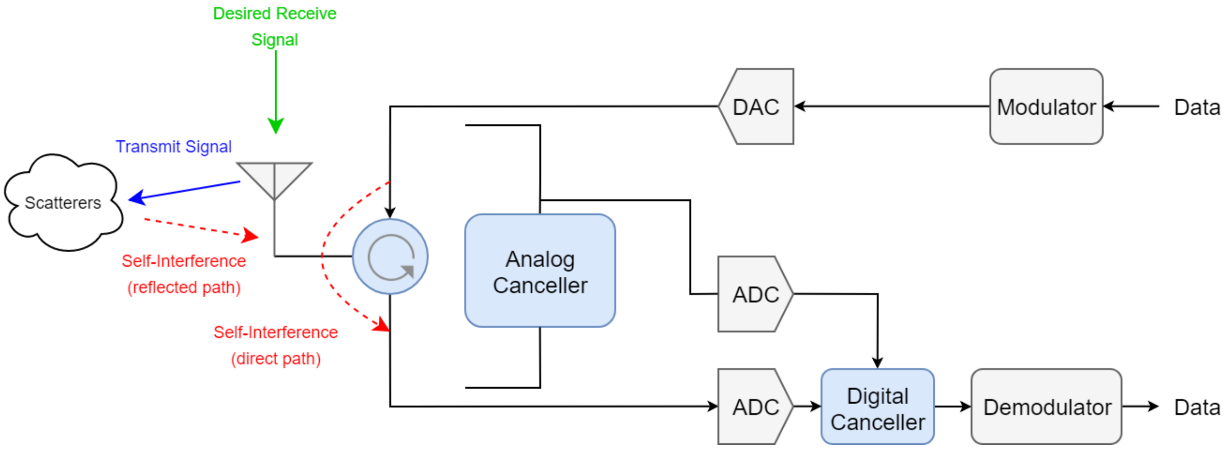

Figure 2.2: Schematic diagram showing a simplistic single-antenna simultaneous transmit and receive (STAR) communication system with relevant signals and circulator, analog-circuit, and digital domain cancellers.

The methods discussed above all rely on either reducing the transmit signal incident upon the receiver or canceling the transmit signal that has leaked into the receiver. Using spread spectrum communication techniques in combination with the above cancellation allows further isolation of the receiver from the transmitter while also implementing multiple access and increasing resistance to jamming, eavesdropping, and fading.

2.2 Spread Spectrum Communication

In the previous section, the focus was on reducing the bandwidth used by a system and increasing spectral efficiency, however, in some multiple access cases it is beneficial to spread the spectrum of the signal to be transmitted.

Spread spectrum communication was developed to provide secure communication driven largely by World War II as detailed in [13]. Spread spectrum communication provides resistance to interference and jamming, a means for reducing the probability of interception, resistance to fading and multipath interference, selectively addressable multiple user access over the same frequency band and communication channel, and ranging capability [14]. Since de-classification in the 1970s, spread spectrum communication has found application in numerous commercial and military systems including cellular systems, Wi-Fi, Bluetooth, and the global positioning system (GPS) [15].

Several technologies exist for implementing spread spectrum technology, but all have the same defining characteristics as stated in [14]. The transmitted signal energy must occupy a bandwidth which is larger than the information bit rate (usually much larger) and which is approximately independent of the information bit rate. Additionally, demodulation must be accomplished, in part, by correlation of the received signal with a replica of the signal used in the transmitter to spread the information signal. This definition excludes wideband frequency modulation which results in a large transmission bandwidth but is not considered spread spectrum. Direct-sequence spread spectrum (DSSS) and frequency-hopping spread spectrum (FHSS) are the two dominant spread spectrum technologies, though chirp spread spectrum (CSS) and time-hopping spread spectrum

(THSS) also exist. These spread spectrum technologies can also be combined to form hybrid spread spectrum systems with some performance improvements [14, 16]

2.2.1 Direct-Sequence Spread Spectrum (DSSS)

One method of spreading a signal is to modulate the signal using a wideband spreading signal, this is referred to as direct-sequence spread spectrum (DSSS). DSSS can be implemented by mapping a digital pseudorandom noise (PN) code to ± 1 to produce a spreading signal, $c(t)$. The spreading signal can then be used to modify the phase of the data signal, $d(t)$, producing a spread spectrum signal, $s_{DS}(t)$. This method of spreading is referred to as binary phase shift keying (BPSK) which is a common form of digital modulation. The spread spectrum signal generated can then be transmitted with all of the inherent advantages described above. Upon reception at the intended receiver the spreading signal, $c(t)$, is used to synchronously de-spread the received signal which can then be demodulated. This despreading operation can be intuitively understood for a BPSK PN sequence by noting that the only possible values are ± 1, which when multiplied by itself always gives 1, since $1 \cdot 1 = 1$ and $-1 \cdot -1 = 1$. A schematic diagram showing a simplistic DSSS transmitter and receiver is shown in Figure 2.3 with example signals shown for a BPSK type system without carrier for visualization. One potential disadvantage of DSSS is that it requires synchronous de-spreading which can sometimes be difficult to maintain, however, but allows use of power and bandwidth efficient modulations that require coherent demodulation, like quadrature amplitude modulation (QAM) [15].

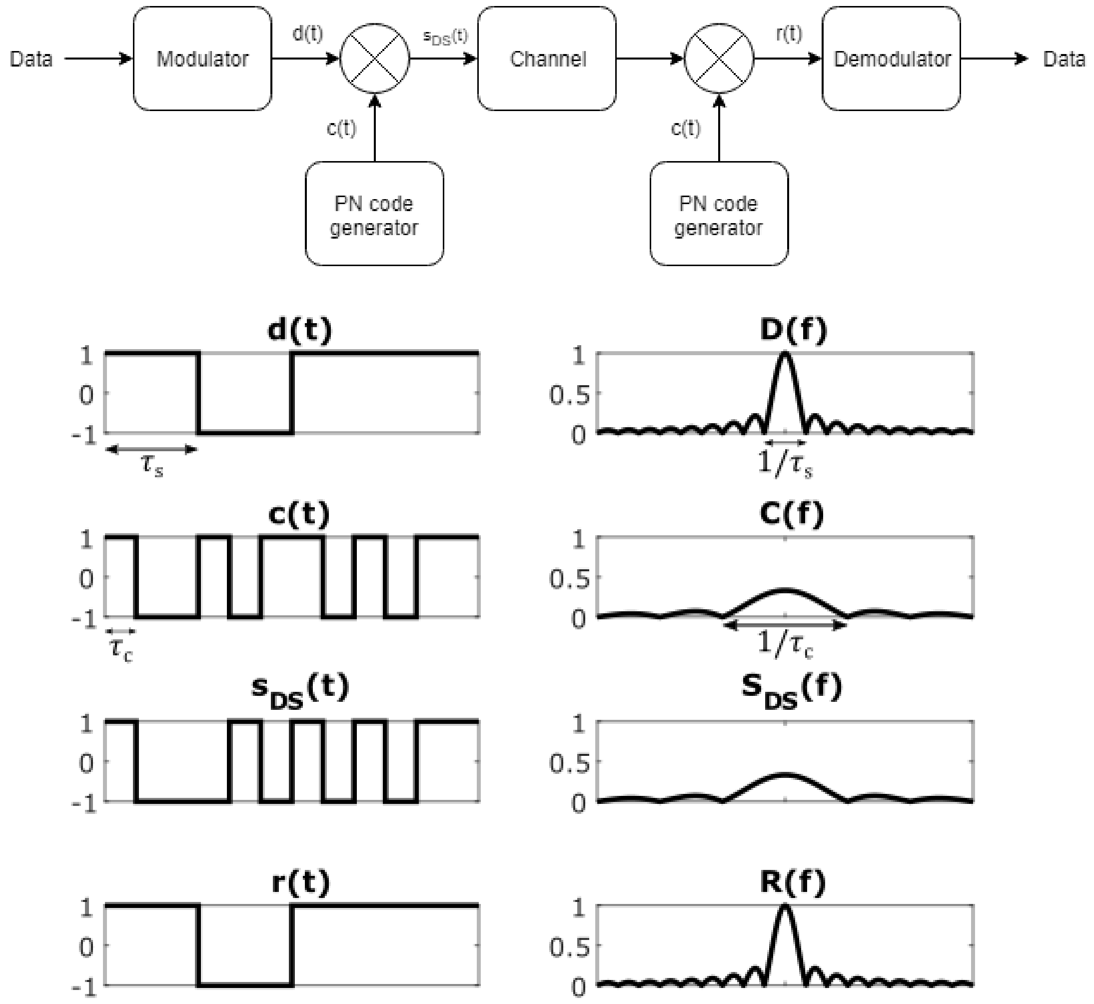

Figure 2.3: Schematic representation of a simplistic direct-sequence spread spectrum (DSSS) system with example signals for a binary phase shift keying (BPSK) system, data signals shown without carrier. The system and signals shown assume that ideal synchronization is maintained between transmitter and receiver.

Using DSSS it is possible to allow multiple systems to communicate over the same frequency band of the same channel by using different spreading signals, this is referred to as code-division multiple access (CDMA). The spreading signals are chosen in a way to facilitate reception by the intended receiver and impede reception by unintended receivers. Additionally, a good spreading signal allows the receiver to discriminate between the intended communication signal and both intentional and unintentional interference. In DSSS, this is accomplished by selecting PN codes with autocorrelation properties similar to that of white noise and that are mutually orthogonal as well as maintaining synchronizing between all systems. Practical systems may only have codes that are partially orthogonal, this results in multiple access interference (MAI), which can be approximated as an increased channel noise floor. Practical systems are also often at least partially asynchronous due to moving systems, resulting in increased MAI and further increasing the effective channel noise floor [15].

An important factor in DSSS systems is the processing gain (PG), which is largely determined by the bandwidth of the spreading signal and can be indirectly defined using one of several equivalent measures as

$$PG = \frac{Spread\ Spectrum\ Bandwidth}{Data\ Bandwidth} = \frac{\tau_s}{\tau_c} = N_{chips/symbol}, \tag{2.1}$$

for a DSSS system. Processing gain is a measure of the improvement gained by using a spread spectrum signal, as described below [14]. Using DSSS provides some immunity in adversarial environments in the form of low probability of intercept / low probability of detection (LPI/LPD) and jammer rejection. LPI and LPD are achieved due to the fact that the transmission signal is spread over a wide bandwidth and thus has a low PSD, sometimes low enough to fall below the noise floor. This low PSD makes it difficult to determine when a system is operating or what frequency band the system uses, and makes both interception and jamming much more difficult. If the frequency band of operation can’t be detected, a jammer may resort to using a wideband jammer over the most likely frequencies or simply guess using a narrowband jammer. The wideband jammer will have some peak and average power limitations, and by forcing this power to be spread over an unnecessarily wide bandwidth, the power in the operation bandwidth will be reduced. The narrowband jammer has a lower likelihood of finding the operation bandwidth, but when it does, it will be spread during the de-spreading operation of the receiver and much of the signal removed by a bandpass filter. The de-spreading operation of the receiver acts to spread the jamming signal by the bandwidth of the spreading signal and reduce the PSD of the jamming signal as illustrated in Figure 2.4, where a jamming signal is superimposed on the desired signal. A simple analysis can be performed for a tone jammer to demonstrate the advantage achieved by using spread spectrum techniques. If a tone jammer with power J is present at the center frequency of the system, then the single to interference ratio is $S/I = P/J$, where P is the power of the desired receive signal. For a spread spectrum system, the analysis must include the despreading and filtering operations. The received signal power spectrum for a spread spectrum receiver is

$$\begin{aligned} S(f) = \frac{1}{2} P\tau_c\left[sinc^2\left((f-f_0)\tau_c\right) + sinc^2\left((f+f_0)\tau_c\right)\right] \\ + \tfrac{1}{2} J[\delta(f-f_0) + \delta(f+f_0)]. \end{aligned} \tag{2.2}$$

Upon reception, the data signal is despread, while power of the jammer is spread. The power spectrum of the received signal is now

$$\begin{aligned} S(f) = \frac{1}{2} P\tau_s\left[sinc^2\left((f-f_0)\tau_s\right) + sinc^2\left((f+f_0)\tau_s\right)\right] \\ + \tfrac{1}{2} J\tau_c[sinc^2\left((f-f_0)\tau_c\right) + sinc^2\left((f+f_0)\tau_c\right)]. \end{aligned} \tag{2.3}$$

The data signal is now despread and has a peak power spectrum of $\frac{1}{2}P\tau_s$ while the jammer spectrum has been spread and now has a peak power spectrum of $\frac{1}{2}J\tau_c$. Due to the spreading, much of the jammer power now lies outside the data bandwidth, and will be removed by a bandpass filter. The signal to interference ratio at center frequency is now $P\tau_s/J\tau_c = PG \cdot P/J$, and since

PG> 1, the effective signal to interference ratio has improved. This shows that for a tone jammer, spread spectrum communication improves the performance proportional to the processing gain. The benefits are strongest for narrowband jammers, and become less effective as the jammer bandwidth increases, as the spreading ratio decreases. A similar analysis can be used to demonstrate increased immunity to interference from other users or fading caused by multipath propagation for DSSS systems, since the multipath signals will not be synchronously despread due to the additional delay [14].

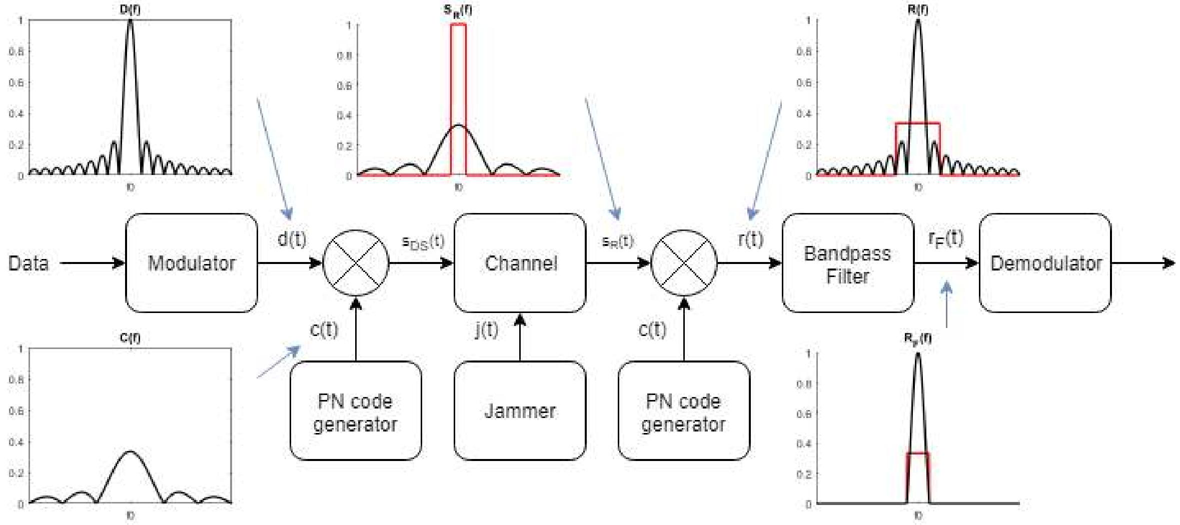

Figure 2.4: Schematic diagram of a DSSS system using a correlator receiver. The schematic and signal plots illustrate how a narrowband jammer is mitigated, the desired signal (black) passes while jammer (red) is attenuated. The system and signals shown assume that ideal synchronization is maintained between transmitter and receiver.

2.2.2 Frequency-Hopping Spread Spectrum (FHSS)

A second method of spreading a signal is to periodically change the carrier frequency of the data signal. In this case the PN code is used to control the sequence of the carrier frequencies, and this is referred to as frequency-hopping spread spectrum (FHSS). FHSS can be implemented by mapping a digital PN code sequence to a set of N_c carrier frequencies, the PN code selects the carrier frequency of the hopping signal, $f_h(t)$, used to modulate the data signal, $d(t)$, producing a spread spectrum signal, $s_{FH}(t)$. The spread spectrum signal generated can then be transmitted with all of the inherent advantages described above. A schematic representation of this transmitter is shown in Figure 2.5 with example signals shown for a fast hopping system using BPSK, data signals are shown without carrier. The hopping pattern from Figure 2.5 can be seen based on the frequency of the signals shown but is also shown in a time-frequency plot in Figure 2.6. Upon reception at the intended receiver the hopping signal, $f_h(t)$, is used to synchronously de-spread the received signal which can then be demodulated. FHSS is described as fast hopping if the hopping period, τ_c, is shorter than the period of the data signal, τ_s, ($\tau_c < \tau_s$), or slow hopping if the hopping period is equal to or greater than the period of the data signal ($\tau_c \geq \tau_s$). Fast hopping is of most interest as each bit is spread across multiple frequencies so each bit sees the spread spectrum benefits as opposed to only seeing spread spectrum benefits over a sequence of bits for slow hopping. One potential disadvantage of FHSS is that it is often difficult to maintain carrier synchronization while hopping, often limiting systems to noncoherent or differentially coherent modulation instead of more power and bandwidth efficient modulations that require coherent demodulation, like QAM [15].

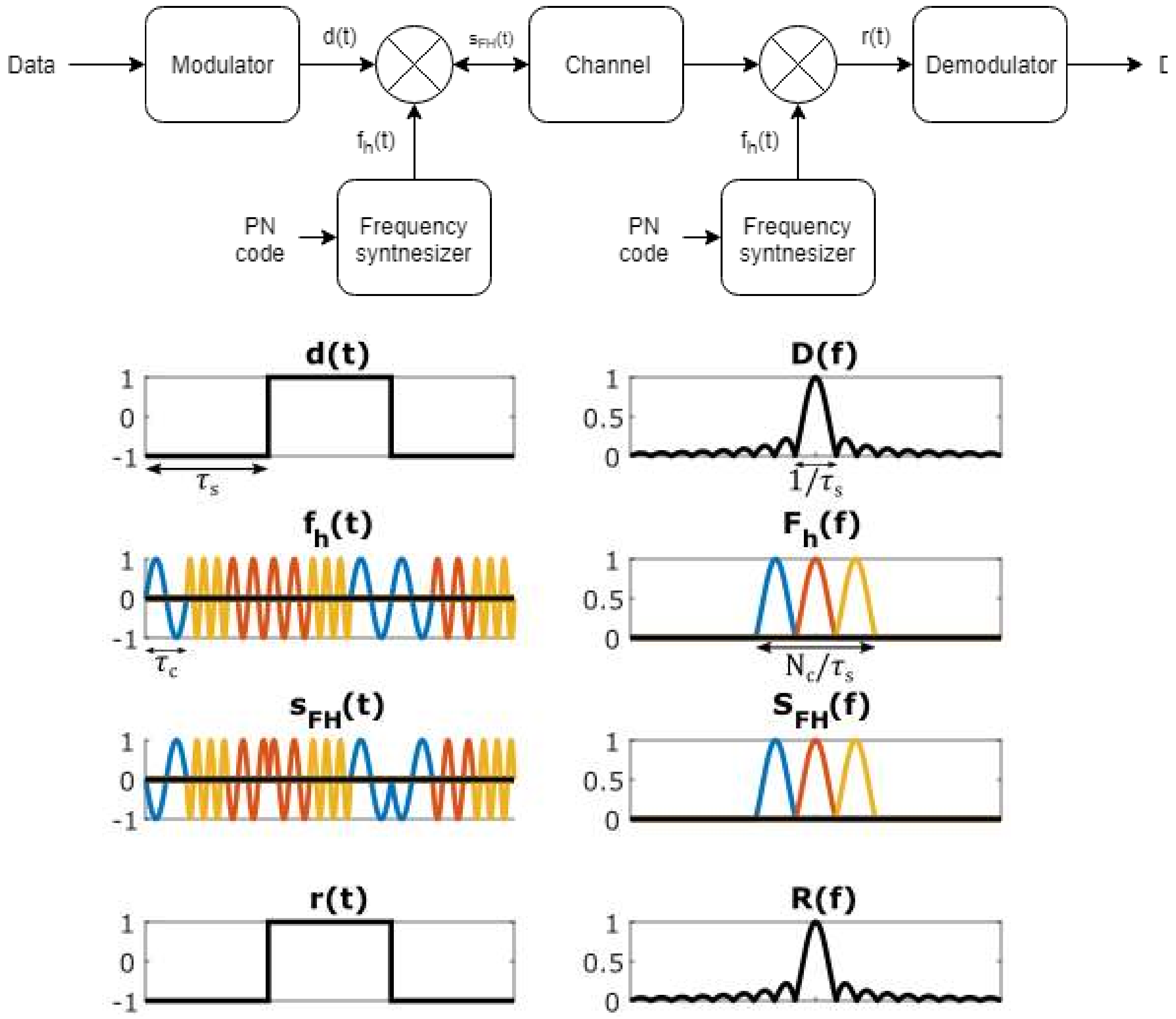

Figure 2.5: Schematic representation of a simplistic frequency-hopping spread spectrum (FHSS) system using a correlator receiver. Example signals are shown for binary phase shift keying (BPSK), and data signals are shown without carrier for simplicity. The system and signals shown assume that ideal synchronization is maintained between transmitter and receiver.

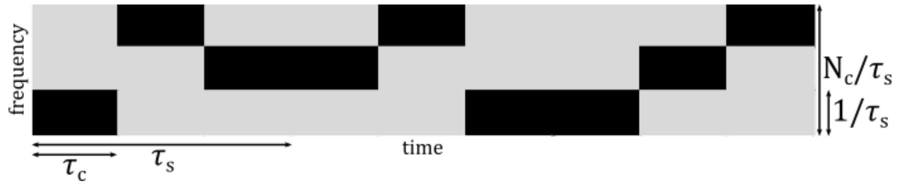

Figure 2.6: Time frequency diagram showing the hopping pattern for the example system in Figure 2.5.

Using FHSS it is possible to implement CDMA over the same frequency band by using different spreading signals, similar in effect to DSSS. This spreading signal is chosen in a way to facilitate reception by the intended receiver and impede reception by unintended receivers. Additionally, a good spreading signal allows the receiver to discriminate between the desired signal and both intentional and unintentional interference. In FHSS, this is accomplished by choosing codes such that systems are never using the same channel at the same time and maintaining synchronizing between all systems. When two systems use the same channel at the same time the likelihood of an error occurring is increased in a way similar to partial band jamming, this is referred to as a collision and is a form of MAI. Practical systems are often at least partially asynchronous, increasing the likelihood of a collision or partial collision and resulting in MAI, which increases the effective channel noise floor. Additionally, if a system has fewer channels than users, collisions will always occur resulting in additional MAI [15].

Using FHSS provides some immunity in adversarial environments in the form of low probability of intercept / low probability of detection (LPI/LPD) and jammer rejection. LPI and LPD are accomplished by spreading the signal to achieve a wide bandwidth signal with low PSD, similar in effect to DSSS. FHSS shows similar jamming immunity to DSSS, however it is accomplished in a different way. In DSSS, a narrowband jammer is spread during the despreading operation and subsequently filtered – reducing the jammer signal level. In FHSS a symbol, or bit, is transmitted over multiple frequencies, a narrowband jammer only affects some of these and thus the effect of the jammer is only a fraction of what it would be for narrowband communication. This effect is illustrated in the time frequency diagram of Figure 2.7 with a jammer superimposed over the center frequency channel (red). In this case only one of the three chips is affected for every symbol, reducing the effect of the jammer by a factor of three. Similar to the analysis for the DSSS system earlier, the suppression of the jammer depends on the ratio of the spread bandwidth to the jammer bandwidth, giving better suppression for narrowband jammers [17].

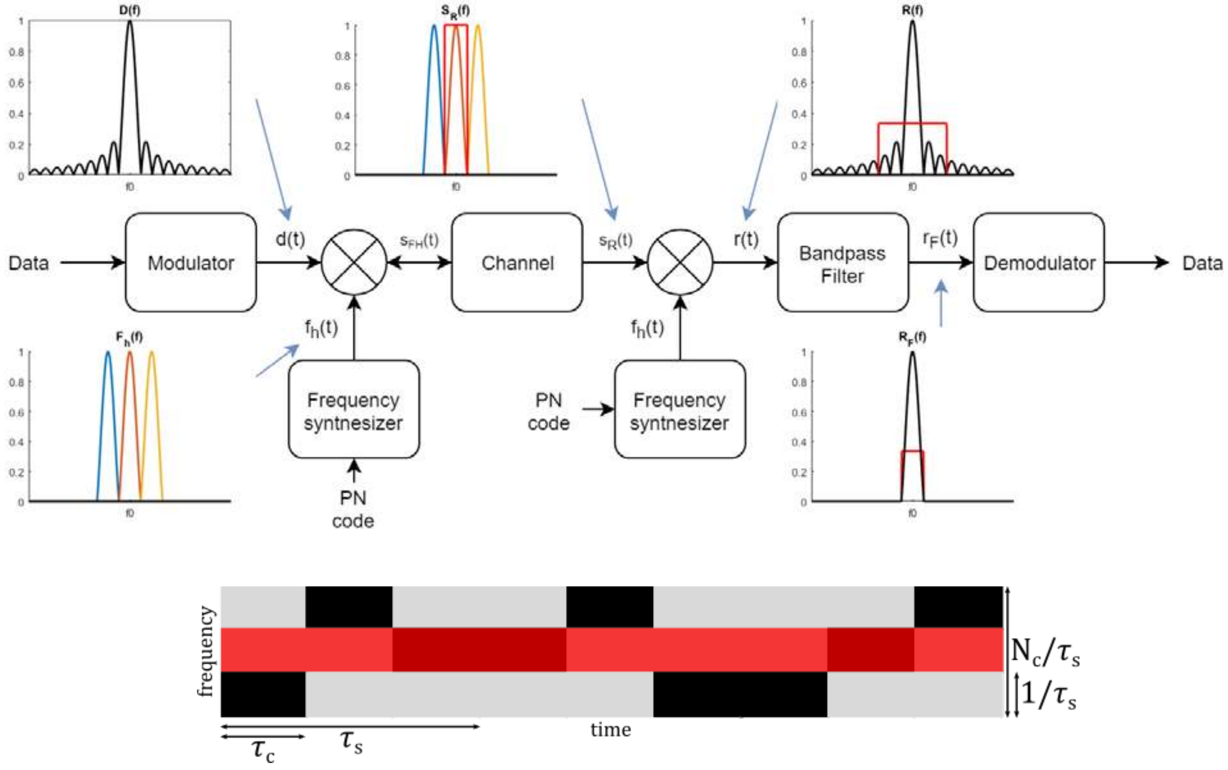

Figure 2.7: Schematic diagram illustration of an FHSS system using a correlator receiver. The schematic and signal plots illustrate how a narrowband jammer is mitigated, the desired signal (black) passes while jammer (red) is attenuated. The jamming signal is also shown superimposed on the desired signal in a time-frequency plot. The system and signals shown assume that ideal synchronization is maintained between the transmitter and receiver.

2.2.3 Spread Spectrum Receivers

There are two common receivers used in spread spectrum communication systems, the correlator receiver and the matched filter receiver. While the implementation of the two receivers are different, both minimize the probability of error by maximizing the signal to noise ratio at the sampling, or decision, instant. The correlator and matched filter receiver are both optimal receivers for the additive white Gaussian noise (AWGN) channel [16]. While both are optimal, practical considerations may make one receiver simpler or more practical to implement depending on the application.

A simple correlator receiver is depicted schematically in Figure 2.8, consisting of a multiplier, integrator, and sampler. The received signal is synchronously multiplied by the same spreading signal used in the transmitter (despread), integrated over a bit length, and sampled. It is common to use BPSK for this spreading modulation, but many other types of angle modulation can be used with some modifications to the receiver structure [14].

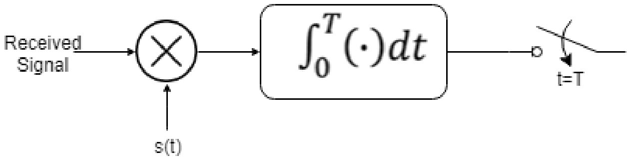

Figure 2.8: Schematic of a simple correlator receiver. The received spread spectrum signal is synchronously multiplied by the same waveform that was used by the transmitter to spread the signal. This multiplication removes the spreading signal from the data signal, a process called despreading. Following the despreading, the signal is integrated over the period of one bit and then sampled. At this sampling instant, the signal to noise ratio is maximized, and the probability of error minimized for an additive white Gaussian noise channel.

The despreading operation requires the transmitter and receiver to be closely synchronized, and if synchronization is off by even a fraction of a carrier cycle the receiver will be unable to perform the despreading operation. Synchronization is typically established using a two stage process, often called course and fine acquisition. The initial synchronization of the code (code acquisition, or course acquisition) is the most intensive, and generally involves a search through possible delays and frequency shifts. Initial synchronization is performed at startup or when the system falls too far out of synchronization, and typically reduces phase uncertainty to an accuracy of less than a chip length, at which point code tracking takes over. Code tracking (fine acquisition) continually works to maintain fine synchronization between the transmitter and receiver, and operates similarly to a phase locked loop (PLL) [14].

A simple matched filter receiver is depicted schematically in Figure 2.9, consisting of a linear filter and sampler. The output of the matched filter is the convolution of the input signal with the impulse response of the filter

$$y(t) = x(t) \star h(t) = \int_0^T x(t)h(t-\tau)d\tau, \tag{2.4}$$

where $\star$ denotes convolution, $x(t)$ is the input signal, and $h(t)$ is the filter impulse response [18]. The filter impulse response is the time reversal of the signal to be detected

$$h(t) = s(T-t), \tag{2.5}$$

where T is an arbitrary delay. This can be stated equivalently in frequency domain using the conjugation property of the Fourier transform as

$$H(f) = S^*(f)e^{-j2\pi fT}, \tag{2.6}$$

where * denotes the complex conjugate. The output of the matched filter to the desired signal is

$$\begin{aligned} Y(f) &= S(f)S^*(f)e^{-j2\pi fT} \\ &= \left[S_{real}(f) + S_{imag}(f)\right] \cdot \left[S_{real}(f) - S_{imag}(f)\right]e^{-j2\pi fT} \\ &= |S(f)|^2 e^{-j2\pi fT}, \end{aligned} \tag{2.7}$$

which is purely real when the signals are matched and delay is zero. The additional exponential term is just a delay term due to system and propagation delays. This can be qualitatively described as a compressed pulse with a time delay T. A significant advantage of the matched filter is that synchronization is not required [4]. In fact, matched filters are sometimes used in course acquisition for correlator receivers [14].

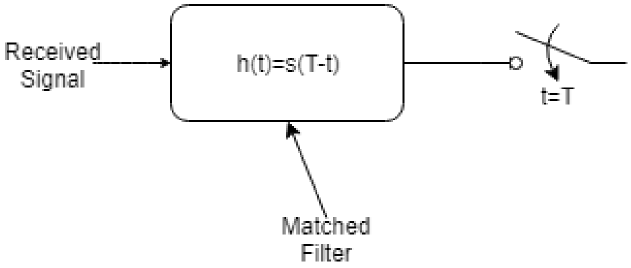

Figure 2.9: Schematic of a simple matched filter receiver. The received signal is passed through a filter and sampled. The impulse response of the filter is the time reversal of the signal to be detected with some additional delay to make the filter realizable. There is no synchronization necessary for the filter, but synchronization is necessary for accurate sampling of the output. If an envelope detector is used after the matched filter, the synchronization requirements can be further relaxed. At this sampling instant, the signal to noise ratio is maximized, and the probability of error minimized for an additive white Gaussian noise channel.

The processing gain described earlier is realized in different ways for the two receivers, but with the same effect. In a correlator receiver, the processing gain is realized during the synchronous de-spreading and integrating operations. This is effectively removing the coding and summing all pulses in time through integration. In a matched filter receiver, the processing gain is realized through the matched filter. In the matched filter, the coding is also removed, and the delays of all signal components are equalized, resulting in all chips arriving simultaneously at the output of the matched filter – a compressed pulse. The two operations both implement a correlation operation, and the output at the sampling instant is identical, however the waveforms are not. The correlation receiver produces a ramp waveform due to the integration of a rectangular pulse, which is sampled at the end of integration. The matched filter receiver produces a compressed pulse, which is sampled at the peak.

A spread spectrum system is spectrally inefficient for a single user, but by supporting many simultaneous users over the same frequency band in the same channel, the network can become quite efficient. In order to support multiple users over the same channel, different codes are assigned to each user. If all users are synchronized, codes can be chosen which are fully orthogonal, and no multiple access interference (MAI) is experienced. In some network topologies this synchronization is possible to maintain, for instance the down-link from a base-station, however it is not possible to maintain this synchronization among all users for many network topologies. In the case where users are asynchronous, it is not possible to maintain a mutually orthogonal code set for all possible delay combinations while maintaining suitable correlation properties for matched codes. There exists a joint lower bound on the maximum sidelobe level for matched codes and peak cross-correlation level for mismatched codes, described in [19]. In this case, codes are pseudo-orthogonal and the difference between the correlation peak of matched code pairs and the maximum cross-correlation of mismatched code pairs over all delays determines the worst-case level of rejection for mismatched codes. This level of rejection depends heavily on the relative delay and the specific codes used, and when multiple systems operate simultaneously this level of rejection is related to the MAI that will be incurred. The full code set must be considered when selecting codes in order to minimize MAI within the set. The topic of multiple users is revisited with figures in Chapter 4.

2.3 Orthogonal Frequency Coding

Orthogonal Frequency Coding (OFC) is a type of spread spectrum coding which uses sequential chips with differing orthogonal carrier frequencies to spread the data signal. As a spread spectrum encoding, OFC has all inherent advantages discussed in the previous section including code division multiple access (CDMA), resistance to interference, jamming, fading, and multipath effects, low probability of interception and detection, and increased signal processing gain due to the increased time-bandwidth product [20]. The remainder of this chapter will focus on OFC as a concept and its applications to surface acoustic wave (SAW) devices.

An OFC waveform consists of a number of chips taken from an orthogonal basis set as described in [20]. The orthogonality constraints are satisfied by rectangular chips with equal time length (τ_c) and center frequency spacing (${\tau_c}^{-1}$) such that at the peak of each chip's frequency response all other chips are at a null, as in Figure 2.10. The response for a rectangular chip in time is described by

$$h_{chip_i}(t) = a\cos\left(2\pi f_{c_i} t\right) rect\left(\frac{t}{\tau_c}\right)$$
$$rect(t) = \begin{cases} 1, & |t| < 0.5 \\ 0.5, & |t| = 0.5 \\ 0, & |t| > 0.5 \end{cases} \tag{2.8}$$

where a is a constant. In frequency domain the chip responses are sinc functions, sometimes referred to as sampling functions, of the form:

$$H_{chip_i}(f) = \tau_c/2\left[sinc\left(2\pi\left(f - f_{c_i}\right)\tau/2\right) + sinc\left(2\pi\left(f + f_{c_i}\right)\tau/2\right)\right]. \tag{2.9}$$

The orthogonality described here is orthogonality between chips within a symbol, which is similar in concept to the orthogonality within a set of codes discussed earlier. A symbol, or bit, is divided into an integer number of chips, the chips are normally contiguous in frequency but may be shuffled in time to provide a level of coding. If the order of the chip frequencies is chosen to be monotonically increasing or decreasing, a stepped up- or down-chirp is formed, respectively. If there are N_c chips all having differing carrier frequencies, then there are $N_c!$ possible codes available due to chip shuffling. The bandwidth for this OFC bit is

$$BW_{OFC} = N_c \cdot {\tau_c}^{-1}, \tag{2.10}$$

and the time length is

$$\tau_{OFC} = N_c \cdot \tau_c, \tag{2.11}$$

giving a processing gain of

$$PG = \tau_{OFC} \cdot BW_{OFC} = {N_c}^2, \tag{2.12}$$

as calculated using the time-bandwidth product. The time response for the bit is a time summation of all chip responses,

$$h_{OFC}(t) = \sum_{i=0}^{N_c-1} h_{chip}(t - i \cdot \tau_c). \tag{2.13}$$

In addition to OFC, an additional level of coding can be achieved by modifying the amplitude or phase of each chip. In this dissertation the polarity of the chips will be varied between ± 1, effectively superimposing a PN code using BPSK on the OFC sequence, sometimes referred to as PN-OFC. While the additional BPSK code does not increase the time-bandwidth product and therefore does not increase the signal processing gain, it does expand the code space significantly [20]. For a bit consisting of N_c BPSK coded chips there are 2^{N_c} possible codes, thus for a bit with OFC and BPSK coding there exist $N_c! \cdot 2^{N_c}$ possible codes. An example time and frequency response for a 4-chip PN-OFC waveform is shown in Figure 2.10.

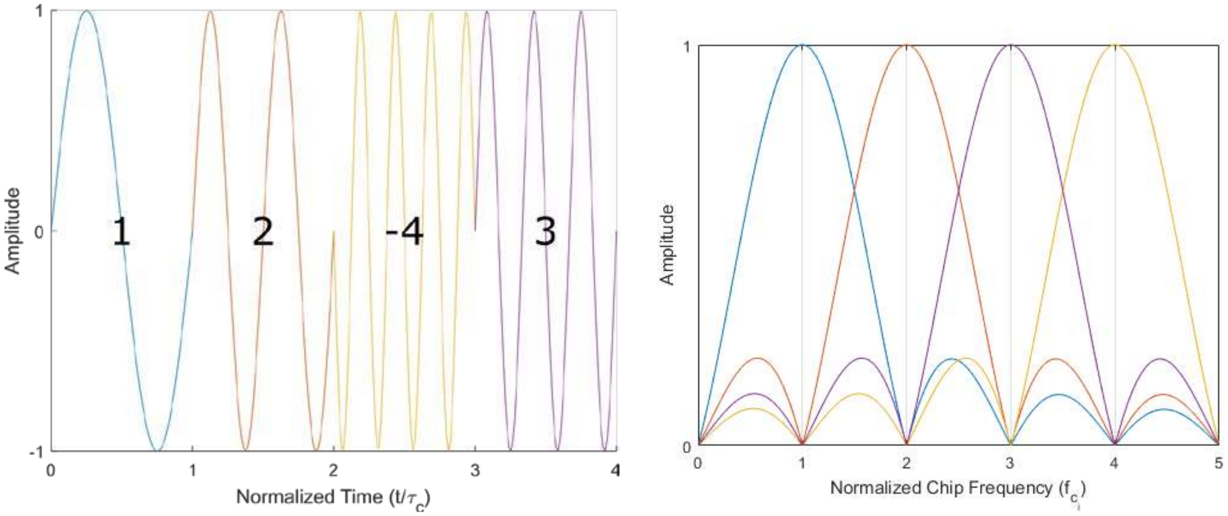

Figure 2.10: Plots showing example time (left) and frequency (right) domain chip responses for a four chip orthogonal frequency coded signal with added BPSK encoding. The OFC sequence is [1,2,4,3] as can be seen by the colors of each chip in time and frequency domain, and the BPSK code is [1,1,-1,1] seen by the phase of the signal in time domain, giving an overall code of [1, 2, -4, 3].

A simple OFC spread spectrum communication system can be implemented using a filter to encode an OFC waveform onto the transmit signal and another filter to decode the waveform followed by a sampler, called a matched filter receiver. In a matched filter receiver, the received signal is fed through a matched filter which has an impulse response that is a time-reversed version of the OFC signal used to encode the desired transmit signal. When the desired receive signal is incident upon the receiver, the dispersion introduced by the transmit encoder is removed and the output of the matched filter is a time-delayed compressed pulse with equal group delay and linear phase over the filter bandwidth. The filter convolves the input with its impulse response and for the matched code, the output is effectively the autocorrelation of the OFC signal delayed in time. The time delay at which the compressed pulse is sometimes called the sampling (or decision) instant, and is equal to the sum of the group delay of the transmit encoding filter and the matched filter plus any system and propagation delays. When a mismatched signal is incident upon the receiver, the dispersion introduced by the transmit encoder is not removed and the receive filter introduces further dispersion. A similar result occurs for interference and jamming signals, resulting in jammer rejection similar to FHSS and DSSS due to the multiple carrier nature of OFC and the BPSK chip encoding.

In order to support multiple users over the same channel, different OFC codes are assigned to each user. If all users within the network are synchronized, OFC codes can be chosen which are fully orthogonal, and there is no MAI. It is often not possible or feasible to maintain synchronization across the entire network, and in this case fully orthogonal codes are not possible. In this case, codes are pseudo-orthogonal and the difference between the correlation peak of matched code pairs and the maximum cross-correlation of mismatched code pairs over all delays determines the worst-case level of rejection for mismatched codes.

The simulated output of an OFC matched filter receiver over time is shown in Figure 2.11 for a matched code and three mismatched codes operating synchronously and simulated independently. With systems using all four codes operating simultaneously, the output of the system using the first code would be the summation of the four signals shown. If the systems are perfectly synchronized and using orthogonal codes as shown, there is no MAI. If systems are asynchronous, the codes will no longer be fully orthogonal and some MAI will occur, the dotted blue line shows the MAI for a single interferer with worst-case asynchronous delay.

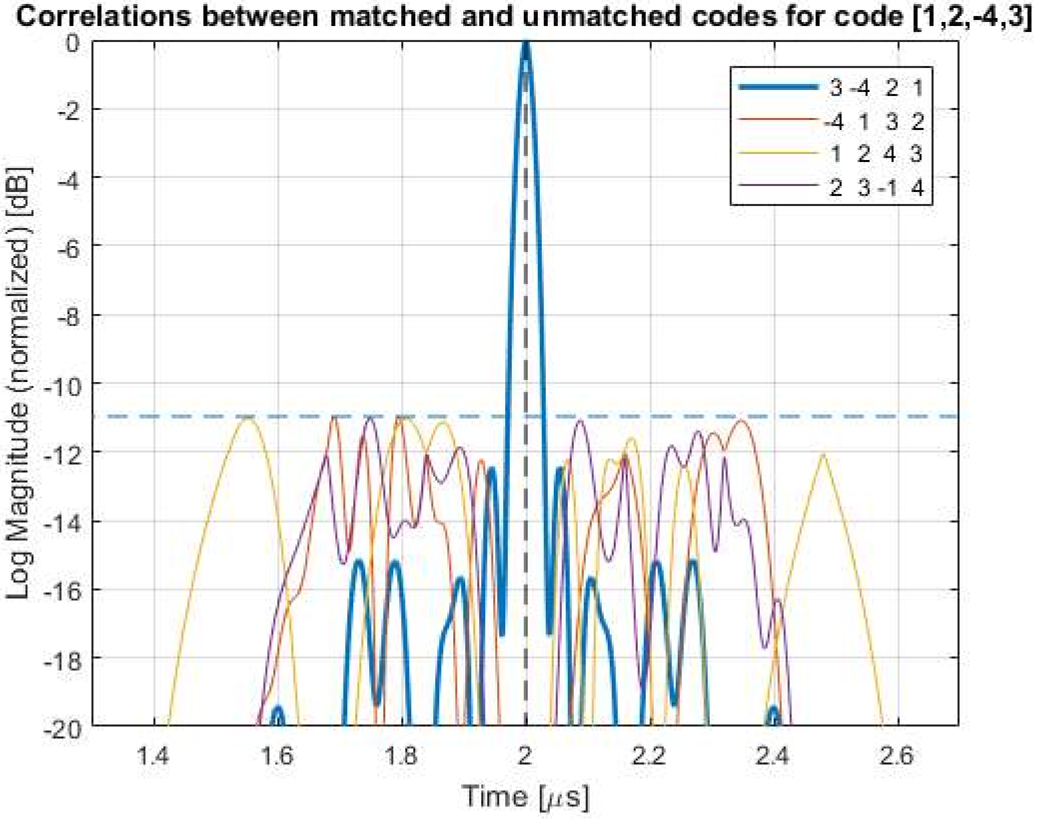

Figure 2.11: Plot showing the output of a matched filter receiver for one matched code (blue, bold) and three mismatched codes. In this example all systems are synchronous, and at the decision instant (2 µs, black dashed) the mismatched orthogonal codes provide no interference to the matched code. In asynchronous systems this is not the case and the interference at the sampling instant can be as high as the peak cross-correlation shown by the dashed line in blue, or higher if interference from multiple mismatched codes combines constructively.

2.3.1 Orthogonal Frequency Coded Surface Acoustic Wave Design

The applications of orthogonal frequency coding to surface acoustic wave (SAW) devices have been known since the early 2000's with the first work being published in 2004 [20]. Since then, a body of work has grown demonstrating OFC SAW sensor systems based on reflective delay line structures for temperature, strain, chemical gas, and magnetic field [21] as well as filters using OFC transducers for ultra-wideband (UWB) spread spectrum communication systems [22]. SAW devices provide a well-known platform for implementing OFC waveforms and are passive, light, small, radiation hard, and can operate from cryogenic to high temperatures [21, 23]. SAW devices are limited in frequency range on the upper end by lithographic limitations and propagation loss and on the lower end by the physical size of the substrate, practical devices can range from low MHz up to several GHz. The remainder of this section will be a brief description of how an OFC waveform can be implemented by a SAW transducer.

A SAW transducer can be designed to produce the desired OFC signal by matching the transducer periodicity to frequency and number of finger pair to the time length on a per-chip basis. A transducer's fundamental center frequency (f_c) and periodicity are related through the SAW substrate velocity by

$$\lambda_c = \frac{v}{f_c}, \tag{2.14}$$

where λ_c is the wavelength of the transducer chip. A transducer's time length and number of finger pair are related through fundamental center frequency by

$$N_p = \tau_c \cdot f_c, \tag{2.15}$$

where N_p is the number of finger pair, which is spatially equivalent to one wavelength at fundamental center frequency. In many cases, N_p for a transducer may be required to be an integer or half-integer number based on the electrode pattern chosen. In an OFC transducer chips are often placed contiguously in time in order to minimize space, though this is not a requirement.

One common embodiment of an OFC filter is the two port configuration shown in Figure 2.12 with a wideband transducer and an OFC transducer separated by some delay. The wideband transducer is designed to cover the OFC spectrum without introducing any unnecessary distortion or loss. The OFC transducer illustrates the different periodicity for different chip frequencies and different number of finger pair to keep a constant time length.

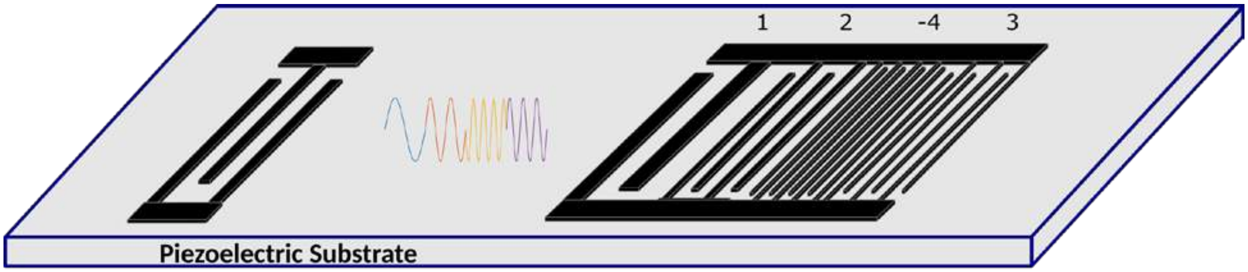

Figure 2.12: A schematic representation of an OFC SAW device comprised of a wideband transducer (left) and an OFC transducer (right) separated by some delay. The OFC waveform generated by this filter would have a code [1,2,-4,3], denoting the order of the frequency hopping pattern and the BPSK code, and the signal produced is shown in the gap between the two transducers.

SAW transducers exhibit harmonic responses in addition to the fundamental response, depending on the electrode pattern. The harmonics present in a uniform transducer with regular electrodes are typically determined using an element factor and an array factor. The simplest element factor is the electrostatic charge density for a single electrode with an infinite array of ground electrodes on either side, called the tap element factor. The array factor is the summation of a number of delta functions corresponding to the hot electrodes in the transducer. The time domain convolution, or frequency domain product, of these factors gives the overall transducer harmonic response. Often these harmonics are considered undesirable and unused for filter applications, but there are some benefits to harmonically operated transducers. The primary advantage is the reduced photolithography requirements due to the larger line widths. For a transducer operating at harmonic M, the electrode widths are M times larger than for a similar transducer at the same frequency operating fundamentally. Harmonic operation allows very high frequency devices to be fabricated using standard processes.

Harmonic OFC design is similar in concept to fundamental OFC design but exact implementation of the desired OFC response may not be possible and approximations may be necessary. The goal in harmonic design is to implement the same waveform as for fundamental design, meaning identical chip frequency, time length, and bandwidth, but using a structure that is operated harmonically. In an OFC design, in order to keep τ_c constant, as f increases N_p also increases. A transducer operating at harmonic M has a time length

$$\tau_c = \frac{MN_p}{f_c}, \tag{2.16}$$

where f_c is the chip frequency at the harmonic of operation, and N_p is the number of finger pair. One finger pair is spatially equivalent to one wavelength at the fundamental frequency, but is spatially equivalent to M wavelengths at the harmonic of operation. For a transducer using fundamental operation, N_p increases by one (equivalent to one additional cycle of the chip frequency) as the chip frequency increases by ${\tau_c}^{-1}$. For a transducer operating harmonically the number of cycles in a chip still needs to increase as the chip frequency increases, but since N_p is now spatially equivalent to M wavelengths, N_p needs to increase by $1/M$ as the chip frequency increases by ${\tau_c}^{-1}$. In many cases it is not possible to increase a N_p by $1/M$ and an approximation must be made. Often the exact N_p is truncated in order to make a realizable transducer design, resulting in a decreased chip length and increased chip bandwidth. The result of this is that the nulls of the chip's frequency response shifts slightly away from the peak of other chip's frequency response and the chips become only pseudo-orthogonal.

OFC designs used in this dissertation show about 1% error in time length due to truncation, as shown with an example design in Chapter 3, and the impact on orthogonality doesn't cause any noticeable effect. Chips with shorter time lengths and higher harmonic operation will be more susceptible to these truncation errors, as the fractional error becomes larger. Similar to the fundamental frequency OFC transducer design, chip frequency and periodicity are related through the SAW substrate velocity and the harmonic of operation by

$$\lambda_c = \frac{v}{f_c/M}, \tag{2.17}$$

where λ_c is the wavelength of the transducer at its fundamental frequency and f_c is the frequency at the harmonic of operation. A further discussion of SAW harmonics is given in the following chapter, with measured responses and design considerations.

Before moving on to the design considerations, some terminology needs to be clarified. The correlator receiver and matched filter receiver are both optimal receivers for the AWGN channel as discussed earlier, and both maximize the signal to noise ratio at the time of sampling. The correlator receiver is implemented by a multiplier followed by an integrator and sampler, and requires that the receiver be synchronized with the transmitter. The matched filter receiver is implemented by a filter with an impulse response that is the time reversal of the waveform to be detected followed by a sampler, and does not require carrier synchronization with the transmitter. While these receivers are distinct, it is common in SAW literature to refer to a filter that performs that matched filter operation as both a correlator and matched filter interchangeably [3, 4], since the operation performed is essentially a cross-correlation of the received waveform with the waveform which the receiver is attempting to detect. In this dissertation the same terminology will be adopted, with correlator and matched filter both referring to a filter performing the matched filter operation.

The remainder of this dissertation will detail the design of OFC SAW correlator filters. SAW correlator filters have been investigated for use in radar and communication systems, and entire chapters in [3] and [4] are dedicated to the subject, and with greater detail in the earlier edition [24]. Some desirable properties of a correlator filter, also called a matched filter, are low insertion loss, programmability, high processing gain, and temperature stability, depending on application. This dissertation focuses on two of these, with low loss design being discussed in Chapter 3, and programmability being discussed in Chapter 4. The fabrication of SAW correlators is briefly discussed, but is not a primary focus of this work. The design of the correlator filter is the primary focus of the work, but system and network level considerations are discussed to give context to the design goals for correlator filters.

CHAPTER 3: LOW LOSS OFC SAW CORRELATOR FILTERS

The previous chapter introduced orthogonal frequency coding (OFC) as a form of spread spectrum communication and discussed the basic method for designing an OFC surface acoustic wave (SAW) filter. A simplistic model for a uniform SAW transducer was used to implement the desired OFC waveform on a per-chip basis with the transducer periodicity (λ), number of finger pair (N_p), and harmonic of operation M, being the primary design parameters. In this chapter, the detailed design of OFC SAW transducers will be discussed and measurements from fabricated devices will be presented with the end result being a set of low loss OFC SAW correlator filters. The chapter is broken into subsections which describe a particular aspect of the overall filter design, all designs considered here are for the inline two-transducer SAW filter embodiment depicted in Figure 2.12. In this dissertation, the transducer on the left is referred to as the wideband transducer and the transducer on the right referred to as the OFC transducer. The design goal for the wideband transducer is to cover the full OFC transducer bandwidth with minimal insertion loss. The design goal for the OFC transducer is to implement the OFC waveform with maximum accuracy and minimal insertion loss. The space between the two transducers is also an important design criteria and will be discussed later in the chapter. A final concern is the substrate material on which the SAW filter is built, and the electrode material. In this dissertation all devices presented use YZ Lithium Niobate ($LiNbO_3$) as the substrate with Aluminum electrodes. YZ Lithium Niobate is chosen for its self-collimating velocity profile, relatively high coupling coefficient, and for the large body of knowledge on the substrate's SAW properties, summarized in Table 3.1. Aluminum is a commonly used electrode material with low resistivity and well-known properties on YZ Lithium Niobate for SAW devices [3].

Table 3.1. Summary of some relevant material properties for YZ Lithium Niobate. The parameter dγ/dθ is used to characterize diffraction in an anisotropic material, and when $d\gamma/d\theta \approx -1$ diffraction spreading is greatly reduced and the material is referred to as a minimal-diffraction orientation [3].

Parameter	***Value or Description***
Material	YZ Lithium Niobate
Orientation (Euler Angles: <λ, μ, θ>)	(0°, -90°, -90°)
Free Surface Velocity (v_f)	3488 m/s
Coupling Coefficient (k^2)	4.8 %
Temperature Coefficient of Delay (TCD)	94 ppm/°C
Derivative of Power Flow Angle ($d\gamma/d\theta$)	-1.08
Relative Effective Dielectric Constant ($\varepsilon_\infty/\varepsilon_0$)	46
Coupling Coefficient (k^2)	4.8%

OFC SAW correlator filters have previously been presented [7, 25] and prototype ultra-wideband (UWB) communication system has been implemented using these devices [22]. The devices presented have a little under 20 dB insertion loss at 250 MHz [7] and around 30 dB insertion loss at 1 GHz [25]. SAW correlators have also focused heavily on devices using various forms of phase shift keying (PSK) [3-5],with results showing an insertion loss of about 14 dB at 2.43 GHz using binary phase shift keying (BPSK) [6]. In this chapter, the design process for achieving low insertion loss is detailed, and a commercially fabricated pair of correlator filters using matched codes is presented with insertion loss as low as 6 dB.

3.1 Transducer Electrode Sampling

The interdigital transducer (IDT) is one of the most fundamental elements of a SAW device and is the structure which serves to convert electrical signals to SAWs and vice versa. An IDT consists of a periodic series of conductive strips called electrodes deposited on a piezoelectric substrate. When an electric potential is applied to a conductive strip the piezoelectric effect creates an elastic stress and displaces the electrode. When this potential is applied periodically to the electrodes in an IDT, an acoustic wave is generated which propagates along the surface of the substrate. This process of generating an acoustic wave from an electric signal is called transduction, and is the primary function of a transducer. In this dissertation, the term transducer always refers to an interdigital transducer, and transducer will be used interchangeably with IDT. This section gives a brief description of transducers and describes how the pattern and polarity of the electrodes within an IDT affect SAW devices with an emphasis on low loss design.

3.1.1 Regular Electrodes

Transducers with regular electrodes, meaning electrodes with constant electrode width (a) and spacing between electrodes (p) are common and detailed analysis is available in the literature [3]. The a/p ratio is an important parameter in analysis and often chosen to be ½ nominally, unless otherwise specified $a/p = ½$ for all transducers with regular electrodes. In addition to the physical geometry, each electrode has a polarity, either positive or negative (sometimes referred to as hot or ground). Two common types of transducers with regular electrodes are shown in Figure 3.1. The single-electrode transducer has two electrodes per wavelength with width $\lambda_0/4$ and spacing $\lambda_0/2$. The double-electrode transducer has four electrodes per wavelength with a nominal width of $\lambda_0/8$ and spacing $\lambda_0/4$. Electrode polarity is determined by which bus bar the electrode is connected to, here we take the upper bus bar to be the hot bus bar and the lower to be ground. This gives electrodes connected to the upper bus bar a polarity of 1, and electrodes connected to the lower bus bar a polarity of 0. Using this definition, the single-electrode transducer electrodes alternate in polarity every electrode (0, 1, 0, 1, …) and double-electrode transducers alternate in polarity every other electrode (0, 0, 1, 1, 0, 0, 1, 1, …). Groups of electrodes that are periodically repeated to create a transducer are often called a finger pair or unit cell. The unit cell is normally spatially equivalent to one wavelength at fundamental center frequency, though this is not required. Transduction is a frequency dependent process in an interdigital transducer, and is strong near the frequency where the wavelength is equal to the spatial length of a finger pair.

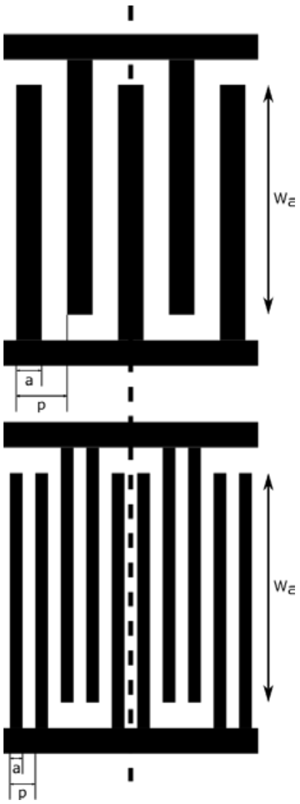

Figure 3.1: Illustration of two common uniform interdigital transducers with regular electrodes, the single-electrode transducer (top) and double-electrode transducer (bottom) with two finger pair each. The horizontal bars at the top and bottom of each transducer are called bus bars and are used to apply voltage to the electrodes. The electrode width (a) and pitch (p) are marked as is the transducer beamwidth (W_a) which will be discussed later in the chapter, and the dashed line denotes the center of both transducers.

The properties of a transducer are largely determined by the placement and polarity of the electrodes, often called the electrode sampling, the number of finger pair (N_p), and the substrate properties. The acoustic conductance for an IDT at fundamental center frequency is

$$G_a(\omega_0) = \omega_0 \varepsilon_\infty^2 N_p^2 W \Gamma_s \tilde{G}_{aM}, \tag{3.1}$$

where ω_0 is the fundamental center frequency, ε_∞^2 is the effective dielectric constant and Γ_s is a modified coupling coefficient determined by the substrate, W is the beamwidth, N_p is the number of finger pair, and $\tilde{G}_{aM}$ is defined by Morgan and depends on the transducer sampling and a/p ratio [3]. The static capacitance of the transducer is

$$C_t = W N_p \varepsilon_\infty \tilde{C}_t, \tag{3.2}$$

where $\tilde{C}_t$ is a normalized capacitance defined by Morgan that again depends on transducer sampling and a/p ratio [3]. Given the conductance and capacitance values above, the electrical Q-factor is the ratio of susceptance to conductance and at center frequency is calculated as

$$Q_t = \tilde{Q}_t / (N_p \varepsilon_\infty \Gamma_s), \tag{3.3}$$

where $\tilde{Q}_t$ is a normalized Q-factor defined by Morgan that again depends on transducer sampling and a/p ratio [3]. The conductance and susceptance terms are frequency dependent, and the overall impedance of the device is comprised of the acoustic conductance, Hilbert transform susceptance, and static capacitance. The acoustic conductance has a frequency dependence that can be approximated as

$$G_a(\omega) \approx G_a(\omega_c) \left[\frac{\sin(X)}{X}\right]^2, \tag{3.4}$$

and the hilbert transform susceptance can be approximated as

$$B_a(\omega) \approx G_a(\omega_c)\left[\frac{\sin(2X)-2X}{2X^2}\right]^2, \tag{3.5}$$

where X is

$$X = \pi N_p \frac{(\omega-\omega_c)}{\omega_c}. \tag{3.6}$$

The full device admittance can be written using these terms as

$$Y_T(\omega) = G_a(\omega) + jB_a(\omega) + j\omega C_t, \tag{3.7}$$

which is also equal to P_{33} in the P maxtrix that will be used briefly in describing unidirectional transducers.

In addition to generating acoustic waves, a process called transduction, electrodes are also capable of reflecting acoustic waves. Reflection occurs due to a change in the acoustic impedance, similar to electromagnetic wave reflections. The presence of the electrodes causes a change in impedance, which can be due to electrical and/or mechanical effects. For a single metal strip, or an electrode, reflections occur at both the beginning and end of the electrode, where the impedance discontinuity occurs. The reflectivity at each interface is typically small, but when multiple reflections combine the effects can become significant. Reflection for a single metal strip is strongest when the width is equal to $\lambda_0/4$, and for multiple $\lambda_0/4$ strips, reflections combine constructively when the spacing (p) is equal to $\lambda_0/2$. At the Bragg frequency, the wavelength is equal to $2p$ and strong reflections occur. For single-electrode transducers the fundamental center frequency of transduction is equal to the Bragg frequency and strong reflections can cause distortions in the electrical response, especially for long transducers or highly reflective electrodes.

For double-electrode transducers, the fundamental center frequency of transduction is equal to half the Bragg frequency where reflections combine destructively, giving fairly weak reflection [3].

Transducers with regular electrodes simplify design and analysis but are all bi-directional, meaning that they launch an acoustic wave in both directions. In a filter with two transducers, bi-directionality means that half of the power launched by a transducer is lost. A similar effect causes half of the power to be lost upon reception by a bi-directional transducer as well, thus in a filter with two bi-directional transducers the minimum achievable insertion loss is 6dB. In addition to the unwanted insertion loss, bi-directional transducers give rise to undesirable multiple-transit signals when connected to finite impedances. Multi-transit effects in bi-directional transducers can be reduced by introducing a mismatch of impedance at the electrical port, but this introduces additional loss [3].

3.1.2 Unidirectional Transducers

It is possible to design a SAW transducer that generates acoustic waves in only one direction, these are referred to as unidirectional transducers (UDTs). Several techniques for designing UDTs have been developed to overcome the issues related to bi-directionality. The primary property of a unidirectional transducer is that it generates waves with unequal amplitudes in the two directions when an electric potential is applied, as depicted in Figure 3.2. The measure of unidirectionality of a UDT is referred to as the directivity and is defined in as the ratio of the forward wave amplitude to the reverse wave amplitude [3]. UDTs can be separated into multi-phase transducers, which require voltages with differing phases to achieve unidirectionality, and single-phase unidirectional transducers (SPUDTs), which achieve unidirectionality without the need for voltages with differing phase. Multi-phase UDTs have some advantage in that wideband devices with high directivity can be achieved and the direction is electrically controllable by changing the phases of the electrical signals. The primary disadvantage of the multi-phase UDT is that at least three bus bars and external phasing networks are required, this problem is compounded for devices using differential acoustic tracks. For these reasons, this dissertation focuses on SPUDTs to achieve low insertion loss.

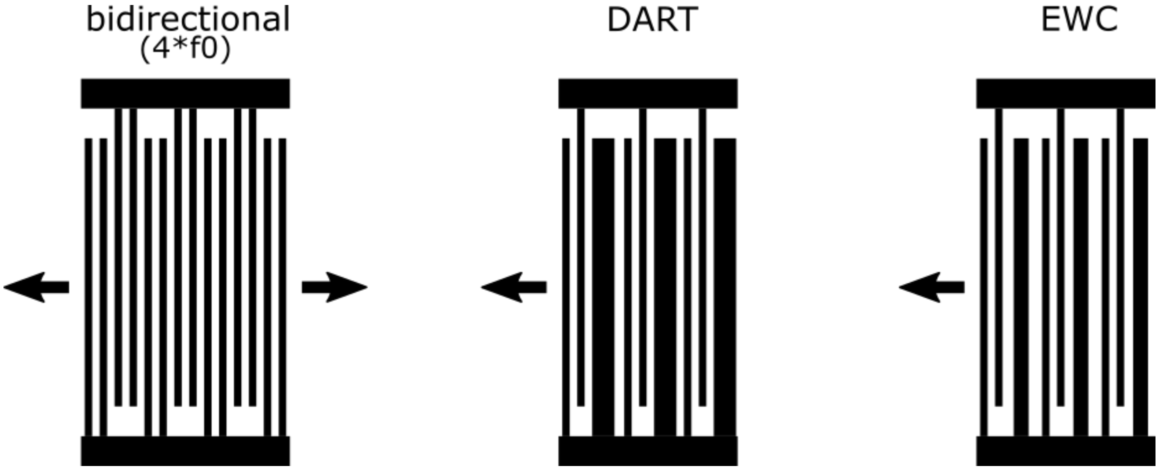

Figure 3.2: Illustration showing a bidirectional double-electrode (4*f0 sampling) transducer and two single-phase unidirectional transducers (SPUDTs), the distributed acoustic reflection transducer (DART) and the electrode width controlled (EWC) SPUDT. The arrows show the direction in which acoustic waves are launched most strongly by each transducer when operated at the device's fundamental center frequency. Each transducer has the equivalent of three unit cells (or finger pairs).

The unidirectional nature of SPUDTs arise due to a distributed internal reflection which is offset in phase from the transduction. The SPUDT is comprised of a number of unit cells, and for the uniform transducers discussed here all unit cells are the same. Typically, a unit cell is one wavelength long at fundamental center frequency, though this is not required. Transduction and reflection processes occur in each unit cell, and can be treated as point sources acting independently [3], which simplifies analysis. The point source from which waves in both directions are generated with the same amplitude and phase is referred to as the transduction center, and can be approximately calculated for an arbitrary SPUDT geometry [26]. Similarly, the reflection center is a point such that the reflection coefficient is the same for waves incident in both directions. If the reflection coefficient at the reflection center is R and the amplitude of the wave generated at the transduction center is T then the total wave at the forward port is proportional to

$$A_1 = T + TRexp(-2jkd), \tag{3.8}$$

where k is the wavenumber and d is the distance between the transduction and reflection centers. At center frequency, the total wave at the forward port is maximized when

$$d = (2n \pm 1/2)\,\lambda_0/4, \tag{3.9}$$

where n is an integer and the sign is determined by the sign of the imaginary reflection coefficient at the reflection center. For the DART and EWC considered here at fundamental frequency, the reflection coefficient is negative imaginary with $n = 1$ and $d = 3\lambda_0/8$ [3]. Choosing a suitable value for d, gives a wave proportional to $T + T|R|$ at the forward port and a wave proportional to $T\sqrt{1-|R|^2}$ at the reverse port. Thus the directivity is the ratio of the total wave amplitude at the forward and reverse ports and is found to be

$$D = \frac{1+|R|}{\sqrt{1-|R|^2}}. \tag{3.10}$$

It is apparent that if the distance between transduction and reflectivity centers is chosen using the above equation, the directivity is determined by the reflection coefficient. For a transducer consisting of multiple unit cells, the directivity is the product of the directivity of all unit cells, which is D^N for N identical unit cells [3]. This shows that strong directivity can be achieved for even weakly reflective structures, though as the number of unit cells increases the device bandwidth decreases. The achievable bandwidth for a given directivity increases as the reflectivity of the structure increases, favoring materials with high coupling coefficients for wideband devices.

The primary goal in SPUDT design is minimizing the reflection coefficient on the forward acoustic port with relatively good impedance matching on the electrical port. Achieving this goal results in a device with low insertion loss and low multi-transit simultaneously, with further reduction in insertion loss due to the elimination of bidirectional loss. This is achieved by the distributed reflection discussed earlier, and for simple analysis, a bidirectional transducer can simply be treated as a SPUDT with no reflection [27]. The reflection coefficient at the forward acoustic port is defined in terms of a mixed matrix called the P-matrix as

$$S_{11} = P_{11} + 2P_{13}^2/(G_L + P_{33}), \tag{3.11}$$

where P_{11} is the reflection coefficient at the forward acoustic port with the electrical port shorted, P_{13} is the acoustic wave amplitude due to an applied potential at the electric port, G_L is the electrical load conductance connected to the SPUDT, and P_{33} is the electrical port admittance of the SPUDT [27]. In this definition, port 1 is the forward acoustic port, port 2 is the reverse acoustic port, and port 3 is the electric port and more details on the P-matrix can be found in [3]. This equation can be broken into two parts, a mechanical reflection term (P_{33}) and an electrical regeneration term ($2P_{13}^2/(G_L + P_{33})$). To achieve a matched forward acoustic port these terms must cancel. For a transducer with no reflectivity, $P_{11} = 0$ and no finite G_L can match the acoustic port. For any value of $P_{11} > 0$, it becomes possible to match the acoustic port for some load impedance, and as reflectivity increases, G_L approaches the condition for a matched load. For an unweighted SPUDT device with optimum matching, meaning the acoustic port is matched, the insertion loss is related to the product of the reflectivity per unit cell and the effective number of cells in the transducer, giving a saw transducer response of

$$|S_{13}|^2 \cong 1 - e^{-2KL_{eff}}, \tag{3.12}$$

where K is the reflectivity per unit cell and L_{eff} is the effective number of unit cells [27]. S_{13} is a scattering parameter from the electrical to forward acoustic port, and is directly related to the filter response. This result shows that as the total reflectivity of the transducer increases, the transmission magnitude approaches unity and the loss approaches zero. This can be achieved by increasing the length of the transducer, but this reduces the transducer bandwidth. The achievable bandwidth for a given directivity increases as the reflectivity of the structure increases, which favors materials with high coupling coefficients for wideband devices. The equation above applies for a matched acoustic port, however, lower insertion loss can often be achieved if increased multi-transit effects can be tolerated. Alternatively, when matching for minimum insertion loss, the multi-transit effects become less significant as the total reflectivity of the transducer increases. In an effort to reduce insertion loss, modified SPUDT cells have also been investigated by varying the electrode widths and position. Results presented in [28] demonstrated nearly double the reflectivity found for a standard electrode width controlled (EWC) SPUDT, but require a critical dimension of $\lambda/16$, reducing the maximum operating to around half of what can be achieved for the standard EWC. It is not currently feasible to produce the 950 MHz devices using this enhanced SPUDT cell with standard processing techniques.

The two types of SPUDTs considered here are depicted in Figure 3.2, the distributed acoustic reflection transducer (DART) and the EWC SPUDT mentioned earlier, along with a double-electrode bidirectional transducer. The DART unit cell consists of two $\lambda/8$ electrodes and one $3\lambda/8$ electrode, with polarity (0, 1, 0, 0, 1, 0, …). The EWC unit cell is nearly identical, except that the width of the thick electrode is reduced from $3\lambda/8$ to $\lambda/4$. The DART unit cell has a distance between transduction and reflection centers of almost exactly $3\lambda/8$, which is ideal, however, the reflectivity of the structure is not maximized. The EWC unit cell increases reflectivity by reducing the thick electrode to $\lambda/4$, however, this introduces a small error in the ideal separation between the transduction and reflection center of about 9° on YZ Lithium Niobate [28]. The unit cell described is usually spatially equivalent to one wavelength at fundamental center frequency, and is roughly equivalent the what was called a finger pair for transducers with regular electrodes. A chapter is dedicated to unidirectional transducer design in [3] with a focus on the DART, and a comprehensive discussion of SPUDT filter design using the EWC SPUDT is found in [27].

Measured results for a pair of forward facing and reverse facing DART and EWC transducers consisting of 36 cells are shown in Figure 3.3, this is the wideband transducer design for the 4-chip OFC transducers designed in this dissertation. The center frequency is 950 MHz with a half-power bandwidth of 25 MHz. These measurements show that the EWC has lower insertion loss and higher directivity, and is the better SPUDT for the wideband transducer design used here. Since the response measured is for a pair of identical forward facing SPUDT transducers, the loss of a single wideband EWC transducer can be calculated to be about 1.5 dB if propagation loss is small, which it should be in this case.

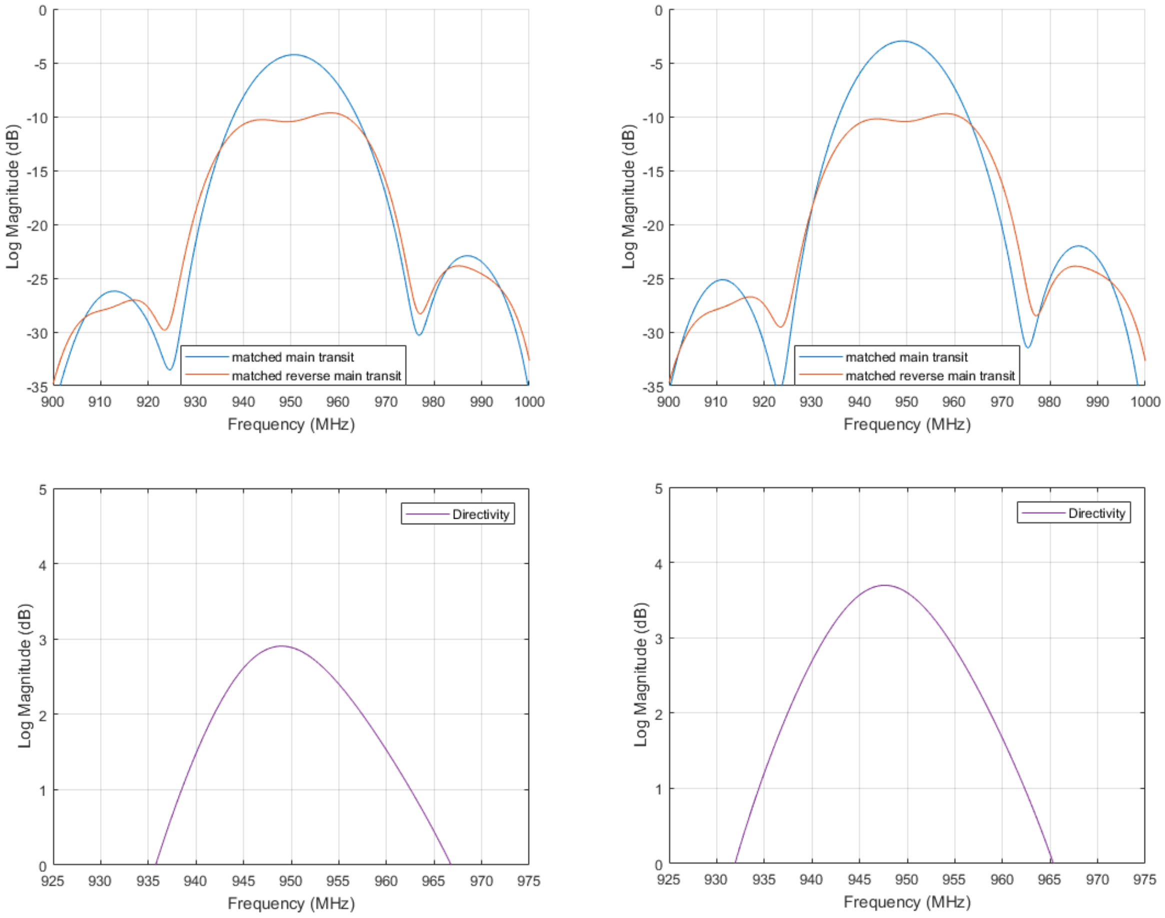

Figure 3.3: Measured log-magnitude S_{21} frequency responses after ideal electrical matching for minimum insertion loss for fabricated DART (left) and EWC (right) SPUDT filters with the main transit gated to remove multi-transit ripple. The blue curves are the frequency response when the two transducers have their forward directions facing one another giving low loss, the orange curves are the frequency response when the two transducers have their forward directions facing away from one another giving higher loss. The purple curves are the directivity of each transducer. Directivity is calculated knowing that the two transducers are identical, so the directivity of each transducer is equal to half the ratio of the forward to reverse response ($D=1/2 \cdot H_{forward}/H_{reverse}$). All devices use the same design other than electrode pattern with 36 cells to allow straightforward comparison. The EWC has lowest loss and highest directivity with a minimum matched insertion loss of 3 dB and peak directivity of 3.7 dB for each transducer giving a 7.4 dB forward-reverse ratio for the full filter. The DART has a minimum matched insertion loss of 4.3 dB and peak directivity of 2.9 dB for each transducer. For this particular design, the EWC is preferable.

In the SAW correlator schematic shown in Figure 2.12, the wideband transducer has one finger pair and the OFC transducer chips have between one and four finger pair. In actual devices, the number of finger pair required is the inverse of the fractional bandwidth of the OFC chip. It is typical to have approximately N_c times more finger pair in the transducers making up the OFC chips than in the wideband transducer, as the wideband transducer must cover the entire OFC bandwidth. The design concerns for the wideband transducer are quite different than those for narrowband OFC chip transducers, and the two are designed somewhat independently. In many cases the bandwidth of the device is constrained by the overall communication system, as is the case for the devices presented in this dissertation and therefore no attempt is made to optimize the device bandwidth for minimum loss. The device presented is a 4-chip OFC correlator with a center frequency of 950 MHz and a bandwidth of 25 MHz. Assuming uniform transducers, this gives a transducer length of roughly 36 cells for the wideband transducer and 150-153 cells for the chip transducers for a transducer operating at the fundamental center frequency.

3.1.3 Harmonic Operation

In addition to the fundamental response, transducers generally exhibit responses at some integer multiples of their fundamental frequency, referred to as harmonics. The harmonics a transducer can generate are determined by the Fourier transform of the electrostatic charge density which is a function of the electrode geometry and polarities of the electrodes. The harmonics for common types of uniform transducers with regular electrodes are well known, and harmonics up to the 3rd order for select transducers are listed below. Though many higher harmonics exist, higher harmonics become increasingly sensitive to a/p ratio tolerances and are not often used. Single electrode transducers don't exhibit either 2nd or 3rd harmonic when $a/p = 1/2$, though the 3rd harmonic appears as a/p increases or decreases from $1/2$. Double electrode transducers exhibit 3rd harmonic responses. While DARTs and EWCs do not have regular electrodes, their transduction can be approximately modelled excluding reflection with a series of λ/8 electrodes with λ/4 spacing with polarities (0 1 0 0). This gives harmonic responses at both the second and third harmonic [3].

Harmonic responses occur at integer multiples of the fundamental frequency and have the same absolute bandwidth regardless of harmonic number. This can be understood by the fact that the physical embodiment of the device is fixed and unchanged by the harmonic of operation. Transducer time response is determined by the physical length of the transducer and the velocity of the substrate, and since bandwidth is the inverse of the transducer time response, the bandwidth remains the same. This means that as the harmonic of operation increases, the fractional bandwidth decreases, and thus devices operating at harmonics will be limited in terms of the achievable bandwidth.

Measurements from a fabricated filter using DARTs in Figure 3.4 show that the first and third harmonic have directivity with opposite forward direction, while the second harmonic doesn't show strong directivity and is somewhat distorted. Measurements from a fabricated filter using EWCs in Figure 3.4 show that the first, second, and third harmonics have directivity with the same forward direction though the second harmonic again shows a somewhat distorted response. The measurements show that for the design used, the EWC gives better performance at fundamental frequency in terms of both insertion loss and directivity. For third harmonic operation, both EWC and DART show good directivity but insertion loss is lower for the DART, making it the better choice. The second harmonic gives a distorted response and does not appear to be useful for the design tested.

Harmonic operation relaxes the critical dimension requirement for device fabrication, but often requires approximations be made in design, as discussed in Chapter 2. For harmonic M, the unit cell of a transducer is typically M wavelengths long and therefore only time lengths that are a multiple of M are realizable. For orthogonal frequency coded (OFC) waveforms, the number of cycles in a chip increases by one as the chip frequency increases, in order to maintain a constant time length and satisfy the orthogonality constraints described in [20]. Transducers operating at fundamental frequency can achieve this, however for harmonic $M > 1$, this is not typically possible. In order to approximate the response, chips must be truncated so that they do not overlap spatially with neighboring chips. An example design for a 4-chip transducer operating at a 3rd harmonic of 950 MHz with a bandwidth of 25 MHz is given in Table 2. The example gives the ideal and approximated actual design, as well as the fractional error in chip time length.

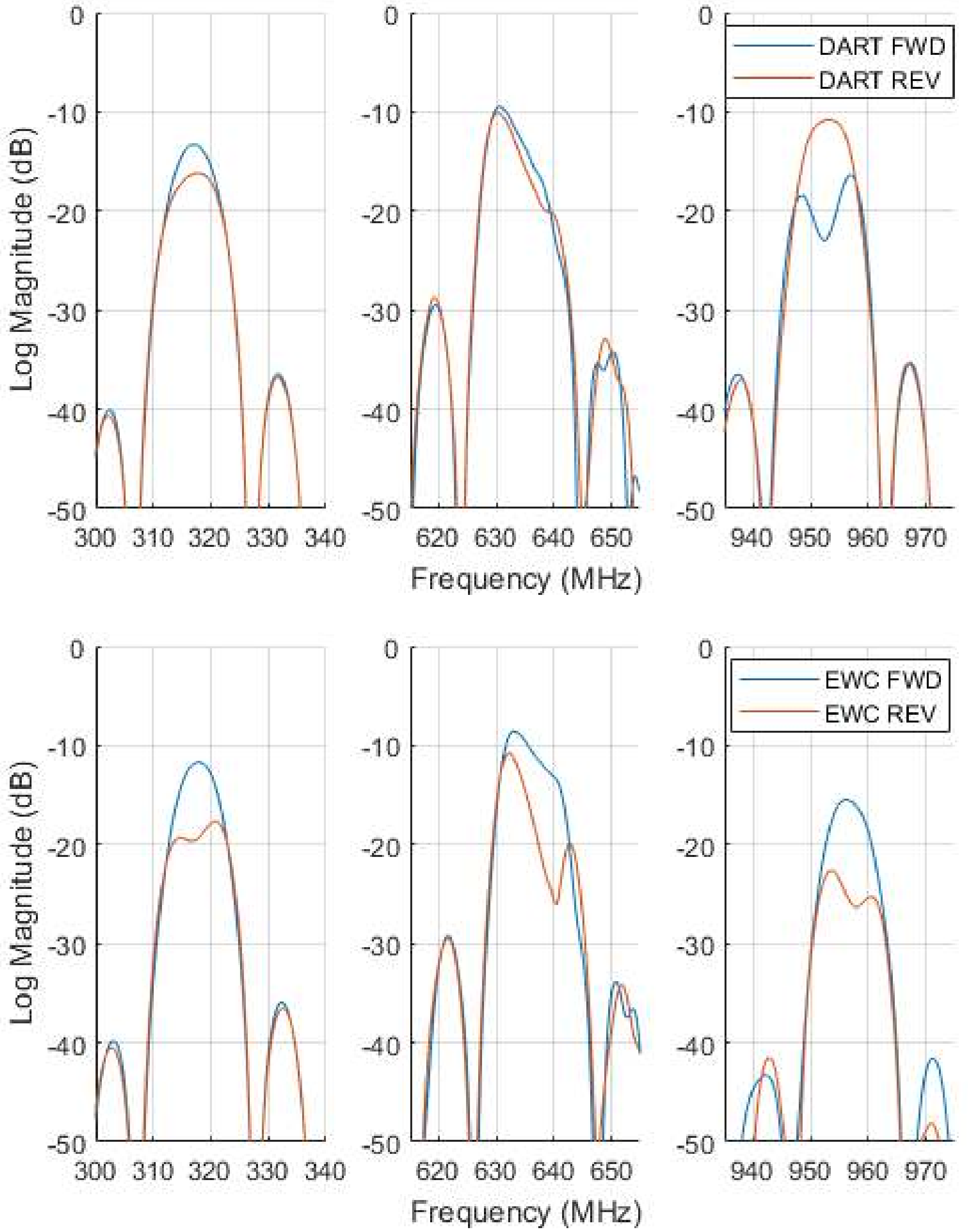

Figure 3.4: Measured log-magnitude S_{21} frequency responses with no electrical matching for fabricated DART (top) and EWC (bottom) SPUDT filters with 31 cells each. Fundamental (left), second harmonic (middle) and third harmonic (right) responses are shown. The blue curves are for transducers with forward directions facing one another and the orange curves for reverse directions facing one another. For the DART, the forward directions are aligned at fundamental, second harmonic shows little directivity, and at the third harmonic the directions have flipped with increased directivity reduced insertion loss. For the EWC, the forward direction is consistent among the first three harmonics, though the second harmonic shows a somewhat distorted response, and the 3rd harmonic shows an increase in directivity but also increased insertion loss.

Table 2. Summary of important design criteria for a 4-chip OFC transducer operating at a 3rd harmonic of 950 MHz with 25 MHz bandwidth for the ideal design and a truncated approximation for SAW implementation. The fractional error is calculated as (1 – $\tau_{c\_actual}/\tau_{c\_ideal}$).

Parameter [units]	***Ideal Design***	***Actual Design***
Device Code (PN-OFC)	[1,2,-4,3]	[1,2,-4,3]
Chip Frequency (f_c) [MHz]	[940.625, 946.875, 959.375, 953.125]	[940.625, 946.875, 959.375, 953.125]
Number of Finger Pair (N_p)	[50.167, 50.500, 51.167, 50.833]	[50, 50, 51, 50]
Time Length (τ_c) [ns]	[160, 160, 160, 160]	[159.468, 158.416, 159.479, 157.377]
Bandwidth (BW_c) [MHz]	[6.25 6.25 6.25 6.25]	[6.271, 6.312, 6.270, 6.354]
Fractional Error [%]	–	[0.332, 0.990, 0.326, 1.639]

The properties of harmonically operated transducers can be calculated in a way similar to what was shown earlier for fundamentally operating transducers. In this dissertation, harmonic transducers are used to approximate the same OFC design as fundamental devices, thus the time length, bandwidth, and center frequency are all pre-determined and will be the same without regard to harmonic operation. Harmonically operated transducers have $1/M$ finger pair when compared to a fundamentally operating transducer at the same center frequency with the same time length and bandwidth, since there are M cycles per wavelength. This reduced number of finger pair affects the transducer impedance and performance. The acoustic conductance for an IDT at harmonic center frequency shown earlier can be generalized to account for the harmonic of operation as

$$G_a(M\omega_0) = M\omega_0 \varepsilon_\infty^2 N_p^2 W \Gamma_s \tilde{G}_{aM}, \qquad (3.13)$$

where M is the harmonic of operation, ω_0 is the fundamental center frequency [3]. For a harmonic of 1, the equation reduces to what was shown earlier for a fundamental transducer. The capacitance is unaffected by harmonic of operation and remains

$$C_t = W N_p \varepsilon_\infty \tilde{C}_t, \tag{3.14}$$

though the susceptance ($j\omega C_t$) does increase by a factor of M due to the increase in frequency with harmonic. Given the conductance and capacitance values above, the electrical Q-factor remains the same regardless of harmonic

$$Q_t = \tilde{Q}_t / (N_p \varepsilon_\infty \Gamma_s). \tag{3.15}$$

In this dissertation, both fundamental and harmonically operating transducers are used to implement the same OFC design. The OFC design determines the time length, bandwidth, and center frequency for each transducer at the harmonic of operation. For a given OFC design with a chosen center frequency, time length, and bandwidth; if only the harmonic M of operation is varied, the number of finger pair must be $N_p' = N_p/M$ to keep the same bandwidth. The conductance is proportional to ${N_p'}^2$, giving the harmonically operated transducer lower conductance than that of a fundamentally operated transducer by a factor of M^2. The capacitance is lower by a factor of M due to the decreased number of finger pair, giving an electrical Q-factor equal to that is a factor of M greater than that of a fundamentally operated transducer.

For SPUDT transducers with a fixed substrate and design, each unit cell will have a certain reflectivity per unit cell. To keep a fixed time length, the harmonically operated transducer again has $N_p' = N_p/M$ finger pair, giving a factor of M less unit cells and therefore a factor of M less total reflectivity for the transducer overall. In addition, the properties of the unit cell in terms of transduction and reflection may change for different harmonics. In the DART transducer response shown in Figure 3.4 the number of finger pair is constant for all harmonics, however, the directivity changes substantially with harmonic which indicates that the unit cell properties vary with harmonic. The EWC shows significant variation in the second harmonic and slight changes between fundamental and 3rd harmonic.

3.1.4 Fabrication

In this dissertation, much of the preliminary work was done with double electrode, DART, and EWC transducers operating at the 3rd harmonic. All of these transducers require a minimum line width and gap of $\lambda/8$ when operating at the fundamental, or $M\lambda/8$ for a transducer operating at harmonic M. The mask fabrication equipment available at the University of Central Florida (UCF) for this work includes a pattern generator (PG) and an image repeater (IR). The PG is capable of writing rectangular features with a critical dimension of about $1.27\ \mu m$, the IR critical dimension is less well defined but is around $0.8\ \mu m$. The PG is direct write and can fill an entire wafer with unique devices whereas the IR is a step and repeat process using a 10x reduction lens, which can fill a wafer with stepped and repeated 0.4 inch squares of unique devices. For preliminary development it is very beneficial to have many unique devices on a wafer, thus the PG is used whenever possible. Wafer processing equipment is limited to 3 inch wafers with 4 inch masks and is capable of processing critical dimension (CD) as low as approximately $0.5\ \mu m$ under optimal conditions. Practical and reproducible CD in this case is mostly limited by the mask processing equipment and is around $0.8\ \mu m$.

For an operational frequency of 950 MHz with 25 MHz bandwidth using YZ Lithium Niobate, the line width required is about $0.44\ \mu m$ for fundamental operation, or $1.33\ \mu m$ for 3rd harmonic operation. Based on the above process limitations, the center frequency of 950 MHz was chosen in order to allow devices operating at 3rd harmonic to be fabricated using the PG at UCF, allowing rapid prototyping and a large number of designs to be tested. While harmonic operation is beneficial in extending the maximum device frequency for a given material and process, fundamental operation gives maximum flexibility in design and is generally preferable.

Devices operating at a fundamental frequency of 950 MHz on YZ Lithium Niobate can't be readily fabricated at UCF using the facilities described above, however, they can be fabricated reproducibly at some commercial facilities. All devices operating at fundamental frequency were fabricated commercially at Qorvo. Commercial fabrication offers a number of advantages over UCF's capabilities, however, the cost and fabrication time are significantly increased. While the majority of the results that will be presented are from commercially fabricated devices, much of the preliminary work was done using 3rd harmonic devices fabricated at UCF.

3.1.5 Weighting

The transducers considered in this dissertation are primarily uniform, however, it is possible to modify the transducer response by weighting. A uniform transducer gives a time response with a rectangular envelope and a frequency response that is a sinc function. A wide range of frequency responses can be obtained by weighting the transducer such that its time response looks like a sampled version of the Fourier transform of the desired frequency response. A common example is to obtain an approximately rectangular frequency response by weighting the transducer with a truncated sinc function. There are several ways to implement a weighted response, apodization is common but suffers from diffraction errors [3]. Withdrawal weighting is a common method of weighting that is well suited to narrowband transducers, such as the OFC chips considered here.

Withdrawal weighting is performed by selectively removing sources from the transducer. Acoustic sources exist where electrodes of different polarity overlap, so by altering the polarity of an electrode such that it is the same as one next to it, a source is removed. By carefully selecting the sources that are removed, a weighted passband can be obtained. In this dissertation, a form of withdrawal weighting that gives an approximately uniform response is used to reduce the effective number of finger pair in an OFC chip. The reduced effective number of finger pair helps to reduce the conductance and capacitance, which can be useful in low loss design.

For a 4-chip OFC transducer at 950 MHz with a 25 MHz bandwidth, each chip has a half-power bandwidth of 6.25 MHz. This gives a fractional bandwidth of less than 0.7% for each chips, corresponding to about 150 finger pair per chip for a uniform transducer operating at fundamental frequency. 150 finger pair is significantly higher than a typical transducer on a high coupling substrate like YZ Lithium Niobate would use, and withdrawal weighting withdrawal weighting is used to reduce the number of active finger pair. Withdrawal weighting terminology used here is WWJ:K, where WW stands for withdrawal weighted and the ratio J:K is the ratio of the effective number of finger pair to the original number of finger pair. For example, WW1:3 would mean that one of every three finger pair is left intact and the other two are grounded. If the fingers are withdrawn in a manner that leaves the transducer approximately uniform over a given section then the response produced will be approximately uniform, but with reduced conductance and capacitance due to the reduced number of active finger pair, $N_{p_{effective}} = N_p J/K$. For an IDT with $N_{p_{effective}}$ finger pair, the acoustic conductance is proportional to the number of finger pair squared, $G_a \propto {N_{p_{effective}}}^2$, and the transducer capacitance is proportional to the number of finger pair, $C_t \propto N_{p_{effective}}$. This gives an electrical Q factor inversely proportional to the number of finger pair, $Q_t \propto 1/N_{p_{effective}}$, which has a bearing on the bandwidth obtainable when electrically matching for minimum loss [3]. If fingers are withdrawn periodically, the transducer can be viewed as being undersampled, and subharmonic alias responses occur. This effect is similar to the one that occurs when operating a transducer harmonically. Another practical effect is the voltage divider formed by the transducer impedance and the parasitic resistance, as discussed later in the chapter. For a fixed parasitic resistance, the parasitic loss will be greater for devices with higher conductance, which favors a reduced number of finger pair. Devices here are withdrawn in a uniform manner that gives a uniform response, unless otherwise stated.

3.2 Reduced Propagation Loss

Surface acoustic wave propagation is affected by propagation loss, diffraction, and waveguide effects. Propagation loss is dependent on the substrate material, orientation, surface condition, and frequency of operation. Propagation loss mechanisms are discussed in [3] and some aspects of interest will be summarized here. Propagation loss on YZ lithium Niobate for a free surface condition at room temperature is found to be

$$\alpha = 0.19f + 0.88f^2 \text{ dB/µs}, \tag{3.16}$$

where f is the frequency in GHz [3].

The most straightforward way to reduce propagation loss is by reducing the propagation distance. The delay described here is the center-to-center delay, which gives the location of the compressed pulse after matched filtering. In an OFC correlator filter, the minimum delay is slightly greater than half the OFC time length due to the width of the wideband transducer. Early in this development, several correlator filters were designed and fabricated with the same design except for delay. The measured time and frequency responses shown in Figure 3.5 indicate that propagation delay has a more significant effect than was expected. These devices use a free surface propagation path and should experience a 0.15 dB reduction in delay when reducing from 0.5µs to 0.35 µs delay, however, a change of 1.3 dB is measured. This suggests that propagation loss is likely not the only factor contributing to the loss, and waveguide or diffraction effects may be present. Diffraction is minimized by using YZ Lithium Niobate, which is a minimal diffraction orientation [3]. Modelling diffraction and waveguide effects requires accurate knowledge of the propagating structure and material properties, and will not be considered here, but these issues will be discussed again later in this chapter with some empirical optimization.

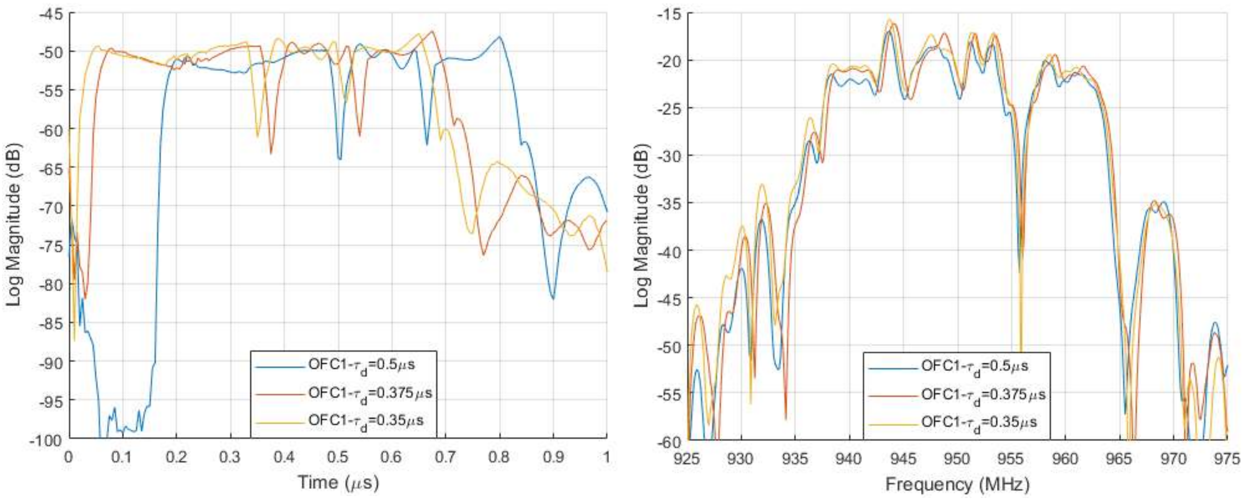

Figure 3.5: Measured log-magnitude S_{21} time (left) and frequency (right) domain response of correlators with free surface propagation paths and center-to-center delay varied from 0.5 µs to 0.35µs. Insertion loss was reduced from 17 dB at 0.5 µs to 15.7 dB at 0.35 µs, a change of 1.3 dB – much more than the expected 0.15 dB reduction.

The above free surface propagation loss is increased with the presence of metal films, and is found to be

$$\alpha = Kf^2 \text{ dB/}\mu\text{s}, \tag{3.17}$$

with $K = 3.0$ for a 500 Å continuous aluminum film and $K = 5.2$ for 2000 Å [3]. The trend shows that thicker aluminum films contribute to higher propagation loss, thus it is desirable to keep metal films thin. At 950 MHz operation, these equations predict about 1 dB/μs propagation loss for free surface and a little over 3 dB/μs for a 650 Å continuous aluminum film. Metal film resistance increases as the films become thinner and the reflectivity of a SPUDT transducer is also modified. There should be an optimum metal thickness, though empirical optimization would require a separate fabrication run for every thickness and becomes a time and material consuming process. At this time metal thickness has not been optimized, though films from 650 Å to 800 Å were tested, with 650 Å showing good results.

3.3 Differential Embodiment

The previous section discussed advantages of reducing the delay of correlator filters in order to reduce insertion loss, however, this can create problems. In a SAW filter an electrical signal in transduced and transmitted acoustically from one electrical port to the other, however, some amount of the signal bypasses the acoustic device and couples capacitively from one port to the other. This effect is called electromagnetic feedthrough, or RF feedthrough, and has the effect of creating ripples that distort the device passband and reduce out-of-band rejection. By designing a SAW transducer with two acoustic tracks, the device can be operated differentially and common mode electromagnetic feedthrough can be suppressed.

This is called the dual-track differential embodiment, or sometimes a balanced-unbalanced configuration and is illustrated in Figure 3.6. The device consists of four transducers making up two tracks, the left two transducers are connected electrically in parallel and the right two transducers are combined in series through a balun. The two acoustic signal paths through the two tracks have a phase shift of 180 degrees, and when combined through a balun the two signals add constructively. The electromagnetic feedthrough signal can be viewed as radiating from the + bus bar of the transducer on the left and being received by the + and – bus bars of the transducer on the right. Since the transducer is nearly symmetric about this point, about the same amount of energy will be received by both bus bars and will approximately cancel when combined at the balun. The two transducers on the left are collectively a single-ended parallel track transducer and the right two transducers are a dual-track differential transducer, and the filter itself can be used as a balun. The amount which the common mode signal is suppressed below the differential signal is referred to as the common mode rejection ratio (CMRR) and is a commonly used metric to compare differential systems. A fabricated device is measured with no electrical matching for both differential and common mode signals and the results are shown in Figure 3.7 giving an average CMRR of 33 dB.

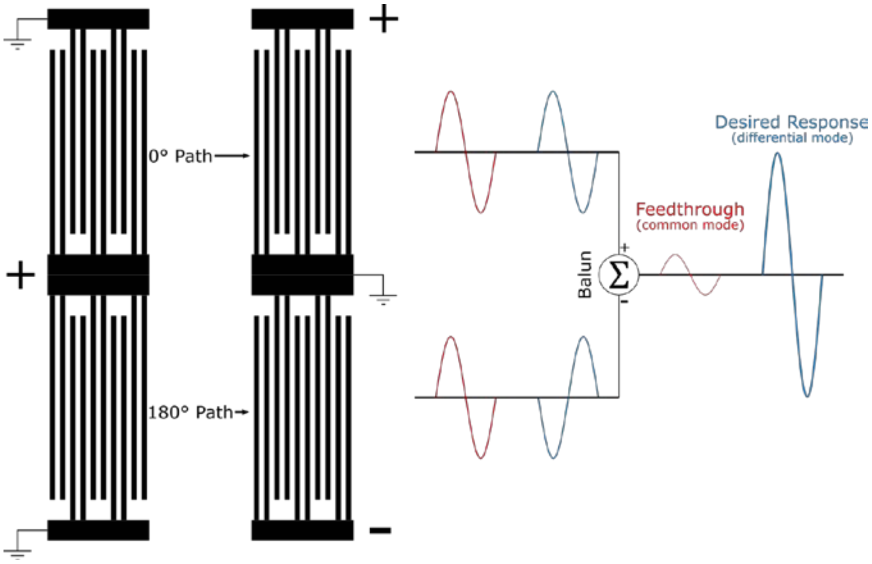

Figure 3.6: Schematic representation of dual-track differential, or balanced-unbalanced, transducer embodiment. The upper and lower tracks have a 180° phase difference for the acoustic signal path, and when combined through a balun the tracks combine constructively as a differential-mode signal. The electromagnetic feedthrough signal can be viewed as radiating from the left transducer at the bus bar marked with a +, the other transducer is symmetric about this point except for a slight difference in the electrode connections. Due to the approximate symmetry, about the same amount of electromagnetic feedthrough is received at the differential + and – bus bars which will approximately cancel at the balun as a common-mode signal.

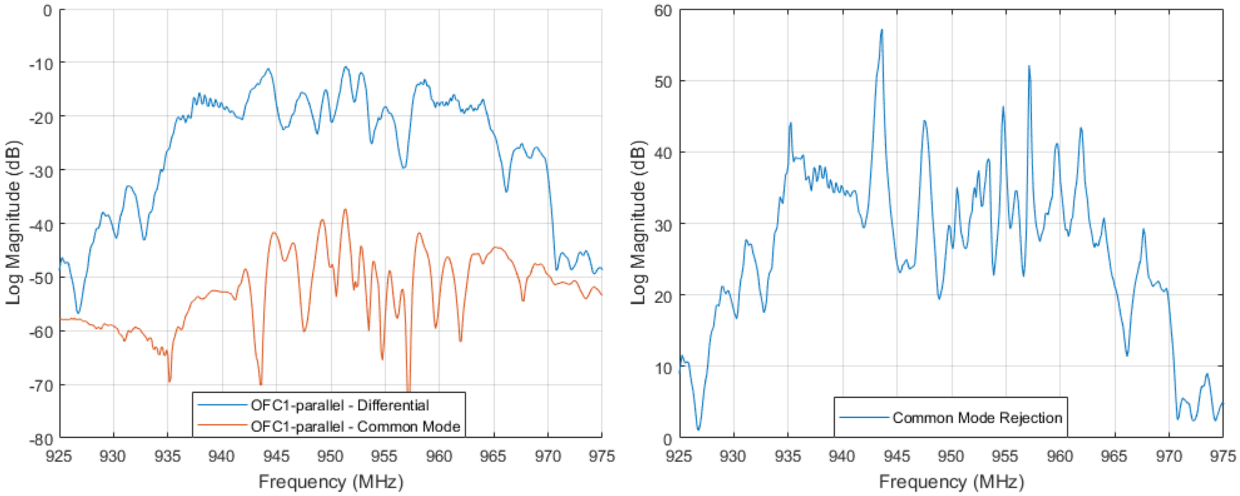

Figure 3.7: Measured log magnitude S21 frequency domain response for a differential and common mode signal (left) and calculated common mode rejection ratio (right) with no electrical matching. The common mode signal is significantly reduced within the OFC passband and the common mode rejection ration ranges from about 20-60 dB with a 33 dB average for the device measured.

3.4 Reduced Parasitic Resistance

Electrodes and bus bars are made by depositing thin metal films on YZ Lithium Niobate. The film thickness and material can significantly affect the performance of the SAW device. Aluminum is a common electrode material and is the only electrode metal considered here, and film thickness is considered in design but not optimized. As the thickness of the electrode metal decreases, propagation loss decreases, but the resistivity of the film increases. This resistivity can have a complicated effect, as it causes the voltage to vary across the beamwidth, but if losses are small it can be modelled as a parasitic series resistance [3] as shown schematically at the top of Figure 3.8. In addition to the electrodes, bus bars also contribute a parasitic series resistance. Neglecting other parasitic elements for simplicity, the effect of parasitic resistance can be modelled by a simple voltage divider between the transducer impedance and parasitic impedance as shown in Figure 3.8. The voltage across the IDT is $V_{IDT} = Z_{IDT}/(Z_{IDT} + R_p)$ and the loss due to the parasitic resistance is V_{IDT}/V_{in}. This simple model shows that resistive loss can be reduced by reducing the parasitic resistance, or increasing the transducer impedance (or both). The approach for reducing the parasitic resistance is described below, while the approach for increasing transducer impedance is described in the next section.

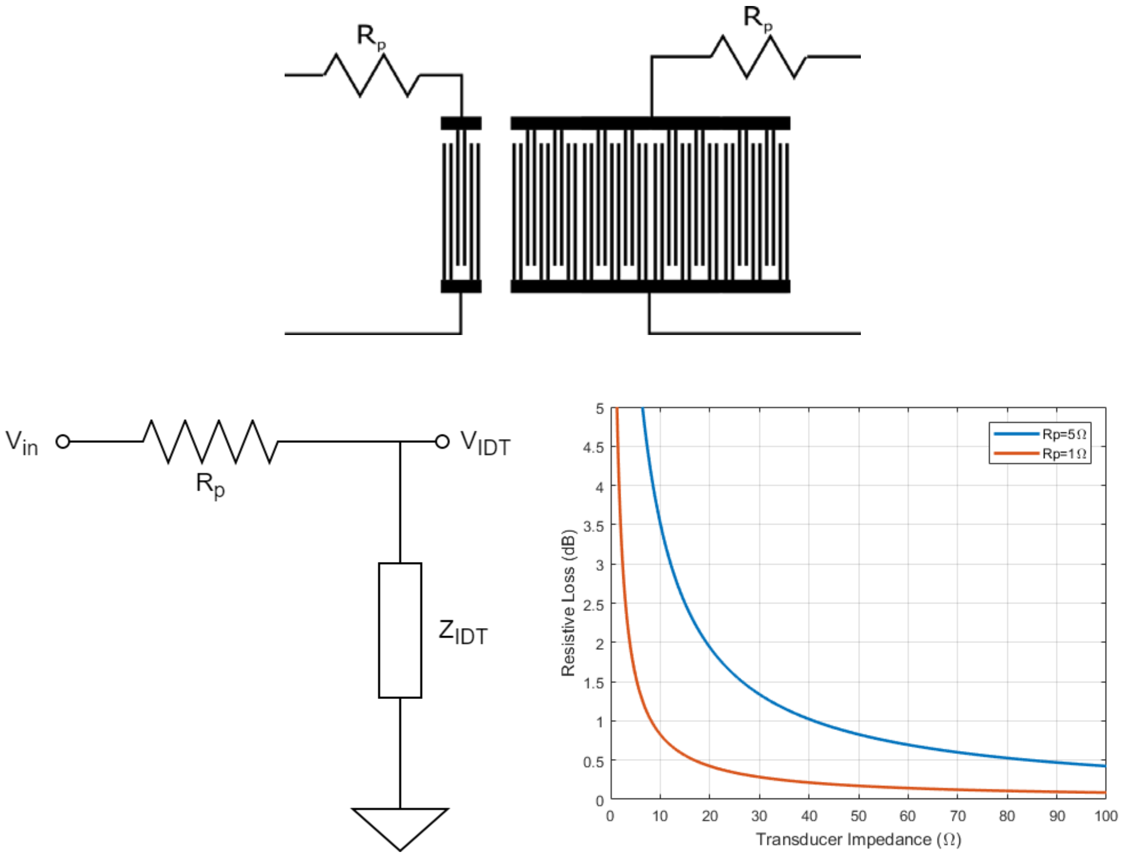

Figure 3.8: Schematic resistance showing series parasitic resistance model (top) and equivalent circuit used to calculate resistive loss (bottom left). Resistive loss is calculated using this simple model as the real part of the transducer impedance is varied from about 1 to 100 ohms for parasitic resistances of 1 and 5 ohms. This simple model shows that resistive loss can be reduced by reducing the parasitic resistance or by increasing the transducer impedance (or both).

In order to keep acoustic propagation loss low, thin 650 Å aluminum electrodes are used, but outside the path thick gold films are deposited over the aluminum bus bar to reduce the parasitic resistance. Adding a gold overlay of about 7500 Å was found to significantly decrease insertion loss after electrical matching. As expected from the plot in Figure 3.8, the reduction in loss is greater devices with lower transducer impedance. Transducer conductance is proportional to the number of finger pair squared and the harmonic of operation ($G_a \propto {N_p}^2$), and for the same time length, a harmonically operating transducer will have N_p/M finger pair. The end result of this is that devices operating fundamentally have greater conductance by a factor of M^2 for the same time length, and therefore much lower impedance. Measured results on identical devices with and without the gold overlay gave an improvement in matched insertion loss of about 4.2 dB for fundamental devices and 2.1 dB on average for devices operating at 3rd harmonic. Additionally, the thick gold films allow more reliable bond wire connections for device packaging. This is a significant improvement in performance with a minor increase in fabrication complexity.

3.5 Empirically Optimized Beamwidth

The beamwidth (W_a), or aperture, of the transducer is an important design parameter in OFC SAW correlator filter. Beamwidth is typically defined as the overlap between the positive and negative electrodes, the acoustically active area, as shown schematically in Figure 3.9. The beamwidth has important effects on both electrical and acoustic performance and both will be briefly described. Upper and lower bounds will be described qualitatively, but ultimately the beamwidth is optimized empirically.

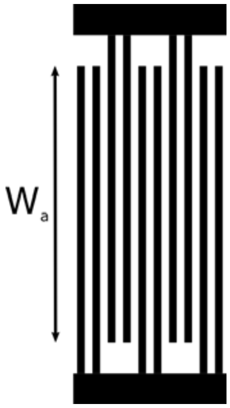

Figure 3.9: Illustration showing the beamwidth for a transducer as defined by the overlap between positive and negative electrodes. A double-electrode transducer is shown but this definition is the same for all electrode patterns discussed in this dissertation.

Acoustically, the beamwidth can have a complicated effect in that it affects both diffraction and waveguide properties. Both diffraction and beamwidth are in general complex to analyze on anisotropic substrates such as YZ Lithium Niobate, but simplified analyses for both are given in [3]. YZ Lithium Niobate is a minimal diffraction orientation, so there is very little diffraction spreading [3] and it is sometimes ignored entirely. Even for a minimal diffraction orientation, at some small aperture size diffraction will become a significant source of loss and thus the lower bound on transducer beamwidth is expected to be limited by diffraction.

On the other hand, waveguide effects are expected to partly limit the upper bound on transducer beamwidth. SAW transducers are known to exhibit waveguide modes, and the total device response will be a sum of the contributions of all excited modes [3]. Each mode propagates with a different phase velocity, and therefore at some frequencies the modes will add in phase and at other frequencies the modes will add out of phase. This can create a beat pattern within the transducer frequency response if multiple modes exist. Additionally, all modes except the lowest velocity mode can only propagate above a certain frequency, called the cutoff frequency. One solution to this problem is to reduce the beamwidth of the transducer to increase the frequency shift of the higher order modes beyond the transducer passband [29].

Electrically, both the acoustic conductance and susceptance are proportional to the transducer beamwidth. The OFC devices considered here often have a considerable number of finger pair, and thus have quite low impedance. This makes the devices sensitive to parasitic loss, as shown in the previous section. While reducing parasitic resistance is taken as a first step, it will also be necessary to maintain a reasonable transducer impedance as there are practical limits to how much the resistance can be reduced. A combination of withdrawal weighting and beamwidth reduction can be used to increase the device impedance to an acceptable value.

The benefit of empirically optimizing the beamwidth is that all of the above mentioned effects, as well as any others that may exist, are taken into account. Several devices with the same design except for beamwidth were fabricated at 3rd harmonic as a first test of the effect of beamwidth on performance. These devices were not optimized for low loss and did not make use of gold films to reduce parasitic resistance, but showed that beamwidth has a significant effect on device performance. The time and frequency responses for the set of devices with varied beamwidth is shown in Figure 3.10 for devices operating at 3rd harmonic. Devices operating at 3rd harmonic have their beamwidth listed in terms of both fundamental wavelength (316.7 MHz) and 3rd harmonic wavelength (950 MHz). Of the 3rd harmonic devices, the device with 5λ beamwidth at fundamental (15λ at 3rd harmonic) show best results in that they have a relatively flat time domain response and lowest overall insertion loss. Following the initial test at 3rd harmonic with no gold overlay, another test was performed for devices operating at fundamental frequency with a gold overlay, and results are shown in Figure 3.11. The devices operating fundamentally have significantly lower loss, with the best results seen for the device with 10λ beamwidth, though the device with 15λ beamwidth is only slightly worse. The results from experiments at fundamental frequency and 3rd harmonic approximately agree that a beamwidth of 10-15λ at 950 MHz for the design used gives best results.

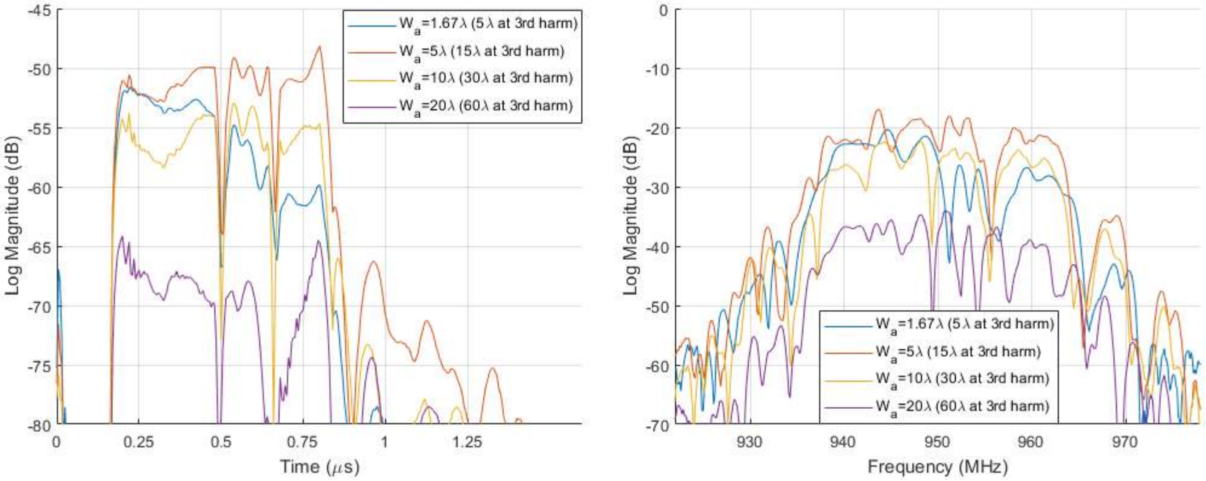

Figure 3.10: Measured log-magnitude S_{21} time (left) and frequency (right) domain response of correlators operating at 3rd harmonic with varied beamwidth. The beamwidth is given in terms of the fundamental wavelength (316.7MHz) and the wavelength at 3rd harmonic operation (950 MHz). The time response shows that the response is relatively flat for a beamwidth of 5λ and 10λ, whereas it shows significant distortion for other beamwidths. It can also be seen in both frequency and time domain that insertion loss is lowest for 5λ beamwidth and decreases significantly for other beamwidths.

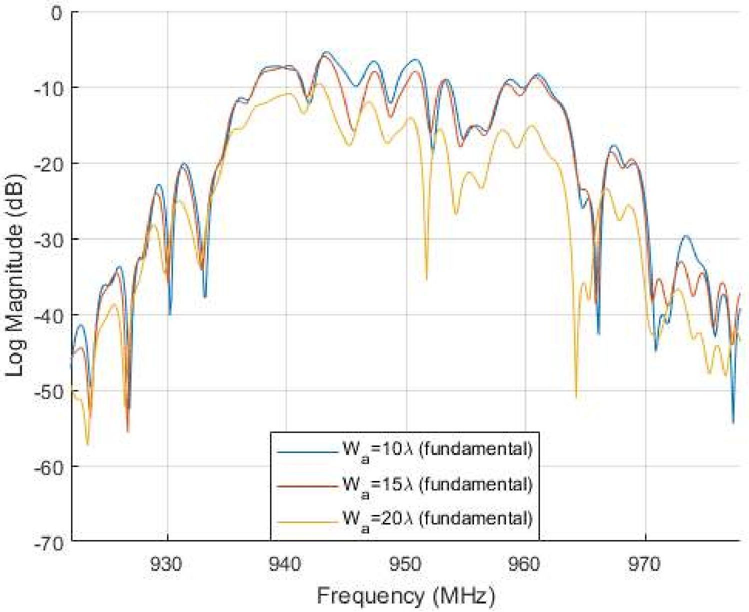

Figure 3.11: Measured log-magnitude S_{21} frequency domain response of correlators operating fundamentally with varied beamwidth. The responses for both 10λ shows the least loss, though the 15λ response is not much different. These results approximately agree with what was seen at 3rd harmonic, in that the effective beamwidth at 950 MHz should be around 10-15λ.

3.6 Low Loss OFC SAW Correlators

Applying the design considerations discussed in this chapter, the end result is reasonably low loss OFC correlators. The layout for the final pair of devices is shown in Figure 3.12, with the forward code on top and reverse code on bottom. The text below indicates some information about the design, and the details summarized in in Table 3.3.

Figure 3.12: Device layout for final low loss OFC correlator filter matched code pair, with a forward code of [1,2,-4,3] (top) and reverse code of [3,-4,2,1] (bottom). On the left is the dual-track differential wideband transducer and on the right is the coded OFC transducer with single-ended parallel tracks. The large rectangles are bus bars and they are tapered at the ends in an attempt to reduce electromagnetic feedthrough, the dark area between bus bars are the electrodes which are too small to resolve. The full design is detailed in Table 3.3.

Table 3.3. Design details for final low loss 4-chip OFC correlator filters, the layout is shown in Figure 3.12.

Parameter		*Value or Description*
Substrate		YZ Lithium Niobate
Electrode Metal		650 Å Aluminum
Pad Metal		7,500 Å Gold over 650 Å Aluminum
Center Frequency (f_0)		950 MHz
Bandwidth (BW)		25 MHz
Time Length (τ_{OFC})		0.64 μs
Number of Chips (N_c)		4
Processing Gain (PG)		12 dB
OFC Code		[1, 2, -4, 3] and [3, -4, 2, 1] – a matched pair
Harmonic (M)		Fundamental
Beamwidth (W_a)		10λ for each track
Center-to-Center Delay (τ)		0.35 μs
Propagation Path		Approximately 45 μm long with free surface condition
Electrode Pattern	Wideband	EWC, uniform with full transduction and full reflection
	OFC	DART, with 1:2 withdrawal weighted transduction and full reflection
N_p	Wideband	36
	OFC	150-153 (75-77 after withdrawal weighting)
Balanced/Unbalanced		Dual-Track with balanced wideband and parallel single-ended OFC

This final correlator design was fabricated commercially and showed good results with low loss with good correlation performance. Devices are measured using a calibrated vector network analyzer (VNA) and an RF probe station for direct on-wafer measurements. Only two-port network analyzers were available for measurement, so a balun is connected to the differential port and the balun s-parameters de-embedded as part of the calibration step. The measured responses for the matched pair are shown in Figure 3.13 before and after ideal electrical matching for minimum insertion loss. The devices show about 6 dB insertion loss after electrical matching and approximately match the desired response, though there is some undesirable loss through the transducer which can be seen in the decreasing response level with time in the time domain plot. Some measured devices using a near-zero length propagation path and EWC transducers were demonstrated with insertion loss as low as 5 dB [11], but the time domain response was significantly distorted and a matched code pair was not fabricated. The design has since been modified significantly, but near-zero propagation devices have not yet been re-investigated.

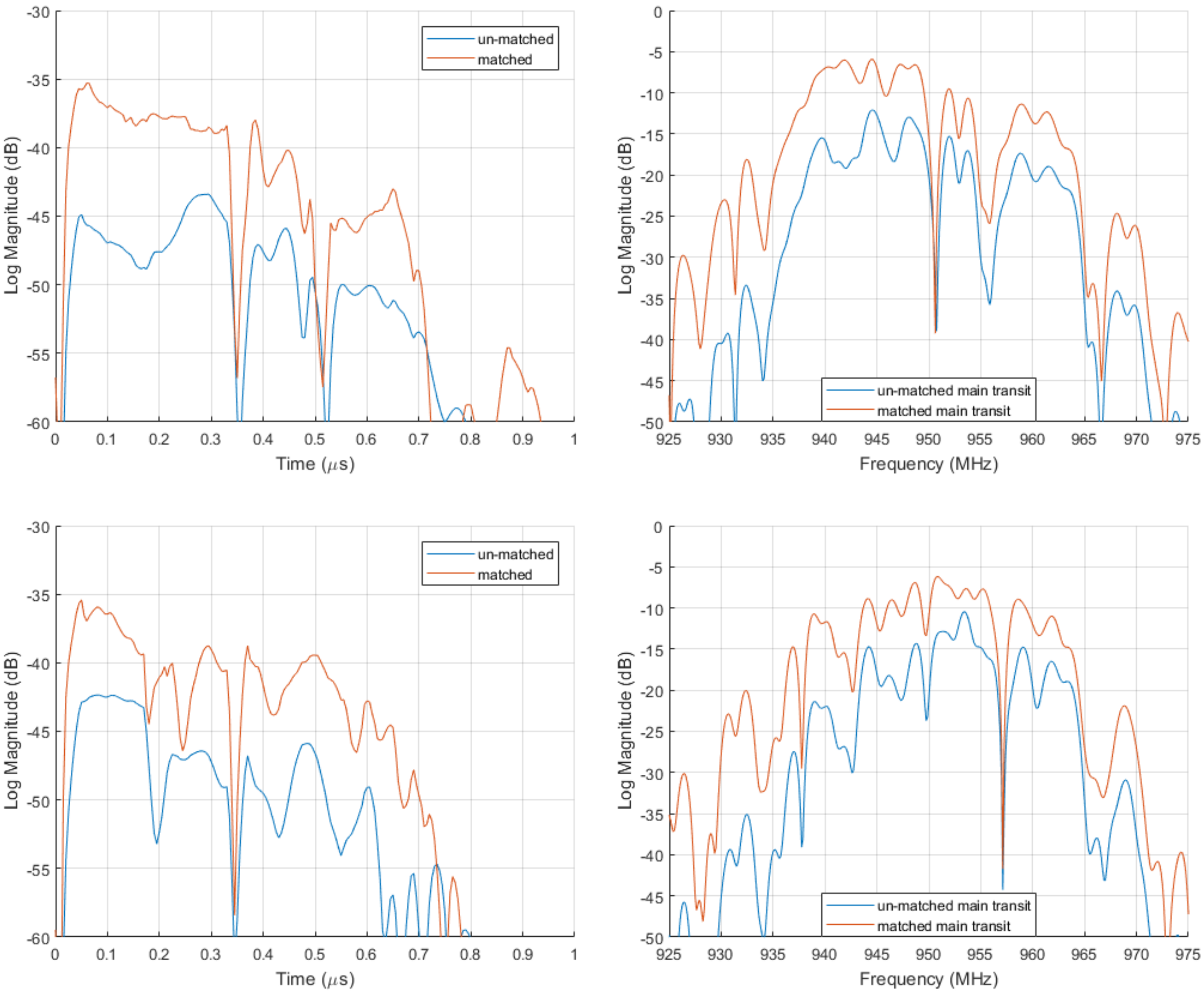

Figure 3.13: Measured log-magnitude S_{21} time (left) and frequency (right) domain response of the final correlator design before and after electrical matching. The responses for both the forward code [1,2,-4,3] (top) and reverse code [3,-4,2,1] (bottom) are shown. The OFC coding isn't directly visible, but the BPSK sequence can be seen in the time domain where abrupt null transitions occur between chips with differing phase. Ideally the frequency response for the two matched codes would be exactly the same, however, the loss through the transducer distorts them both from the ideal response. The loss through the transducer is visible in the time domain as the level of the responses decreases with time. The minimum insertion loss after electrical matching is about 6 dB for both forward and reverse codes.

The measured frequency responses are multiplied in software and then transformed to time domain using a fast Fourier transform (FFT) to produce the correlation or cross-correlation of the two codes. This is mathematically equivalent to the time convolution obtained by cascading the two filters and measuring the response, but allows more flexibility for post-processing. When a pair of matched codes is used, the matched filter (or correlation) response is obtained and the result is a compressed pulse with properties dependent on the processing gain of the sensors and how well they are actually matched including device imperfections. When a pair of mismatched codes is used, the cross-correlation response is obtained which does not result in a compressed pulse for codes that are sufficiently mismatched. The cross-correlation of a pair of mismatched codes can be used to calculate the interference that would be contributed to a system if the devices were used simultaneously, called the multiple access interference (MAI). Some important figures of merit for a matched filter response are the pulse compression and the peak-to-sidelobe level (PSL). For a mismatched response, the cross-correlation at the time of correlation gives the MAI for synchronous operation, the peak cross-correlation gives the worst-case MAI for asynchronous operation, and the average cross-correlation can also be useful in determining what a typical level of MAI may be for asynchronous operation. The measured matched filter response using the two matched codes for the final correlator design is shown in Figure 3.14 before and after electrical matching. In this figure, the electrical matching is optimized to give minimum insertion loss given a minimum PSL spec of 9.5 dB. The matched filter response without electrical matching gives a PSL of 7.7 dB and it was typical to be able to improve the PSL by a couple dB by optimizing the matching network with very little added loss.

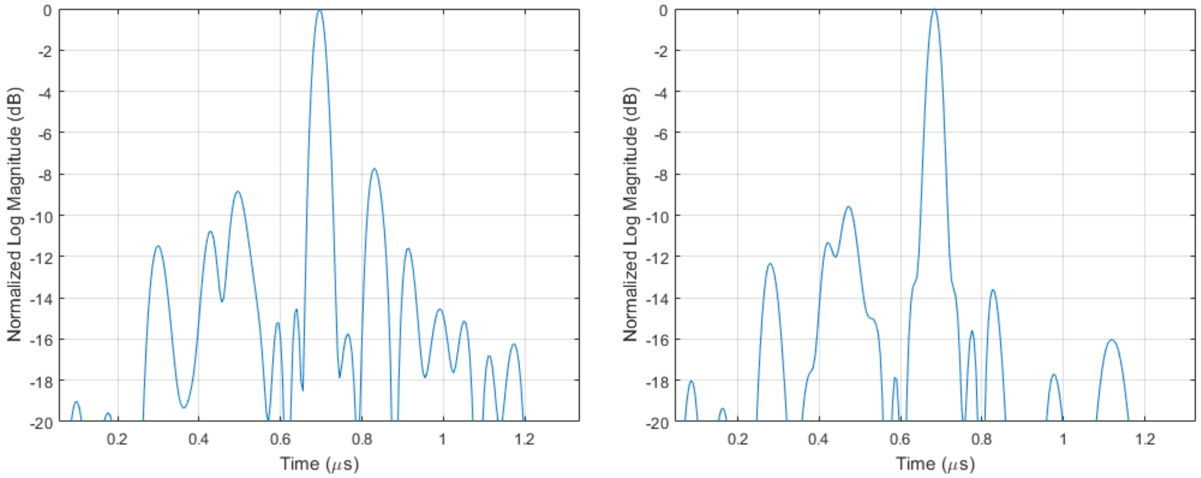

Figure 3.14: Measured normalized log-magnitude S_{21} time domain correlation for the final correlator design before (left) and after electrical matching (right). The electrical matching in this case is optimized to minimize the correlation sidelobes by incorporating a small amount of frequency dependent mismatch that helps to level the chip amplitudes. The matched response gives a peak-to-sidelobe level of 9.6 dB while the unmatched response gives a peak-to-sidelobe level of 7.7 dB.

Simulations using a simple signal based model for the OFC response indicate that loss through the transducer and within individual chips contribute significantly to the degradation of the matched filter response. Exponential decay through the individual chips is attributed to the reflectivity of the transducer, while exponential decay through the transducer as a whole is attributed to propagation loss. The exponential decays are implemented using a straightforward generalization of the OFC signal described in Chapter 2. The chip response becomes

$$h_{chip_i}(t) = a\cos\left(2\pi f_{c_i} t\right) rect\left(\frac{t}{\tau_c}\right) e^{-\alpha_c t} \tag{3.18}$$

where α_c is the exponential decay through the individual chip in nepers/μs (Np/μs). After the chip responses are summed, a second exponential decay through the transducer gives the full OFC response as

$$h_{OFC}(t) = \left[\sum_{i=0}^{N_c-1} h_{chip}(t - i \cdot \tau_c)\right] e^{-\alpha_p t}, \tag{3.19}$$

where α_p is the exponential decay through the transducer as a whole.

Loss through individual chips and the transducer as a whole were found to cause the correlation peak level to be decreased and the resulting PSL to be reduced, depending on the level of roll-off. A simulation of a correlator pair with no losses is compared with the same correlator pair but with a reflective decay of 2 Np/µs and propagation loss of 2 Np/µs, shown in Figure 3.15. These can be expressed equivalently by converting nepers to decibels as approximately 17.4 dB/µs for consistency with earlier discussion. The ideal response with no reflective decay or propagation loss is also shown for comparison, with a PSL of around 14 dB. The simulation including exponential loss terms shows a decrease in PSL to about 11 dB. These findings are consistent with what is seen with measured data, devices measured with flatter chips show higher PSL, one of which is presented in Chapter 4. Compensating for these effects using weighted transducers could likely improve the correlation results.

The measured devices are matched using a simulated matching network with ideal, lossless components. The matching network is implemented in software using a 2-element per port network with inductors and capacitors, with values chosen through an optimization routine. The software is written in MATLAB and takes advantage of the built-in optimization functions to best choose the matching network components based on definable goals and specifications. Typically for simple filters, average insertion loss is minimized over the half-power bandwidth, but it is also possible to match for minimum insertion loss at a single frequency. For correlator filters, devices are typically matched for minimum insertion loss over the bandwidth given a minimum acceptable

PSL. The optimization process does not give an analytic understanding of how the responses are progressively improved, but by analyzing the matched responses, some understanding can be gained. The matching network appears to improve the PSL of the measured matched filter response by introducing a small amount of frequency dependent electrical mismatch loss. The frequency dependent mismatch loss introduced is believed to compensate for the amplitude variation of chips introduced by the decay terms discussed above. It is also possible to simply match for minimum insertion loss over the bandwidth, giving little or no change in PSL over the unmatched response.

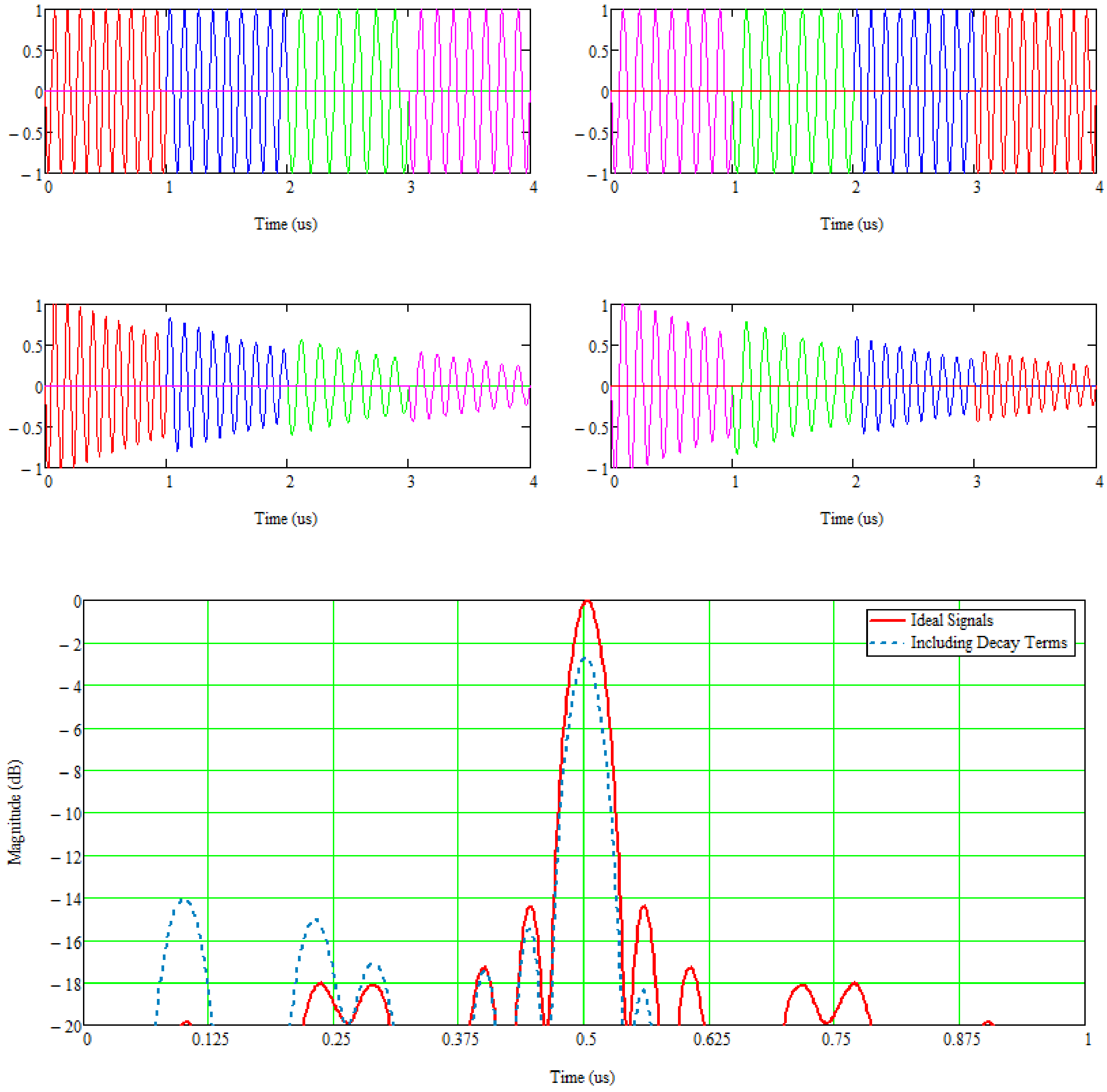

Figure 3.15: Simulated time domain response for the forward (left) and reverse (right) correlator filters with no reflective decay or propagation loss (top) and 3 Np/µs reflective decay through the individual chips and 2 Np/µs propagation loss through the transducer as a whole (middle). The four different colors correspond to the four different chip frequencies. The simulated matched filter responses for both ideal and with exponential loss terms are shown (bottom). The ideal response has sidelobes about 14 dB below the peak of the compressed pulse. The response including exponential loss has a reduced correlation peak and higher sidelobes, giving sidelobes about 11 dB below the peak of the compressed pulse.

3.7 Summary

Low loss correlators were designed and fabricated as part of this work, demonstrating the lowest loss OFC SAW correlators published to date. The procedure for reducing insertion loss was detailed using several parallel approaches resulting in 4-chip OFC devices at 950 MHz with 6 dB insertion loss and 9.6 dB PSL for the matched pair presented with ideal electrical matching, a significant improvement over the 20 dB insertion loss presented in [7] at 250 MHz. This chapter presents only fixed-code correlator filters, the following section will describe an approach to create programmable SAW correlators and demonstrates positive results.

This work demonstrates a significant improvement from previous work, however, there may still be some room for improvement in terms of insertion loss and correlation quality. Some ideas that were considered and tested but not implemented in final devices are described here. It may be possible to further reduce insertion loss by flattening the insertion loss over bandwidth by weighting the wideband transducer. Multi-phase unidirectional transducers could be beneficial since it is possible to achieve high directivity for short transducers like the wideband, where it is difficult to obtain high directivity for SPUDTs. The downside is that these require external phasing networks which complicates design. There may be significant benefits to breaking each chip into individual tracks, referred to as a multi-track device. A multi-track device would suffer less propagation loss since each chip only propagates through a single transducer, though the velocity under each structure must be known accurately to correctly align each chip in time. The devices presented are not temperature compensated, and either passive or active temperature compensation could make the devices more useful in practical systems.

CHAPTER 4: PROGRAMMABLE OFC SAW CORRELATOR FILTERS

The previous chapter described the design of low loss orthogonal frequency coded (OFC) surface acoustic wave (SAW) correlator filters. These devices provide the matched filter operation with relatively low insertion loss but have the distinct disadvantage that the code is fixed. In order to communicate selectively with multiple systems, codes must be programmable. Chapter 2 introduced the concepts of code division multiple access (CDMA) based on OFC SAW correlator filters, Chapter 3 included some experimental results for a matched pair of fixed-code devices, and this chapter focuses on programmable SAW correlator filters.

Programmable SAW correlators allow communication between multiple systems using a single correlator module, and can also allow long code sequences [5] which make communication more secure. Devices using external switches have been investigated [6, 8] at 183 MHz as well as integrated devices on silicon using a piezoelectric film [9] at 100 MHz. It is also possible to create programmable correlators using nonlinear SAW convolvers [10] which can implement convolution with a near-arbitrary time and bandwidth limited signal. In this chapter, SAW correlator filters with a programmable code are designed and positive results presented at 950 MHz using external switches. The SAW device itself is completely passive but external switches to implement programmability require a small amount of power, the devices presented use less than 1 mW of DC power.

4.1 Code Division Multiple Access Networks using OFC SAW Correlator Filters

In a multiple access scenario, a separate code must be used for each communication link within the network. To reduce interference between systems operating simultaneously, each link must have one matched pair of codes that are orthogonal to all other codes used by other systems. This is possible for a network of systems that are completely synchronized, such as the down-link (tower to user) of a cellular system. For networks where complete synchronization is not possible, such as the up-link (user to tower) of a cellular system, it is typically not feasible to maintain full network synchronization and full orthogonality is not achievable [15].

In a synchronized system, the decision instant is the same for all correlators. The decision instant is the point where the output of the matched filter receiver is sampled, and for a matched pair of codes this instant is where the peak of the compressed pulse occurs. The decision instant for the simulated matched filter pairs in Figure 4.1 is 2 μs, and the compressed pulse peaks at this point in time for the matched code. For a mismatched code, the response has no compressed pulse and instead has a reduced response at the decision instant, a zero response at this instant is obtained if the codes are orthogonal. For the synchronized simulated matched filter pairs in Figure 4.1, the decision instant is 2 μs for all codes, and there is no multiple access interference (MAI). While the mismatched codes show no MAI for a synchronized network, the mismatched codes are not orthogonal for all time delays and MAI will occur. These systems have a center frequency of 950 MHz with 25 MHz bandwidth and time length of 0.64 μs giving 12 dB processing gain. The synchronous system is MAI free at the decision instant, while the example asynchronous system shown has MAI about 11 dB below the peak signal level for each mismatched code. An asynchronous system can have any combination of delays between systems, and the level of MAI varies significantly with delay. The asynchronous system shown is only one example, but the worst-case MAI can be calculated from the peak of the cross-correlation response and the expected MAI can be calculated from the average of the cross-correlation response for each mismatched code. All mismatched codes contribute interference, and the sum of the cross-correlations will give the full MAI for the system.

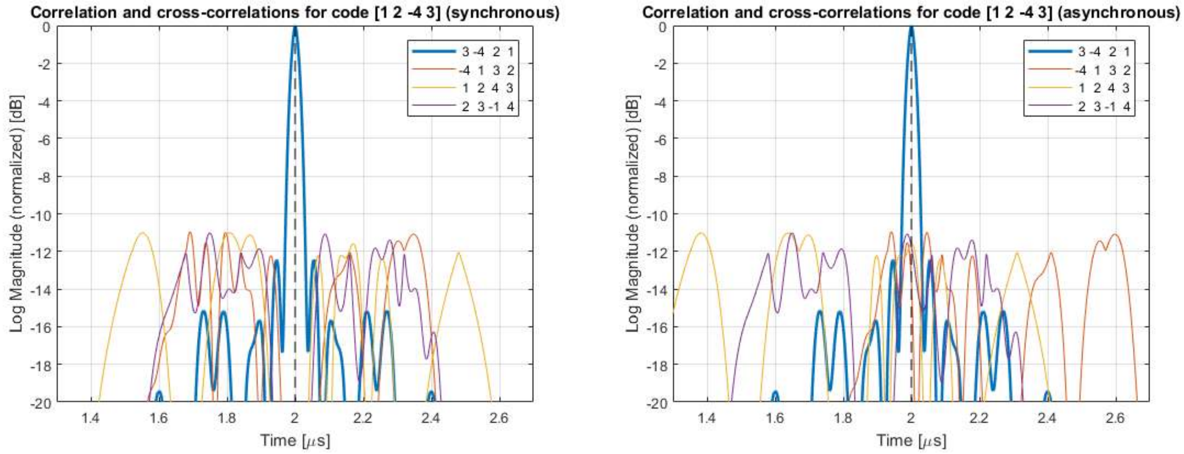

Figure 4.1: Simulated log-magnitude correlation (bold) and cross-correlations for a synchronous system (left) and example asynchronous system (right). The decision instant is indicated by the black dashed line. In the synchronous system, all signals have the same delay giving a decision instant of 2 µs and it can be seen that all mismatched codes trend to zero while the matched code gives a sharp peak. In the asynchronous system, the decision instant for the matched code is still 2 µs but the mismatched codes all have different delays and the signals from mismatched codes are typically non-zero but vary with delay. For the example shown, the MAI for each mismatched code is 10-14 dB below the correlation peak, but can vary significantly for other delays.

In order to communicate selectively within a network of systems, each system must be able to change the codes it uses to transmit and receive. This can be done with multiple correlators using $2N_{code}$ switches to implement N_{code} codes, which becomes costly and difficult to implement for large code sets. It is also possible to create a programmable OFC sequence using $2{N_c}^2$ switches to implement $N_c!$ codes, where N_c is the number of chips in the OFC sequence. For small N_c this requires more switches than codes produces, but as N_c increases the number of codes greatly surpasses the number of switches. The cross-over point is between 4 and 5 chips, but even with only 5 chips the setup requires 50 switches and isn't very practical. Aside from the switches, the actual correlator becomes difficult to build, as it requires switched multi-track correlators which require accurate knowledge of the velocity under all fabricated structures. Another possible embodiment is to use a fixed OFC sequence, but programmable amplitude or phase coding on the individual chips. If binary phase shift keying (BPSK) is used, this embodiment is fairly simple in terms of the switches and the OFC design, which will be discussed in the next section. To create 2^{N_c} codes, only $2N_c$ switches are needed and the number of programmable codes available is greater than the number of switches required for any number of chips greater than 2. The number of codes available and number of switches required for up to 10 chips are shown in Figure 4.2, using single-pole single-throw (SPST) switches. The number of codes vs number of switches are also compared, showing that the switched BPSK code achieves the greatest number of codes for a given number of switches. SPST switches are simple on-off switches, though other types of switches with multiple poles and/or multiple throws may make practical implementation easier. These figures and the above discussion show that programmable correlators using programmable BPSK code with fixed OFC sequence are most practical to implement. The design and measured results for a pair of fabricated 4-chip programmable SAW correlators with programmable BPSK and fixed OFC sequence will be described in the following sections.

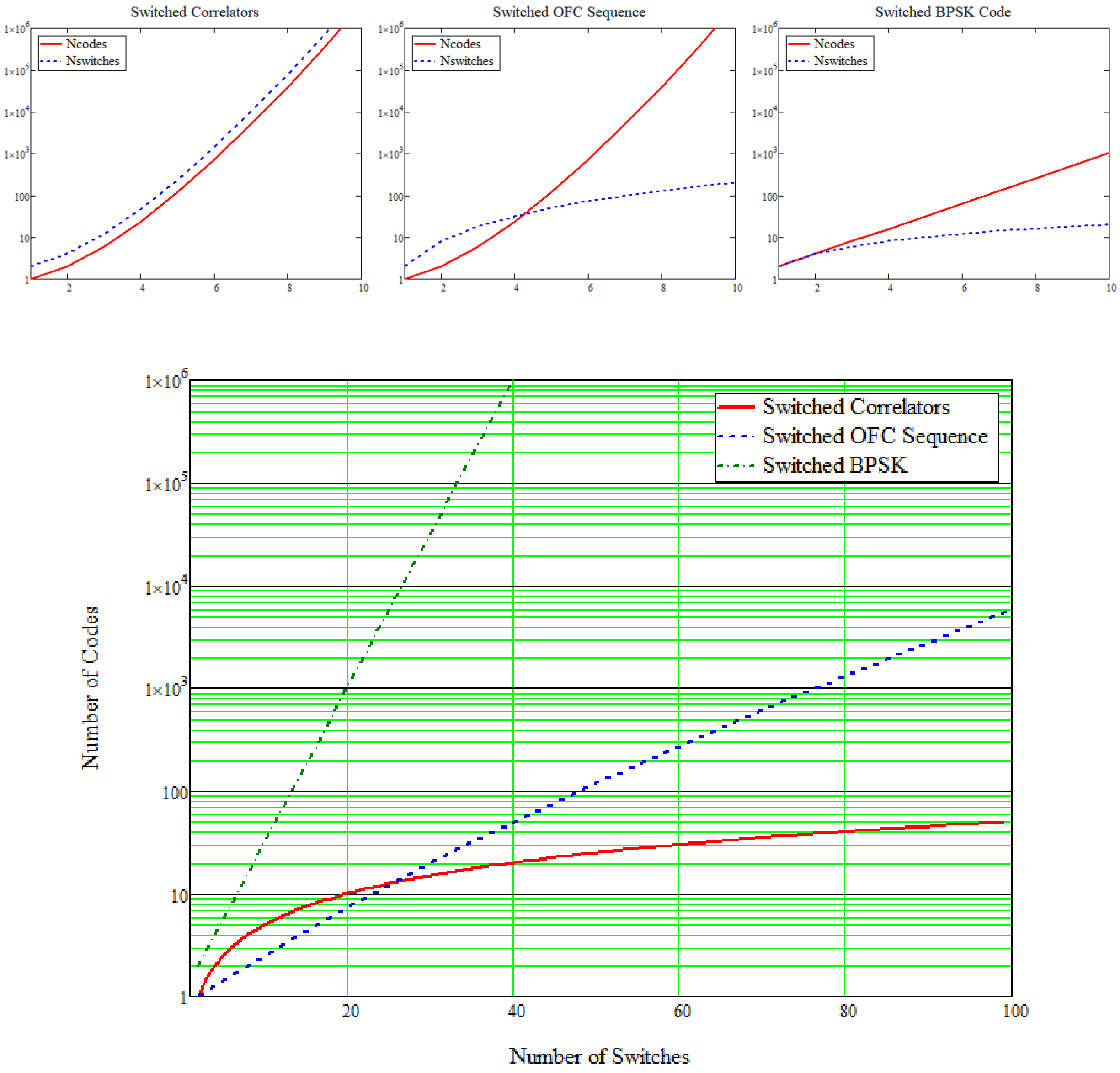

Figure 4.2: Log-linear plots showing the number of switches required compared to the number of programmable correlator codes for the three described programmable embodiments. The switched correlator method (top-left) always requires 2x more switches than codes, the programmable OFC sequence (top-middle) gives more codes than switches for $N_c > 4$, and the programmable BPSK code (top-right) with fixed OFC gives more codes than switches for $N_c > 2$. The bottom plot shows the number of codes compared with the number of switches required for the three embodiments. Devices using programmable BPSK code require far fewer switches to achieve a given number of codes and are also more practical in terms of SAW design.

4.2 Programmable Correlator Filter SAW Design

There is no inherent limitation on programmability for OFC correlator filters, the limitation arises due to the physical embodiment of the device. In the device embodiment presented previously, there are two electrical ports, one for the wideband transducer and one for the OFC transducer. Since the transducer structure is fixed during fabrication and the bus bar connects all chips in a fixed manner, neither OFC sequence nor individual chip amplitude or phase can be modified after fabrication. By breaking the bus bar that connected all chips into individual bus bars for each chip, an $N_c + 1$ port device is created and individual amplitude and phase of chips can be modified independently. Device embodiments for both fixed-code and programmable correlators are depicted schematically in Figure 4.3.

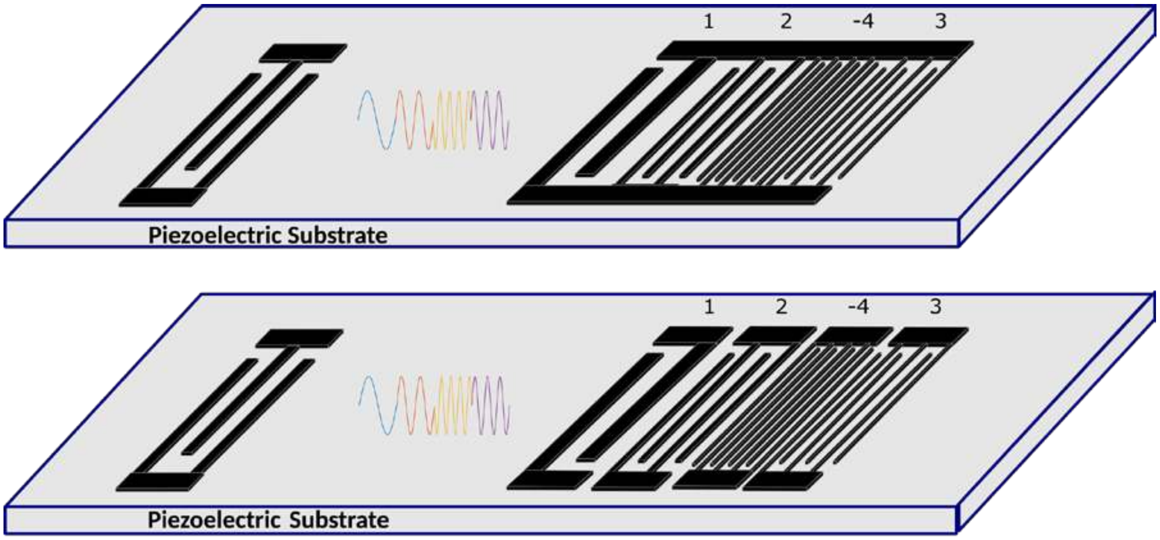

Figure 4.3: Schematic representation of an OFC SAW device comprised of a wideband transducer (left) and an OFC transducer (right) separated by some delay. The upper device implements a fixed-code whereas the bottom device allows amplitude or phase code programmability with a fixed OFC sequence. The OFC waveform generated by these filters has an OFC sequence [1,2,4,3], denoting the order of the frequency hopping pattern. The upper device has a fixed BPSK code of [1,1,-1,1] giving an overall device code of [1,2,-4,3] whereas the bottom code can use arbitrary amplitude and phase coding. An example signal is shown in the gap with the programmable device using the same amplitude and phase coding as the fixed code device.

SAW correlators using a fixed OFC sequence are fabricated in both fixed-code and programmable embodiments using the same design except for bus bars. The layout for the fixed code pair presented is shown in Figure 4.4 and the layout for the programmable correlator pair presented is shown in Figure 4.5. Since the design for the fixed-code and programmable devices is the same with the exception of the bus bars and probe pad structure, and devices should have similar performance, excluding effects of the peripheral components for programmable devices. The fixed-code device was previously fabricated and is used as a known device which can be used for comparison with programmable devices.

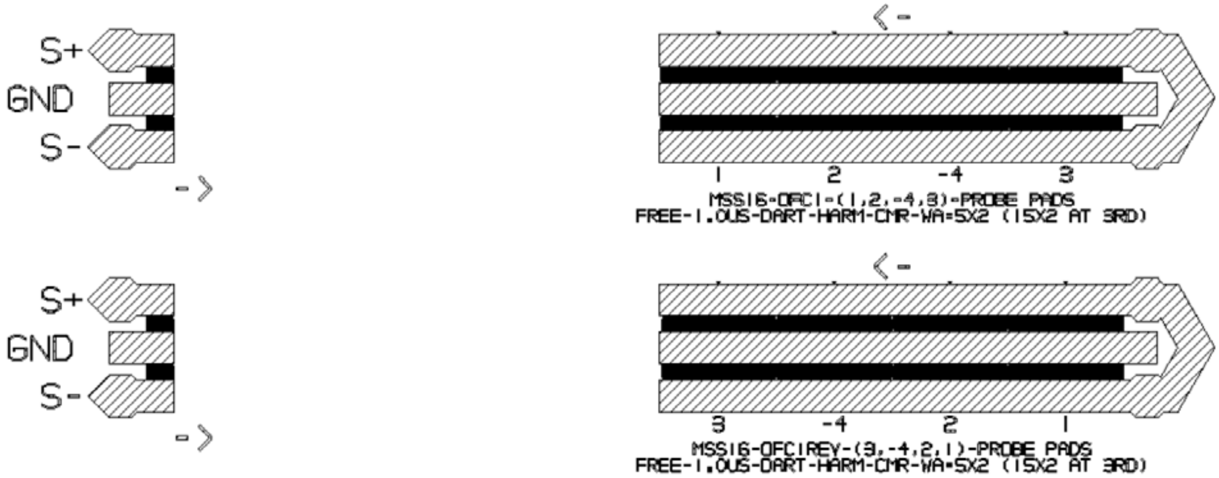

Figure 4.4: Device layout for prototype 4-chip OFC SAW correlator filter fixed-code pair with unified bus bars and probe pads. On the left is the dual-track differential wideband transducer and on the right is the coded OFC transducer with single-ended parallel tracks. The large crosshatched areas are the bus bars with extended areas to accommodate RF probes, the dark area between bus bars are the electrodes which are too small to resolve. The design here is not optimized for low loss.

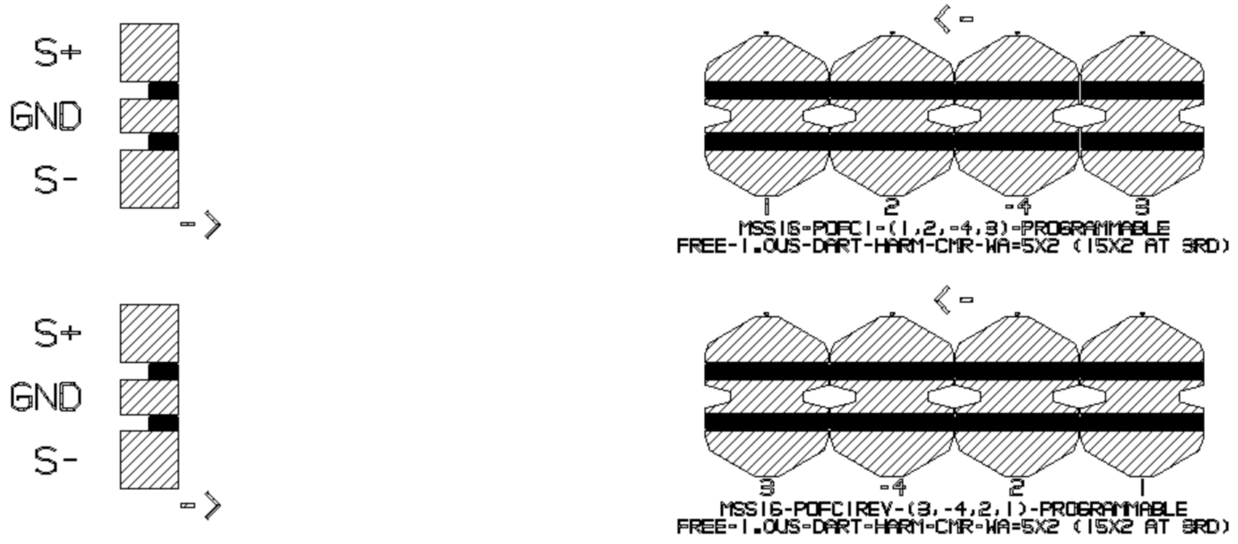

Figure 4.5: Device layout for prototype 4-chip OFC SAW correlator filter code pair with individual bus bars for each chip. On the left is the dual-track differential wideband transducer and on the right is the coded OFC transducer with single-ended parallel tracks. The large crosshatched areas are the bus bars and they are tapered at the ends in an attempt to reduce capacitive coupling between chips, the dark area between bus bars are the electrodes which are too small to resolve. The design here is not optimized for low loss.

4.3 Programmable Correlator Filter PCB Design

Arbitrary amplitude and phase coding allows a wide range of coding options, and in this dissertation binary phase shift keying (BPSK) is chosen for the programmable code. BPSK is a common digital modulation and is relatively easy to implement using electronic switches. A programmable BPSK code can be used in conjunction with the fixed OFC code sequence by modifying the phase of the signal going to a chip by ±180°, which is equivalent to flipping the polarity of a chip. This programmable phase shift can be implemented using RF switches alone, as shown schematically in Figure 4.6 for a 4-chip device. For a device using a fixed OFC code with programmable BPSK code, the achievable processing gain is ${N_c}^2$ and 2^{N_c} programmable codes are possible using a single correlator with N_c DPDT switches (or $2N_c$ SPST switches). The

16 programmable codes for the 4-chip correlators vary from [1,1,1,1] to [-1,-1,-1,-1], with 16 matched codes out of 256 total combinations for a pair of correlators. Simplified waveforms for a fixed OFC code with two differing BPSK codes are shown in Figure 4.7, using codes [1,2,-4,3] and [-1,2,-4,-3]. The phase difference between responses for the two codes is 180 degrees for chips 1 and 3, while chips 2 and 4 have no phase difference. The simplified signals shown here only have a few cycles per chip for illustration purposes, the codes used in the actual devices presented have approximately 150 cycles per chip.

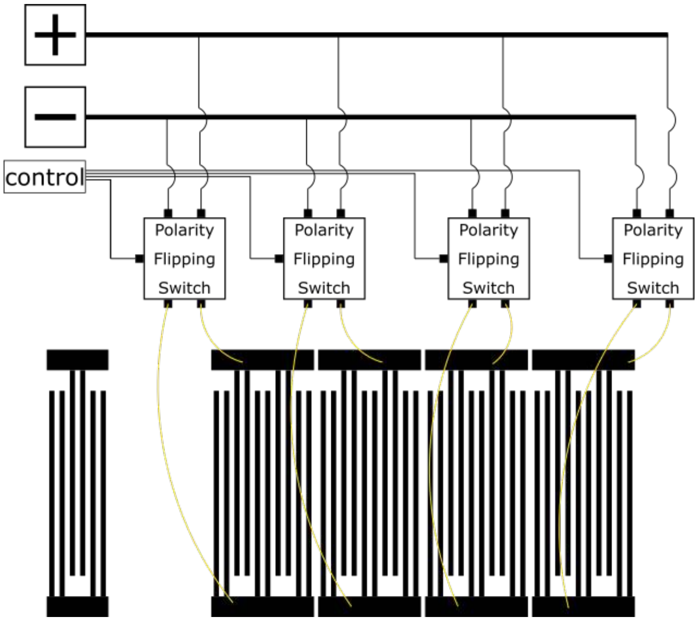

Figure 4.6: Schematic representation of a 4-chip OFC SAW correlator with a programmable binary phase shift keying (BPSK) code implemented using RF switches and a fixed OFC code. When the control signal is changed, the DPDT RF switches swap the connection of the chip, effectively flipping the polarity or changing the phase by 180°. There is one DPDT switch per OFC chip, and this setup can be used with differential signaling as shown or with single-ended signaling.

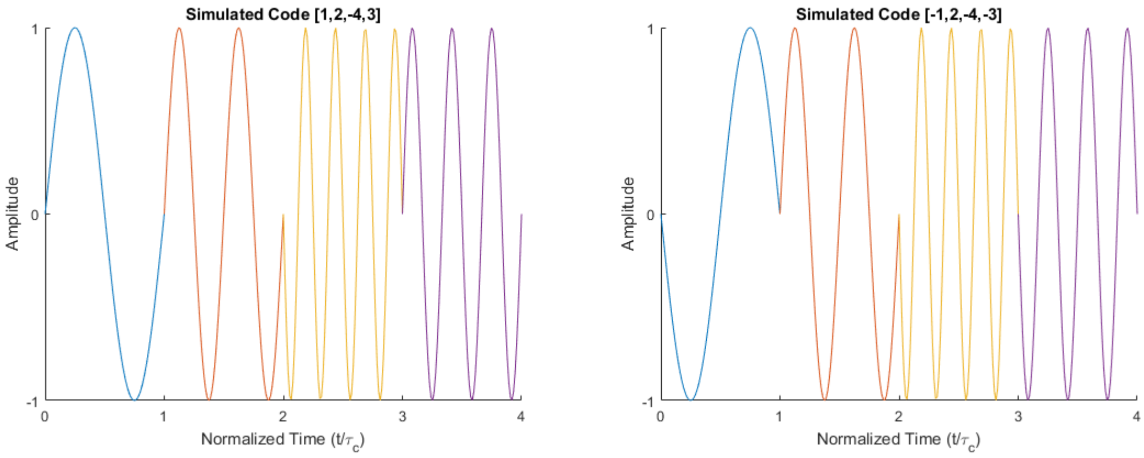

Figure 4.7: Simplified waveform illustrating two chips with the same fixed OFC sequence and two differing BPSK codes. The codes [1,2,-4,3] (left) and [-1,2,-4,-3] (right) are chosen arbitrarily from the set of 16 possible BPSK codes for the 4-chip devices. The phase of the first and last chips (1 and 3) are opposite between the two codes, while the phase of the middle two chips (2 and 4) are the same between the two codes.

A printed circuit board (PCB) is designed to integrate the SAW correlator with the switches and other peripheral components. A populated PCB with a fabricated 4-chip programmable correlator bonded to the front and four DPDT switches on the back is shown in Figure 4.8. This PCB was designed using a simple PCB layout tool and was not simulated before fabrication. The PCB is meant to act as a 4-way splitter with 4 DPDT switches to change the polarity of the chips individually. An ideal 4-way splitter would have equal transmission parameters of -6 dB and equal phase, and would not cause add any unnecessary loss or distortion to the SAW device response. The splitter that was designed and fabricated is not ideal, and simulations performed using ADS after fabrication show phase variation up to 20° and amplitude variation up to 6 dB between chips. This variation is significant, and will degrade the filter response.

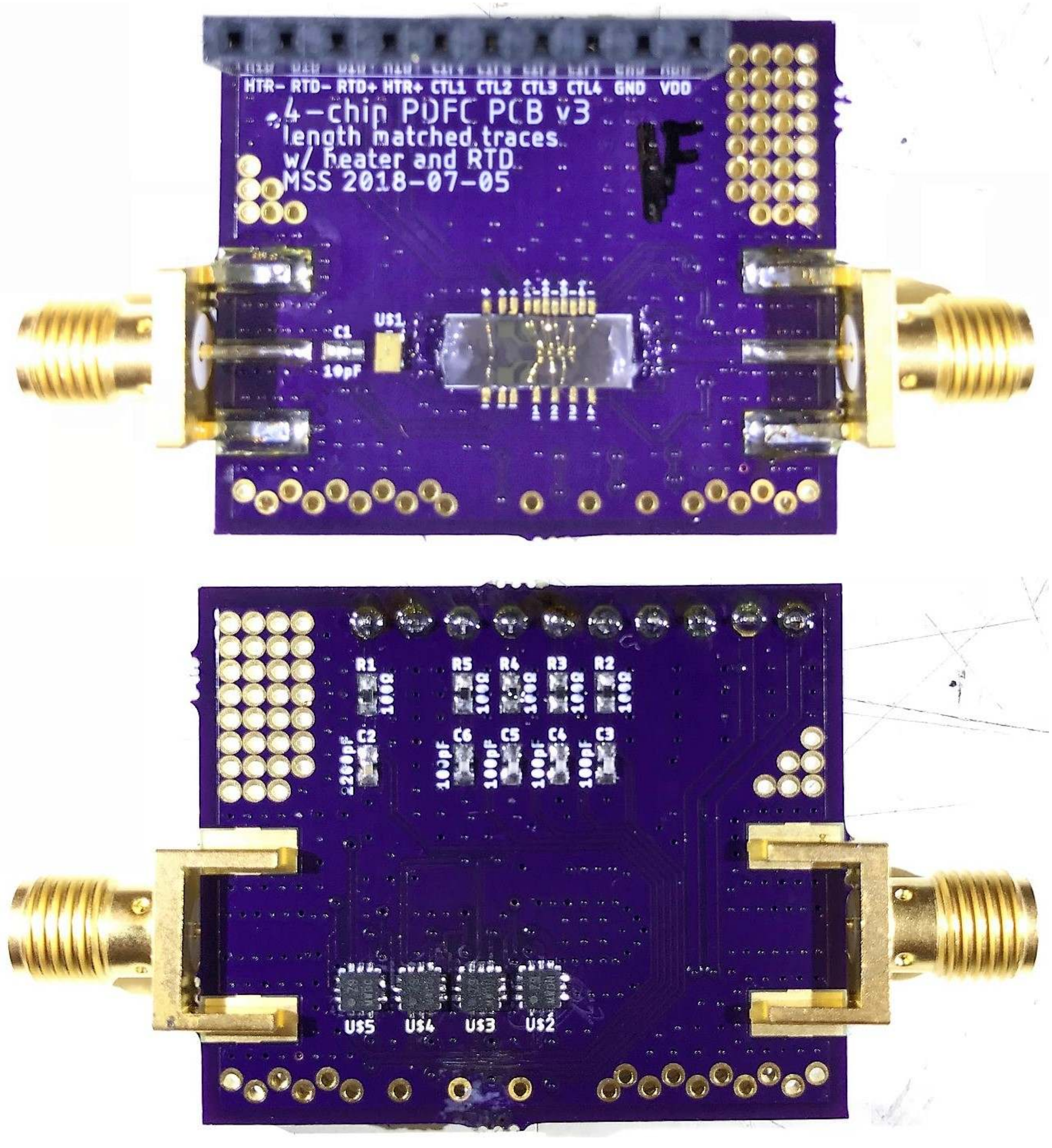

Figure 4.8: Images of the front (top) and back (bottom) of a populated PCB designed to integrate a 4-chip SAW correlator with electronic switches, collectively a programmable correlator. The top image shows the OFC SAW correlator die bonded to the gold pads on the PCB with peripheral components and connectors. The bottom image shows the four RF DPDT switches in QFN packages with peripheral components and connectors. The connectors on the sides provide RF connections and the header on top provides DC connections.

4.4 Experimental Results

A pair correlator filters with matched codes are designed and fabricated for both fixed-code and programmable embodiments. The devices designed are prototypes and are not optimized for low loss as in the previous chapter. The devices are fabricated at UCF on YZ Lithium Niobate with 600 Å Aluminum metallization over a 50 Å Titanium adhesion layer. The design uses 3rd harmonic operation to achieve a center frequency of 950 MHz with 25 MHz bandwidth and 0.64 μs time length giving 12 dB signal processing gain. The fixed OFC sequence for all devices is [1,2,4,3] for the forward code and [3,4,2,1] for the reverse code. Correlators with fixed-code embodiment use BPSK code [1,1,-1,1] and [1,-1,1,1] giving overall PN-OFC codes of [1,2,-4,3] and [3,-4,2,1] – a matched pair. Correlators with programmable BPSK code can use any of the 16 available 4-chip code combinations from [-1,-1,-1,-1] to [1,1,1,1].

All devices are measured using a calibrated vector network analyzer (VNA). Devices with a fixed-code that have probe pads are measured on-wafer using an RF probe station. Programmable devices can't be measured directly on-wafer because the pitch of the RF probes is too small to span the bond pads, and devices must be packaged before measuring. The PCB described above is used for both forward and reverse code devices and they are measured using the RF connectors on the sides. There are 16 possible BPSK codes for each programmable correlator, giving a total of 256 combinations for the forward and reverse correlator. In order to measure the correlation and cross-correlation response for all combinations, the frequency response of both the forward and reverse codes are measured for all 16 BPSK codes and the correlations and cross-correlations are calculated in software. Correlations and cross-correlations for each code combination are calculated by multiplying the frequency domain responses and taking the inverse Fourier transform to convert back to time domain. This is mathematically the same as the time convolution obtained by cascading the two filters, as would be done in a real system. The advantage of using this method is that only $2 \cdot 2^{N_c}$ measurements are required to produce the full 2^{2N_c} combinations, for the 4-chip device presented this reduces the number of measurements from 256 to 32.

When two matched codes are measured, a matched filter (or correlation) response is obtained and a compressed pulse is observed with pulse compression ratio and peak-to-sidelobe level dependent on the processing gain and how well matched the codes actually are. When two mismatched codes are measured, the response is not a matched filter response and no compressed pulse is observed for codes that are sufficiently mismatched. When multiple systems are operating simultaneously, each system will receive a signal from the desired matched code but also every other mismatched code used by other nearby systems. These mismatched codes contribute multiple access interference if the codes are not fully orthogonal. The level of MAI contributed depends heavily on the set of codes chosen and the relative delay between simultaneously operating systems. Codes can be selected based on MAI, and typically for a well-chosen code set, the level of MAI decreases as processing gain for the coding increases.

For fixed-code correlators, two devices with matched code pairs are designed and fabricated. The matched filter response for the pair is shown in Figure 4.9 giving a peak-to-sidelobe (PSL) of 12 dB. This shows that the designs give a good matched pair. These prototype devices haven't been designed for low loss like the last chapter, and fixed-code devices have as low as 16 dB insertion loss after ideal electrical matching.

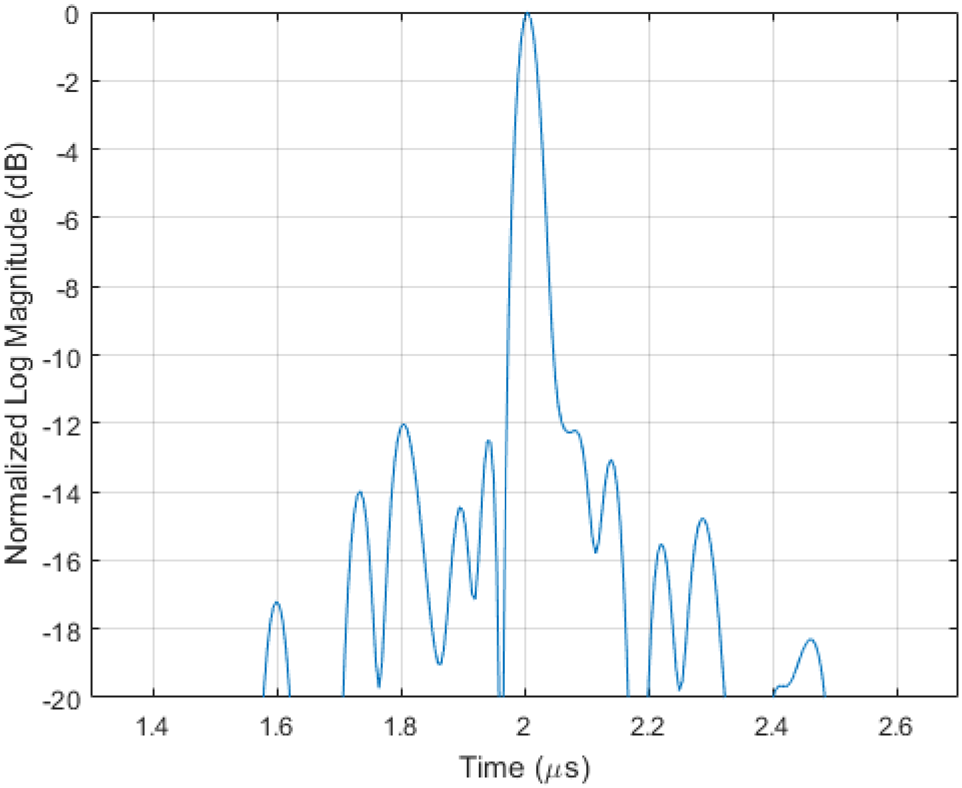

Figure 4.9: Measured normalized log-magnitude S_{21} time domain correlation for fixed-code OFC SAW correlator filters with no electrical matching. The matched response gives a good compressed pulse with a peak-to-sidelobe level of 12 dB, indicating that the codes are well matched.

For programmable correlators, two devices with matched OFC code sequences and programmable BPSK codes are designed and fabricated. These two devices have 16 possible BPSK codes each, so 16 matched pairs out of a total of 256 combinations are possible. The matched filter response for all 16 matched codes are shown in Figure 4.10. When using the full code set, the variation in correlation peak and sidelobes reduces the peak-to-sidelobe level significantly. Simulations indicate that the PCB designed has significant amplitude and phase variation between chips which is believed to be the cause of correlation peak variation. Improving the PCB design should significantly improve the measured matched filter response.

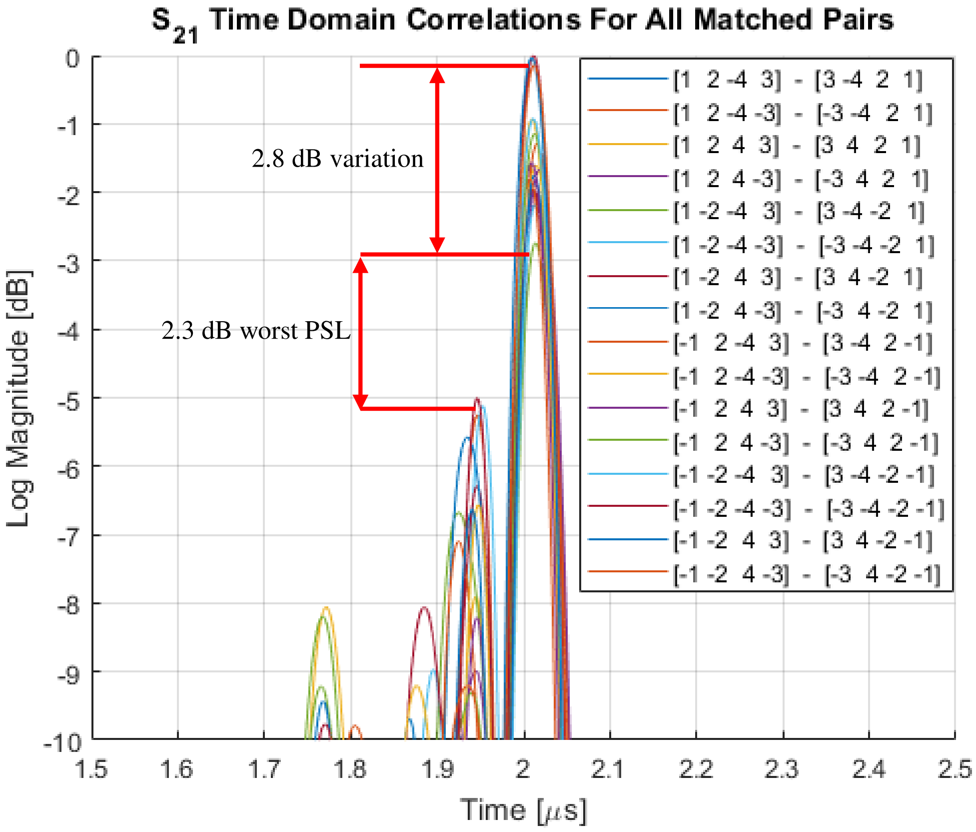

Figure 4.10: Measured normalized log-magnitude S_{21} time domain correlations for all 16 programmable BPSK codes with fixed OFC sequence, no electrical matching. The correlation peak shows significant variation, up to 2.8 dB with a worst case peak-to-sidelobe level of 2.3 dB across the full 16-code set.

Reducing the full 16 code set to a set of 4 codes as shown in Figure 4.11 gives improved performance while still using 25% of the available codes. For a synchronous network using this 4-code set, the worst-case MAI would be about 3.1 dB below the lowest correlation peak, while for asynchronous operation a worst-case MAI 1.9 dB is possible. The programmable correlators presented have as low as 22 dB insertion loss with no electrical matching.

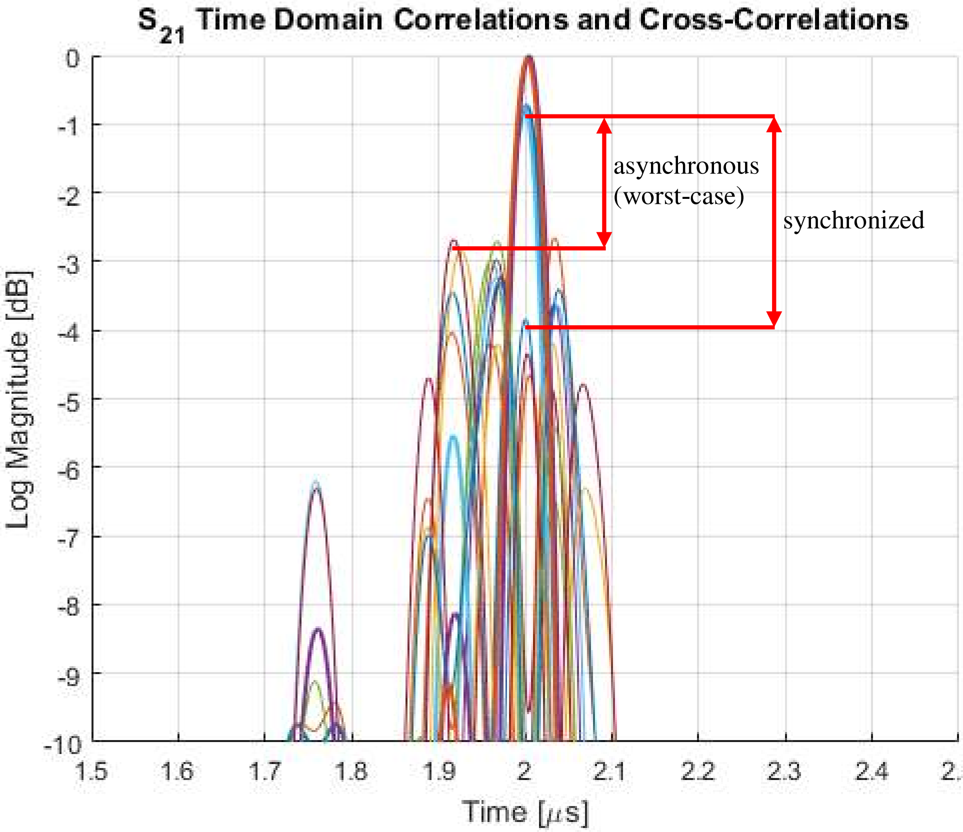

Figure 4.11: Measured normalized log-magnitude S_{21} time domain correlations and cross-correlations for a 4-code programmable BPSK code with fixed OFC sequence, no electrical matching. The correlation responses for matched codes are in bold, and show a compressed pulse with <1 dB variation. The cross-correlation responses show a worst-case MAI of about 3.1 dB for a synchronous system or about 1.9 dB for asynchronous operation with worst-case delay.

Further reducing the full 16 code set to a set of 2 codes as shown in Figure 4.12 gives a further improvement in performance while still using 12.5% of the available codes. For a synchronous network using this 4-code set, the worst-case MAI would be about 8.2 dB below the lowest correlation peak, while for asynchronous operation a worst-case MAI 3.5 dB is possible.

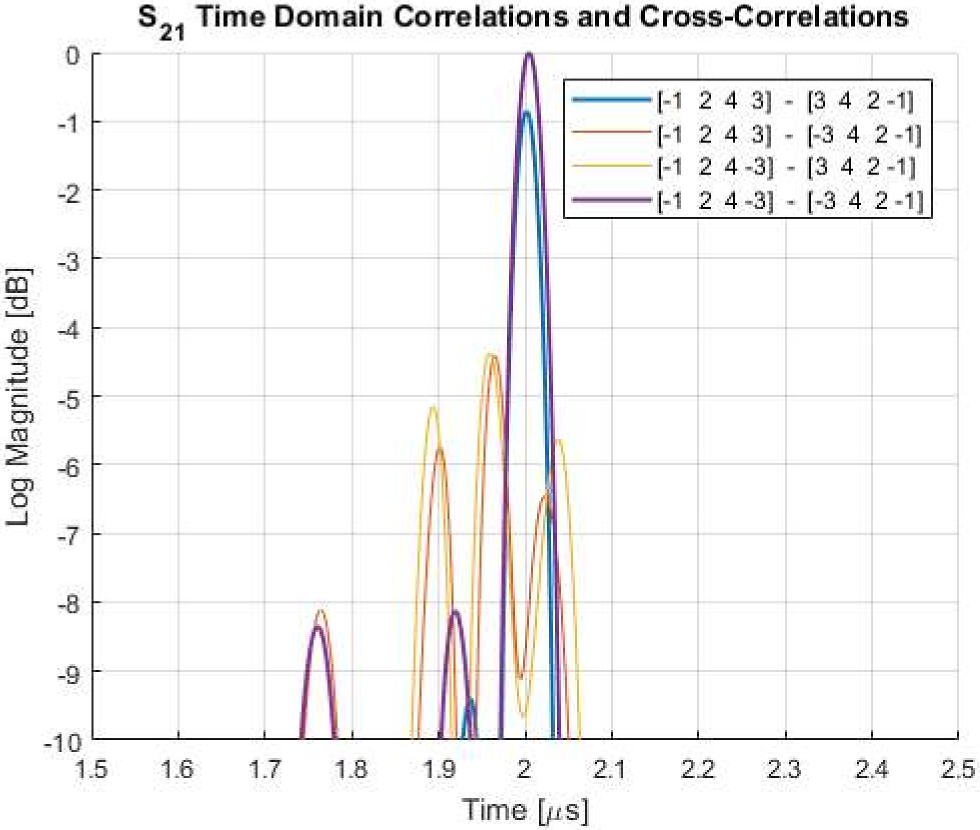

Figure 4.12: Measured normalized log-magnitude S_{21} time domain correlations and cross-correlations for a 2-code programmable BPSK code with fixed OFC sequence, no electrical matching. The correlation responses for matched codes are in bold, and show a compressed pulse with <1 dB variation. The cross-correlation responses show a worst-case MAI of about 8.2 dB for a synchronous system or about 3.5 dB for asynchronous operation with worst-case delay.

The matched filter responses presented for the full and reduced code sets show code discrimination as expected, but the level of discrimination is less than what simulation shows is possible. For a BPSK code with no additional OFC coding, the processing gain is equal to the number of chips, N_c [4]. The OFC coding gives much higher processing gain equal to the number of chips squared, ${N_c}^2$ [21]. Since these filters use fixed OFC sequences with programmable BPSK codes, the compressed pulse experiences the full processing gain equal to ${N_c}^2$, but the discrimination between mismatched codes is proportional to the BPSK processing gain, N_c. The level of discrimination between a pair of mismatched codes is the same as the level of MAI discussed previously. The level of discrimination is dependent on the codes used, but at the decision instant for synchronized systems, it is found to be equal to the difference in the number of chips that are in phase and the number of chips out of phase between the two codes normalized by the total number of chips. For example, if the transmit code has code [1,2,-4,3] and the receive code has code [3,-4,2,1] all chips have the same code and there is no rejection because this is a matched code pair. On the other hand, if the receive code is changed to [-3,-4,2,-1] then two of the chips now have the same phase (2 and 4), and two have opposite phase (1 and 3), giving zero MAI for a synchronized system and making the codes orthogonal. For asynchronous systems no easy calculation was found for worst-case level of MAI but simulations were used to calculate the expected MAI, and the value is typically higher than for synchronous systems.

Code sets can be simulated using simple signal based models or more complex models like the coupling of modes (COM) model that account for some SAW effects. The simple signal based models run quickly (several simulations per second, quick setup even for full code sets) and can be used to compare code sets ignoring SAW effects, while the COM model simulator runs slightly slower (a few seconds per simulation, setup time is longer and not set up for simulating full code sets) but gives more accurate simulations. For simulating large code sets, the COM model becomes impractical and for simulations shown here the simple signal model is used.

The system that these devices are designed for operates asynchronously in a dynamic mobile network. In an asynchronous network, received signals have an unknown delay and code pairs that produce identical amplitude responses with only a phase shift will be indistinguishable. For the BPSK codes used here, half of the codes have the same magnitude response as the other half but with a 180° phase shift, which immediately reduces the code set by a factor of two for asynchronous operation. Secondly, the log-magnitude plots used to clearly display results in this dissertation remove phase information and would make these codes indistinguishable in the plots as well.

The code sets presented above are simulated using a simple signal based model for comparison. The 4-chip 4-code set using measured results in Figure 4.11 achieved 3.1 dB rejection for mismatched codes in a synchronous system and 1.9 dB for worst-case asynchronous operation. The same 4-chip 4-code set is simulated and a rejection of 6 dB is found for a synchronous system and 3.7 dB for worst-case asynchronous operation, as seen in Figure 4.13. The 4-chip 2-code set using measured results in Figure 4.12 achieved 8.2 dB rejection for mismatched codes in a synchronous system and 3.5 dB for worst-case asynchronous operation. The same 4-chip 2-code set is simulated and a rejection of 6 dB is found for both synchronous and worst-case asynchronous operation, as seen in Figure 4.14. This indicates that it should be possible to improve the performance for the measured results with the exception of the unexpectedly high 8.2 dB rejection for synchronous operation found for the 2-code set.

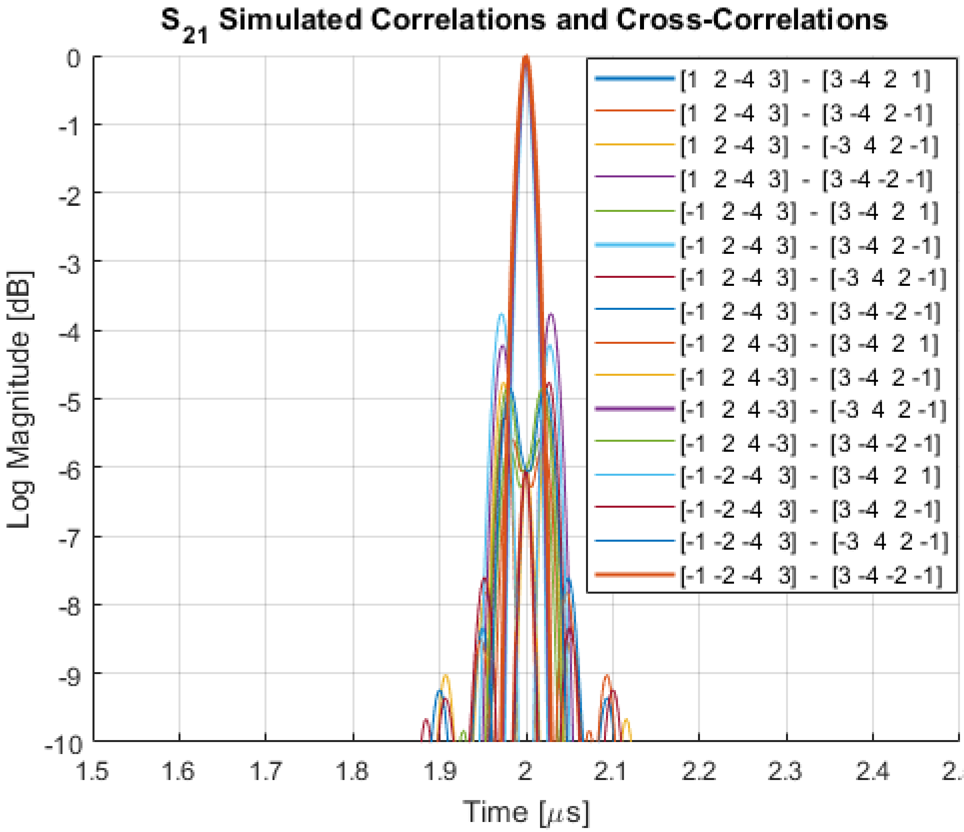

Figure 4.13: Simulated normalized log-magnitude S_{21} time domain correlations and cross-correlations for the 4-code programmable BPSK code with fixed OFC sequence presented above using measured devices. The correlation responses for matched codes are in bold, and show a compressed pulse with no variation. The cross-correlation responses show a worst-case MAI of 6 dB for a synchronous system or about 3.7 dB for asynchronous operation with worst-case delay.

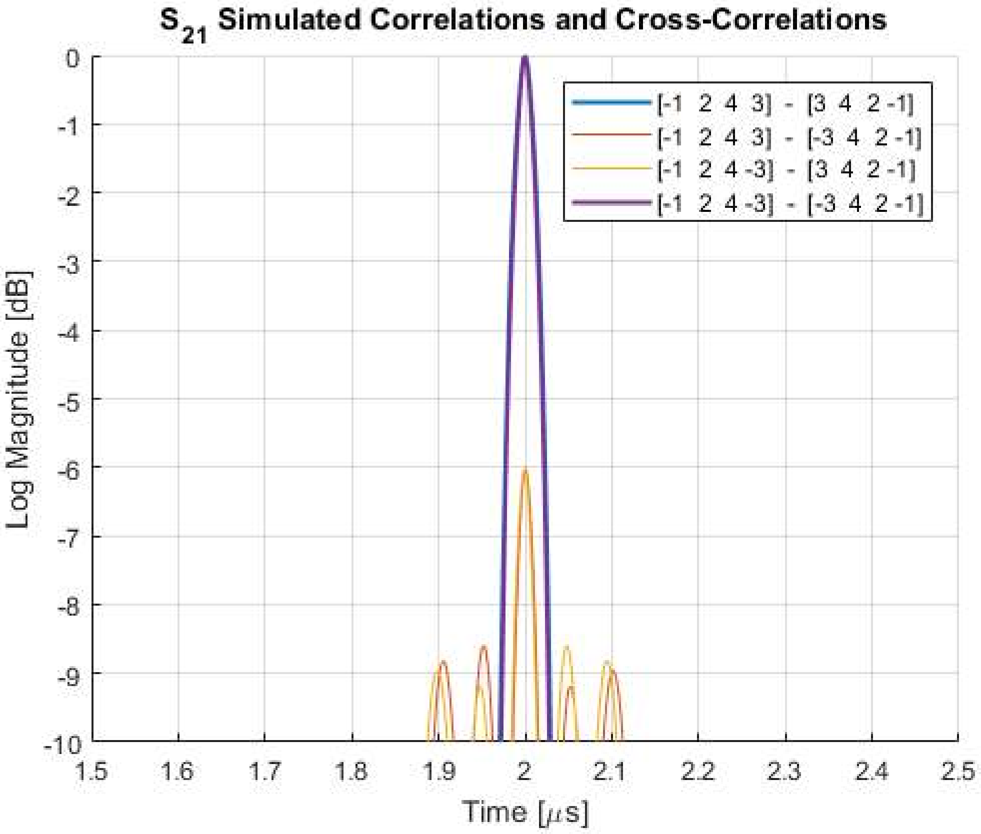

Figure 4.14: Simulated normalized log-magnitude S_{21} time domain correlations and cross-correlations for the 2-code programmable BPSK code with fixed OFC sequence presented above using measured devices. The correlation responses for matched codes are in bold, and show a compressed pulse with no variation. The cross-correlation responses show a worst-case MAI of 6 dB for both synchronous and worst-case asynchronous operation.

4.5 Summary

A pair of prototype programmable SAW correlator filters were developed using a programmable 4-chip BPSK code with fixed OFC code and positive results were presented. The results presented demonstrate the first programmable SAW correlator using OFC encoding. The programmable SAW devices and PCB are both in the early stages of development, and are not optimized. The SAW device is believed to give good performance based on the results for the fixed-code device with the same design, but has higher insertion loss than is desired. Based on the ADS simulation of the PCB and device simulations incorporating these errors, it is believed that amplitude and phase variation on the PCB are the primary contributor to the increased peak-to-sidelobe level for matched codes and increased MAI for mismatched codes. It should be possible to reduce the amplitude and phase variation of the PCB using simulation and iterative designs. It may be possible to reduce the SAW device loss to as low as 5-6 dB based on the previous chapter though the PCB and the PCB and switches will add a small amount of additional insertion loss. The switches used have approximately 0.35 dB of insertion loss between all paths at 950 MHz and are well matched for 50 Ω systems. The SAW device itself is completely passive but the external switches require about 210 μW each [30], so the full 4-chip programmable correlator uses less than 1 mW of DC power.

CHAPTER 5: CONCLUSION

The work described in this dissertation constitutes a significant improvement in low loss surface acoustic wave (SAW) correlator filters, particularly in the context of simultaneous transmit and receive (STAR) radio systems. The advantages of spread spectrum encoding using correlator filters for use with STAR radios was described in Chapter 2, and a low loss design methodology using orthogonal frequency coded (OFC) SAW filters was presented in Chapter 3. The insertion loss was reduced from about 20 dB presented in previous work [7] down to as low as 6 dB with ideal electrical matching for the correlator pair presented.

A second contribution is the design and fabrication of programmable SAW correlator filters using OFC. The filters use a fixed OFC sequence with programmable binary phase shift keying (BPSK) code using external DPDT RF switches. The design of both the SAW device and the printed circuit board (PCB) for integrating switches and peripheral components in described in Chapter 4, with measured device results. The resultant devices show positive results, and using the approach of Chapter 3 it should be possible to create low loss programmable SAW correlator filters with some modifications.

The introduction and Chapter 2 provide the motivation for this work and the theory necessary to understand the significance of the results presented. The desire for spread spectrum correlator filters with low insertion loss is presented in the context of STAR radio systems and the concepts of spread spectrum communication are outlined with illustrative examples. OFC, a type of multi-carrier spread spectrum coding, is described with applications to SAW devices.

Chapter 3 outlines design goals and describes a detailed approach to reducing the insertion loss of SAW correlator filters using fixed OFC sequences. Interdigital transducer (IDT) design is described with an emphasis on low loss design including some pertinent aspects of fabrication and device embodiment. Loss mechanisms are described and some design tradeoffs are described and empirically analyzed to improve performance. The results from the analysis and experiments described are used to design a final set of fixed-code OFC SAW correlators are designed and commercially fabricated, resulting in the low loss devices presented.

Though this work represents a significant improvement, it may be possible to further reduce insertion loss. Some of these modifications were considered in design, but found to be difficult to design or fabricate. One alternate embodiment is the multi-track configuration, which may reduce loss through the transducer [31], but presents additional design difficulties and tighter constraints on fabrication. Another area for improvement is temperature compensation. The devices presented use YZ Lithium Niobate, which has a temperature coefficient of delay (TCD) of about 94 ppm/°C. Temperature changes cause a change in velocity which introduces errors in the device response. It is possible to modify the temperature TCD of the crystal by depositing a dielectric film with a TCD of opposite sign, and at some thickness the TCD at the interface is zero. This has been described for Lithium Niobate substrates using a Silicon Dioxide (SiO_2) film, and results in a material with increased coupling coefficient with some increase in propagation loss [32]. This temperature compensated approach shows good promise, and temperature compensated correlators are under development using this approach, though results are not yet ready to be presented. A third area for potential improvement is the waveguide structure of the OFC transducer. The simple solution of empirically optimizing the beamwidth could likely be improved by modifying the structure to launch a so called ‘piston mode’ as has been described for reducing loss and issues associated with multiple transverse modes in resonators [33]. Once losses are at a minimum, it may be possible to reduce any remaining amplitude variation or distortion by weighting the response to compensate for these effects. The weighting may slightly increase insertion loss, but should improve correlation properties.

Chapter 4 presents programmable SAW correlator filters using fixed OFC sequences with programmable BPSK code. Some system and network level topics are discussed to provide the context needed to interpret the results that follow. The SAW design is described and a PCB for integrating the SAW die, switches, and other peripheral components is presented. Programmable correlator filters are fabricated, and measured results are presented and compared with measurements for a pair of fixed code devices as well as simulated responses. Small code sets using a single pair of programmable correlator filters are presented, emulating a small network of systems, with positive results.

The programmable correlator filters presented are not optimized and can be improved in terms of insertion loss, as well as amplitude and phase errors on the PCB. Simulations and iterative design should allow these PCB errors to be minimized and the methodology of Chapter 3 can be followed to reduce insertion loss. Furthermore, devices using greater code lengths will increase the processing gain, which will bring STAR systems closer to an achievable reality. The PCB presented integrates the programmable correlator into a component that is about 1.35 by 1.125 inches component, whereas the SAW device itself is only about 0.15 x .025 inches. This size is mostly due to peripheral components and allows easy placement of parts in a prototyping environment, it should be possible to significantly decrease size in future versions. Furthermore, incorporating SAW devices directly on semiconducting substrates using this piezoelectric films is becoming a more feasible reality. Thin single-crystal Lithium Niobate films have been investigated as a means of integrating on-chip photonic components, which should also be applicable to SAW devices. Using a process called ion slicing, freestanding micrometer thick films can be separated and bonded to other substrates, while maintaining properties very similar to those found in the bulk material properties of the parent sample [34]. This overcomes issues associated with thin film growth, and may allow improved integration and the ability to eliminate the need for a PCB with discrete external components.

This final chapter is intended to bring together what was achieved in a short summation, and suggests some areas that may benefit from further research. The work presented serves as a demonstration of the capabilities of spread spectrum SAW correlator filters for applications requiring low insertion loss. The incorporation of programmability extends the range of applications and will hopefully spur future developments.

LIST OF REFERENCES

[1] A. Sabharwal, P. Schniter, D. Guo, D. W. Bliss, S. Rangarajan, and R. Wichman, "In-Band Full-Duplex Wireless: Challenges and Opportunities," *IEEE Journal on Selected Areas in Communications,* vol. 32, no. 9, pp. 1637-1652, 2014.

[2] T. Riihonen, D. Korpi, O. Rantula, H. Rantanen, T. Saarelainen, and M. Valkama, "Inband Full-Duplex Radio Transceivers: A Paradigm Shift in Tactical Communications and Electronic Warfare?," *IEEE Communications Magazine,* vol. 55, no. 10, pp. 30-36, 2017.

[3] D. P. Morgan, *Surface Acoustic Wave Filters with Applications to Electronic Communications and Signal Processing*, 2nd ed. Amsterdam ; London: Academic Press, 2007.

[4] C. Campbell, *Surface Acoustic Wave Devices for Mobile and Wireless Communications*. Academic Press, Inc., 1998, p. 631.

[5] E. A. Ash, "Fundamentals of Signal Processing Devices," in *Acoustic Surface Waves*, A. A. Oliner, Ed.: Springer, 1978.

[6] R. W. Brocato *et al.*, "Programmable SAW Development," Sandia National Laboratories, Online, 2004.

[7] D. R. Gallagher and D. C. Malocha, "Ultra wide band saw correlators using dual orthogonal frequency coded transducers," in *2009 IEEE International Frequency Control Symposium Joint with the 22nd European Frequency and Time forum*, 2009, pp. 24-27.

[8] R. Brocato, E. Heller, G. Onidahl, J. Wendt, S. Jones, and D. Palmer, "High frequency SAW correlator module," in *53rd Electronic Components and Technology Conference, 2003. Proceedings.*, 2003, pp. 458-463.

[9] F. S. Hickernell, M. D. Adamo, R. V. D. Long, J. G. Hinsdale, and H. J. Bush, "SAW Programmable Matched Filter Signal Processor," in *1980 Ultrasonics Symposium*, 1980, pp. 104-108.

[10] G. S. Kino, "Acoustoelectric interactions in acoustic-surface-wave devices," *Proceedings of the IEEE,* vol. 64, no. 5, pp. 724-748, 1976.

[11] M. S. Smith, A. R. Weeks, and D. C. Malocha, "Low Loss Orthogonal Frequency Coded Surface Acoustic Wave Correlator Filters," presented at the IEEE International Frequency Control Symposium, Olympic Valley, CA, 2018.

[12] Z. Zhang, K. Long, A. V. Vasilakos, and L. Hanzo, "Full-Duplex Wireless Communications: Challenges, Solutions, and Future Research Directions," *Proceedings of the IEEE,* vol. 104, no. 7, pp. 1369-1409, 2016.

[13] R. Scholtz, "The Origins of Spread-Spectrum Communications," *IEEE Transactions on Communications,* vol. 30, no. 5, pp. 822-854, 1982.

[14] R. L. Peterson, D. E. Borth, and R. E. Ziemer, *Introduction to spread-spectrum communications*. Englewood Cliffs, NJ: Prentice Hall, 1995.

[15] B. P. Lathi and Z. Ding, *Modern digital and analog communication systems*, 4th ed. New York: Oxford University Press, 2009.

[16] J. G. Proakis and M. Salehi, *Digital communications*, 5th ed. Boston, MA; Bogotá: McGraw-Hill, 2008.

[17] R. Pickholtz, D. Schilling, and L. Milstein, "Theory of Spread-Spectrum Communications - A Tutorial," *IEEE Transactions on Communications,* vol. 30, no. 5, pp. 855-884, 1982.

[18] G. Turin, "An introduction to matched filters," *IRE Transactions on Information Theory,* vol. 6, no. 3, pp. 311-329, 1960.

[19] C. Sturm and W. Wiesbeck, "Waveform Design and Signal Processing Aspects for Fusion of Wireless Communications and Radar Sensing," *Proceedings of the IEEE,* vol. 99, no. 7, pp. 1236-1259, 2011.

[20] D. C. Malocha, D. Puccio, and D. Gallagher, "Orthogonal frequency coding for SAW device applications," in *IEEE Ultrasonics Symposium, 2004*, 2004, vol. 2, pp. 1082-1085 Vol.2.

[21] D. C. Malocha, M. Gallagher, B. Fisher, J. Humphries, D. Gallagher, and N. Kozlovski, "A Passive Wireless Multi-Sensor SAW Technology Device and System Perspectives," *Sensors,* vol. 13, no. 5, 2013.

[22] D. R. Gallagher, N. Y. Kozlovski, and D. C. Malocha, "Ultra-wideband communication system prototype using orthogonal frequency coded SAW correlators," *IEEE Transactions on Ultrasonics, Ferroelectrics, and Frequency Control,* vol. 60, no. 3, pp. 630-636, 2013.

[23] W. J. Stapor, J. H. Hines, and D. H. Wilson, "Ionizing space radiation effects on surface acoustic wave resonators," *IEEE Transactions on Nuclear Science,* vol. 38, no. 6, pp. 1329-1335, 1991.

[24] D. P. Morgan, *Surface-Wave Devices for Signal Processing*. Amsterdam ; London: Elsevier, 1991.

[25] D. R. Gallagher and D. C. Malocha, "Ultra wide band dual orthogonal frequency coded SAW correlators using harmonic operation," in *2010 IEEE International Frequency Control Symposium*, 2010, pp. 301-306.

[26] S. Malocha and B. P. Abbott, "Calculation of COM parameters for an arbitrary IDT cell," in *2002 IEEE Ultrasonics Symposium, 2002. Proceedings.*, 2002, vol. 1, pp. 267-270 vol.1.

[27] C. S. Hartmann and B. P. Abbott, "Overview of design challenges for single phase unidirectional SAW filters," in *Proceedings., IEEE Ultrasonics Symposium*, 1989, pp. 79-89 vol.1.

[28] J. D. Galipeau, "Enhanced SPUDT cells for high coupling substrates," in *IEEE Ultrasonics Symposium, 2005.*, 2005, vol. 2, pp. 1052-1055.

[29] C. K. Campbell, "Modelling the transverse-mode response of a two-port SAW resonator," *IEEE Transactions on Ultrasonics, Ferroelectrics, and Frequency Control,* vol. 38, no. 3, pp. 237-242, 1991.

[30] Qorvo, "QPC6222 General Purpose DPDT Transfer Switch," ed. Online, 2016.

[31] H. Odagawa, D. C. Malocha, and K. Yamanouchi, "High stable and sensitive orthogonal frequency coded SAW tags and sensors using unidirectional IDT and high coupling zero TCF substrates," in *2011 IEEE International Ultrasonics Symposium*, 2011, pp. 814-817.

[32] K. Yamanouchi, H. Satoh, T. Meguro, and Y. Wagatsuma, "High temperature stable GHz-range low-loss wide band transducers and filter using $SiO_2/LiNbO_3$, $LiTaO_3$," *IEEE Transactions on Ultrasonics, Ferroelectrics, and Frequency Control,* vol. 42, no. 3, pp. 392-396, 1995.

[33] M. Solal *et al.*, "A method to reduce losses in buried electrodes RF SAW resonators," in *2011 IEEE International Ultrasonics Symposium*, 2011, pp. 324-332.

[34] M. Levy and A. M. Radojevic, "Single-Crystal Lithium Niobate Films by Crystal Ion Slicing," in *Wafer Bonding: Applications and Technology*, M. Alexe and U. Gösele, Eds. Berlin, Heidelberg: Springer Berlin Heidelberg, 2004, pp. 417-450.